FOSSIL

DOE/PC/90293--T15
(DE95009310)

HIGH-TEMPERATURE MEMBRANES FOR H_2S AND SO_2 SEPARATIONS

Final Report

By
J. Winnick

January 1995

Work Performed Under Contract No. FG22-90PC90293

For
U.S. Department of Energy
Pittsburgh Energy Technology Center
Pittsburgh, Pennsylvania

By
Georgia Institute of Technology
Atlanta, Georgia

MASTER

DISCLAIMER

DOE/PC/90293--T15
(DE95009310)
Distribution Category UC-113

HIGH-TEMPERATURE MEMBRANES FOR H_2S AND SO_2 SEPARATIONS

DE-FG22-90PC90293

FINAL REPORT

JANUARY 1995

Georgia Institute of Technology
Jack Winnick, P.I.

Table of Contents

List of Figures

List of Tables

EXECUTIVE SUMMARY

Electrochemical cells which separate H_2S and SO_2 from hot gas streams have two important materials issues that limit their successful industrial application: (1) membranes and (2) electrodes. These were the focus of the present study.

For the H_2S work, experimental analysis incorporated several membrane and electrode materials; densified zirconia provided the best matrices for entrainment of electrolytic species, ionic mobility, and a process-gas barricade hindering the capabilities of gas cross-over, alternate reactions. In-lab densification of a zirconia weave/knit mat using sub-micron particles of zirconia in an aqueous suspension provided the most efficient and economical manufacturing technique. Electrode materials of lithiated Ni converted to NiO in-situ were successful in polishing applications; however H_2S levels > 100 ppm converted the NiO cathode to a molten nickel sulfide necessitating the use of Co. Lithiated NiO for the anode material remained morphologically stable and conductive in all experimentation.

High temperature electrochemical removal of H_2S from coal gasification streams has been shown on the bench scale level at the Georgia Institute of Technology utilizing the aforementioned materials. Experimental removals from 1000 ppm to 100 ppm H_2S and 100 ppm to 10 ppm H_2S proved over 90% removal with applied current was economically feasible due to high current efficiencies (~100%) and low polarizations; therefore low power requirements for removal applications in the above ranges. Polishing of H_2S from 10 ppm to < 1 ppm tested the most stringent application of the

electrochemical cell due to the low concentration of H_2S compared to CO_2. Removals over 90% were achieved; power requirements for this level of removal are negligible.

For the SO_2 work, an extensive search was conducted for a suitable membrane material for use in the SO_2 removal system. The most favorable material found was Si_3N_4, proven to be more efficient than other possible materials. In addition, tape casting was proven to be the method of choice for delivery of the ceramic matrix in full cell testing. New lithiated NiO electrodes were also developed and characterized, proving more stable than previously used pervoskite electrodes.

The combination of these new components led to 90% removal at near 100% current efficiency over a wide range of current densities. Cells proved highly stable over the unprecedented period of 30 days, showing identical characteristics from beginning to end of experimentation.

The highest levels of current density are commensurate with economic cell design; they are limited only by mass-transfer from the bulk gas, as expected from modeling of the system. With the high current densities tested, SO_2 generation was observed at the cathode due to chemical and electrochemical complications. This generation was characterized with respect to O_2 partial pressure. Electrodes with higher reaction area were being tested for the ability to eliminate this limitation as the research period ended.

INTRODUCTION

Use of selective membranes for separating gaseous components from mixtures is experiencing escalating interest. Most rely on a pressure or concentration difference to provide a chemical potential driving force:

$$\Delta\mu_i = \mu_i - \mu'_i = RT \ln (a_i / a'_i) \quad (1)$$

where the activities of component *i* in the two phases separated by the membrane are noted a_i and a'_i. Facilitated transport through a chemical or surface reaction can sometimes be employed to aid selectivity and permeability. In certain instances, an electric field can be employed as an alternative. For species with a net charge, z_i, the driving force across a membrane becomes the electrochemical potential difference, $\Delta\bar{\mu}_i$:

$$\Delta\bar{\mu}_i = \bar{\mu}_i - \bar{\mu}'_i = RT \ln(a_i / a'_i) + z_i F \Delta\Phi \quad (2)$$

where $\Delta\Phi$ is the potential difference across the membrane.

The simplest application of this technique is the preparation of nearly pure oxygen from air[1]. An asbestos mat or a few sheets of filter paper, soaked in aqueous KOH (electrolyte) serves as the membrane. The electric field is created by a low voltage DC power supply (or battery) attached across two nickel screens (or porous electrodes) pressed to either side of the membrane. Air passes by the negative screen (cathode) where oxygen is reduced:

$$1/2\ O_2 + H_2O + 2\ e^- \Rightarrow 2\ OH^- \quad (3)$$

At the positive screen (anode), hydroxide is oxidized:

$$2\ OH^- \Rightarrow H_2O + 1/2\ O_2 + 2\ e^- \quad (4)$$

producing nearly pure oxygen (water saturated, but free of nitrogen, argon, and carbon dioxide). The minimum voltage, from equation (2), is but a few tens of millivolts.

The propensity for this alkaline electrolyte to scrub carbon dioxide from the air led to its application as a life-support subsystem in manned spacecraft[2]. When the electrolyte reaches a steady-state composition it is an alkaline carbonate solution, with a pH near 12 at the cathode and, with hydrogen supplied to the anode in place of electric power, a pH near 7 at the anode.

The same principle can be, and has been, applied to high temperature gas mixtures encountered in coal utilization. These are the two general types of processes: reducing, as from gasification processes; and oxidizing, as in combustion flue gas. The primary gaseous pollutant in each case is a sulfur species; in the first case H_2S and in the second case SO_2. Since the membrane is exposed to the same pressure on both sides, there is no theoretical limit to the pressure at which the process operates. While the electrochemical principle is the same for each, the chemistry is quite different; the main thrust of this research is the purification of fuel gases (specifically coal gasification product gases, or synthetic-gas) of H_2S.

Four major task were designated, as stated in the proposal for H_2S & SO_2 removal:

H_2S

1. Find a suitable anode material capable of high current density while maintaining structural and chemical stability in the harsh cell environment.

2. Optimize and utilize membrane matrix materials sustaining morphology and providing a barrier to process gas-crossover in full-cell experiments.

SO_2

3. Manufacture of a suitable matrix by tape-casting, sintering, or pressing.

4. Determine viability of components in full-cell tests designed to achieve 90% removal.

H_2S SUMMARY

The gas resulting from coal gasification has a broad range of compositions depending on the coal as well as the gasification process; that is, the temperature, pressure, and amount of air (or oxygen) and steam employed. However, the level of H_2S is set by the sulfur content in the coal; for example, 3% sulfur coal will yield about 0.6 - 0.7% H_2S. A lesser amount of COS is found as well. The corrosive and toxic nature of these contaminants make it essential that they be removed down to sub-ppm levels.

Since gasification processes are quite varied, the product gas also has a large variety of compositions:

CO	18. - 60. %
CO_2	3. - 30. %
H_2	15. - 60. %
N_2	1. - 60. %
H_2O	2. - 30. %
H_2S	0.2 - 1.5%

Processes to remove the H_2S generally rely on low to ambient temperature absorption, followed by sorbent regeneration and Claus treatment for conversion of concentrated H_2S to elemental sulfur. Hot gas desulfurization has been limited to employment of metal oxide sorbents which suffer most of the same drawbacks as the lower temperature processes. That is, they require desorption and Claus treatment.

The hot-gas electrochemical membrane process is illustrated schematically in Figure 1. The product gas, cleansed of particulates, is passed by the cathode. Here, the most easily reduced component, that is, the strongest Lewis acid, will be electronated.

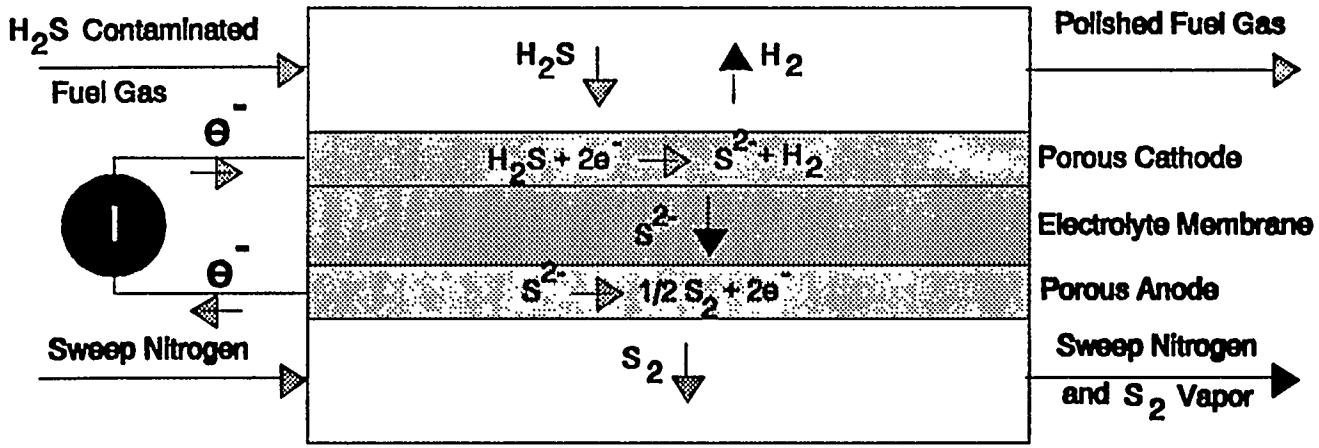

Figure 1 Electrochemical Membrane Separation Process

Under these conditions, it is H_2S:

$$H_2S + 2\,e^- \Rightarrow H_2 + S^{2-} \qquad (5)$$

A membrane which contains sulfide ions in a molten state will act to transport sulfide across to the anode where, in the simplest case, hydrogen can be supplied to form H_2S. If the membrane is capable of preventing diffusion of hydrogen from the cathode side, an inert sweep gas such as N_2 can be used at the anode to carry away oxidized sulfide ions as vaporous sulfur, S_2.

This concept has been used with success for gases containing only H_2S in N_2[3], simulated coal gases[4], and simulated natural gases[5]. For this last work, a membrane was constructed of alkali metal sulfides and carbonates retained in a porous MgO stucture a few millimeters in thickness. The cathode was made of porous carbon and the anode of porous CoS_2. Polishing of simulated coal gases, testing the most stringent application of this technology, has recently been shown using the electrochemical membrane separator. Successful polishing experiments utilized a porous cubic zirconia membrane of the same order thickness as previous membrane materials. Electrodes were lithiated-NiO. The cell is shown schematically in Figure 2. As anticipated, applied current acted to remove H_2S from the cathode gas, as shown in Figure 35 & 36. It was simultaneously produced at the anode:

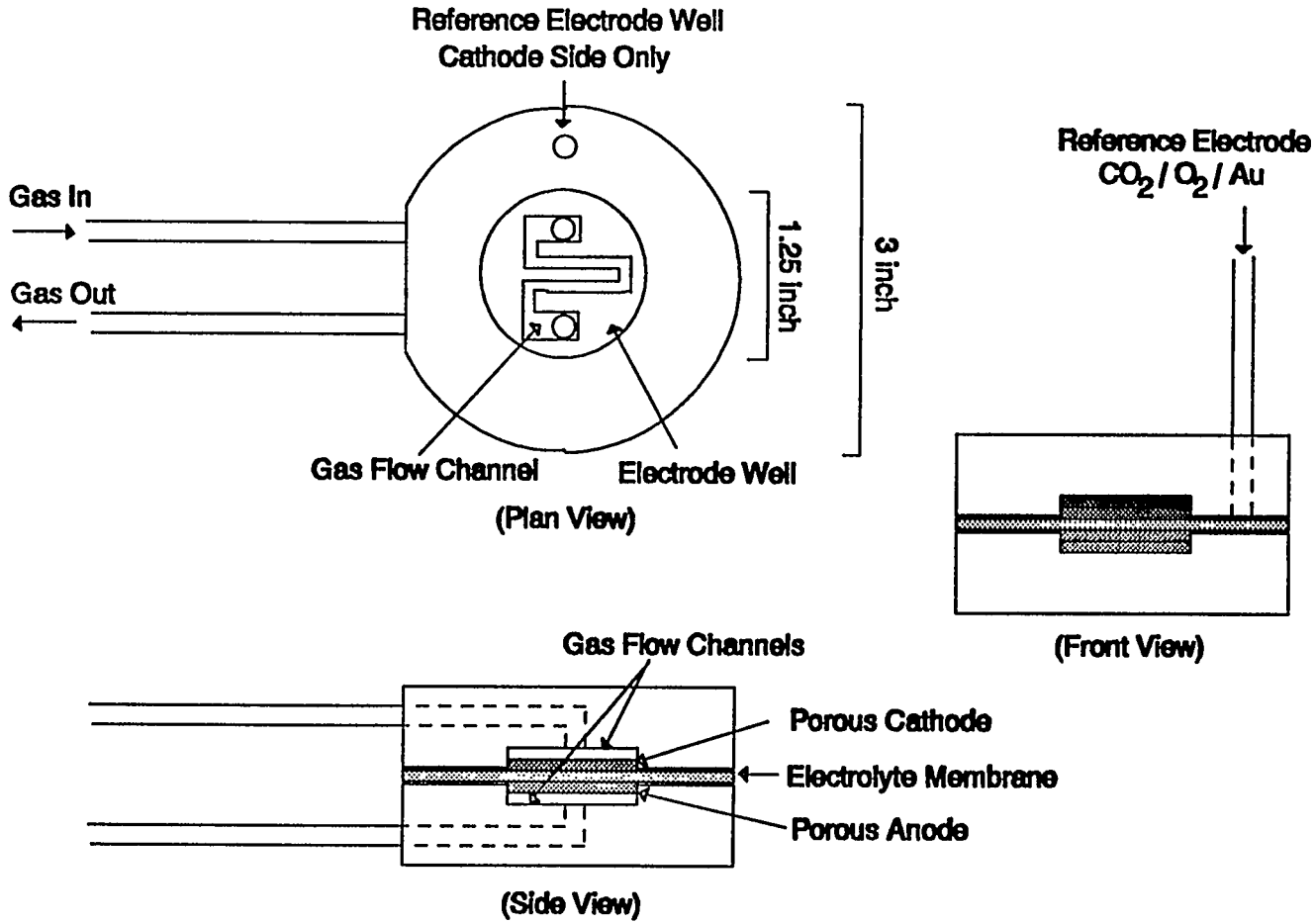

Figure 2 Schematic of Electrochemical Cell

$$S^{2-} \Rightarrow 1/2\ S_2 + 2\ e^- \quad (6)$$

The situation is complicated, however when realistic gas mixtures are involved. Carbon dioxide and water vapor compete in the reduction reaction by:

$$CO_2 + H_2O + 2\ e^- \Rightarrow CO_3^{2-} + H_2 \quad (7)$$

As reaction (7) proceeds at about the same standard potential as reaction (5), the electrolyte becomes richer in carbonate. The ionic flux through the membrane depends upon the relative mobilities of the carbonate and sulfide as well as their concentrations.

Since the oxidation reactions (6) and (8):

$$CO_3^{2-} + H_2 \Rightarrow CO_2 + H_2O + 2\ e^- \quad (8)$$

also occur near the same standard potential, about 1 Volt positive of the reductions, CO_2 will be transferred at a far greater rate than H_2S, since it will be present in the process gas at an order of magnitude higher concentration.

$$E = E^\circ - [RT/nF] \ln(a_{prod.} / a_{react.}) \quad (9)$$

The situation is favorably altered if no reductant is available at the anode. The direct oxidation of carbonate:

$$CO_3^{2-} \Rightarrow CO_2 + 1/2\ O_2 + 2\ e^- \quad (10)$$

occurs at a standard potential some 700 mV more positive than that for sulfide:

$$S^{2-} \Rightarrow 1/2\ S_2 + 2\ e^- \quad (6)$$

Thus, a concentration (or activity) ratio of 10^5 could exist in the anolyte, assuming equivalent electrode kinetics for the two reactions, before significant (e.g. 1%) carbonate is oxidized. This mode of operation is preferable for commercial application, with direct

production of elemental sulfur vapor, eliminating the need for a Claus reactor. The net effect, under these conditions, is continuous removal of H_2S from the process gas accompanied by enrichment of the process gas with H_2 and direct generation of elemental sulfur. The only reagent required is electric power at a potentially attractive rate.

The equilibrium potential for a single cell, given by equation (9), for the cathodic and anodic reactions (5) and (6), is 587 mV for a process gas containing 100 ppm H_2S and an anode product of pure sulfur vapor. To this must be added the overpotentials needed for both electrode reactions and ohmic loss. The electrode reactions have been studied in free electrolyte on graphite electrodes[6,7]. Potential step experiments showed very rapid kinetics, with exchange currents in both cathodic and anodic directions near 40 mA/cm^2. Cyclic voltammetry verified a 'catalytic' reaction mechanism with disulfide as the electro-active species. At the cathode:

$$H_2S + S^{2-} \Rightarrow H_2 + S_2^{2-} \quad (11)$$

and

$$S_2^{2-} + 2\,e^- \Rightarrow 2\,S^{2-} \quad (12)$$

At the anode:

$$S_2 + 2\,S^{2-} \Rightarrow 2\,S_2^{2-} \quad (13)$$

$$S_2^{2-} \Rightarrow S_2 + 2\,e^- \quad (14)$$

Surprisingly, enhanced cathodic H_2S removal was found with CO_2 and H_2O in the gas, probably due to another 'catalytic' scheme, reaction (7) followed by:

$$CO_3^{2-} + H_2S \Rightarrow CO_2 + H_2O + S^{2-} \quad (15)$$

Another unexpected result was the concurrent removal of the COS down to levels below the analytical limit (ca. 1 ppm). This occurs apparently due to rapid equilibrium between H_2S, CO, CO_2, and COS at these temperatures.

A study of potential cathode materials[4] showed several promising alternatives. It was conducted using a configuration similar to anticipated designs (see Figure 2). Since the working membrane will be mostly carbonate at steady-state, Molten Carbonate Fuel Cell(MCFC) 'tiles', purchased from IGT, were used. Other membrane materials such as a tape cast MgO, zirconia felt, and rigid zirconia each infiltrated with molten carbonate in the same cationic mole composition($Li_{0.62}K_{0.38}$) used in the MCFC, sulfided in-situ, provided sufficient barriers to process gases and electrolyte entrainment to attain high removal of H_2S (over 90%). Several electrode materials were found acceptable; including nickel and cobalt, formed from powders, sulfided in-situ.

Studies of 'tile' compositions have also been performed. By analyzing the equilibrium of reaction (16), it is possible to know the electrolyte composition which would be in equilibrium with a given process gas at a given process temperature. This has been done with some success by Alexander (see Figure 3)[5]. Theoretical tile compositions were calculated by thermodynamic analysis of the tile equilibrium reaction (16). Since standard MCFC tiles were used in this analysis, the cations present were K and Li in a ratio corresponding to the low melting carbonate eutectic ($Li_{0.62}K_{0.38}$).

$$(Li_{0.62}K_{0.38})_2CO_3 + H_2S \;<=>\; (Li_{0.62}K_{0.38})_2S + CO_2 + H_2O \qquad (16)$$

This analysis was performed by finding the Gibbs free energy of reaction (16) at the process temperature and relating this to the equilibrium constant, K_a, by the relation:

$$\ln K_a = \frac{\Delta G}{RT} \qquad (17)$$

with K_a defined as:

By this analysis, a process gas with a composition of 0.88% CO_2, 1760 ppm H_2S, 12% H_2O, and the balance methane (for the natural gas process mentioned above) with a run

$$K_a = \frac{P_{CO_2} P_{H_2O} a_{(Li_{0.62}K_{0.38})_2S}}{P_{H_2S} a_{(Li_{0.62}K_{0.38})_2CO_3}} \qquad (18)$$

temperature of 610° C will have an equilibrium constant of 6.9. If the activity coefficients of the molten phase constituents (namely the sulfide and carbonate in the electrolyte) are assumed to be unity, this translates to an electrolyte composition of 19.5% sulfide and 80.5% carbonate. This was verified by exposing a tile which was originally 100% carbonate to the above process gas for 34 hours in an operating removal cell. The tile was subsequently analyzed by wet test methods and found to have a composition of 20.3% sulfide and 79.7% carbonate.

If a 'tile' is manufactured already in equilibrium with the gas to be treated, it will not have to undergo the stresses inherent in the density changes associated with 'sulfiding' a carbonate tile or 'carbonating' a sulfide tile. While techniques for manufacturing such a tile are still under study, the concept has been used successfully in both the coal gasification process cell[8] and the natural gas process cell[5].

The key to successful anode performance; that is, oxidation of sulfide but not carbonate, will depend upon identifying an anode material capable of overpotentials below about 500 mV at current densities of 100 mA/cm^2. This would seem possible

since it has been achieved with graphite and since cathodes have been operated at relatively high current densities well within this limit. Several potential anode materials have been identified[8] and anodes of CoS_2 have been used with some success in the natural gas process cell[5]. Anodes constructed of these materials do not have the chemical decomposition problems inherent in the carbon electrodes. NiO used primarily in molten carbonate fuel cells have also shown promise in full-cell experimentation as an adequate anode material.

MATERIALS

Electrodes

The electrodes used as sites for the electrochemical reduction and oxidation reactions in this removal cell must meet certain criteria with respect to their materials and their pore characteristics. They must be electronically conductive within the temperature range of operation for the cell and they must be chemically stable in the corrosive process gas and the oxidizing environment of the anode. The pores through the electrode must offer little gas phase diffusion resistance since reagents must be able to move from the bulk gas phase to the reaction sites at the electrode/electrolyte interface. The overall pore structure must have a high interfacial surface area in order to maximize the sites for electrochemical reaction. Finally, the electrode pores must offer low capillary forces on the electrolyte within the membrane matrix. The electrolyte must only wet the walls of the electrode pores, not completely flood the electrode. If the

electrode floods, the interfacial surface area is decreased and the membrane matrix is depleted of electrolyte.

Several potential electrode materials were identified by Weaver[8]; of these, porous carbon, $La_{0.8}Sr_{0.2}CrO_3$, Co, CoS_2, MoS_2, Ni and NiO were used in full-cell experiments. Since Weaver has surveyed possible cathode materials, interest in this study was placed on possible anode materials tested in a removal cell with a gas-impermeable membrane.

Carbon: Carbon is highly conductive and remains solid to an extremely high temperature. Electrodes were obtained from Ultra Carbon pre-formed with dimensions of 1.25" diameter and 0.8 mm thick (porosity of 54%). While useful for short duration bench-scale experimental runs, carbon would not be useful in an long duration or industrial application because of degradation reactions. At the cathode it is eroded by steam or CO_2:

$$C + H_2O \rightarrow CO + H_2 \qquad (19)$$

$$C + CO_2 \rightarrow 2\,CO \qquad (20)$$

And at the anode it can act as a reductant for carbonate:

$$CO_3^{2-} + C \rightarrow CO + CO_2 + 2e^- \qquad (21)$$

Since reaction **(21)** occurs at a potential about 300 mV below the sulfide oxidation reaction, this provides a 'short-cut' for carbonate transport. Thus, carbon was not useful

as an anode material. However, since carbon electrodes were inexpensive and easily available, they were used as cathode materials in experimental runs of limited duration, specifically in natural gas application studies. Carbon cathodes were used successfully in runs 37, 40, and 42.

Carbon anodes act as a reducant for CO_3^{2-} by (21); therefore, carbon was not the material of choice for use as the anode. Carbon anodes showed sever degradation over the course of relatively short runs (around 48 hours). Since they were easily available some runs did use carbon anodes with limited success.

$La_{0.8}Sr_{0.2}CrO_3$: The high melting temperature, corrosion resistance, and high electrical conductivity of certain ceramic materials identify them as possible candidates for removal cell electrodes. Lanthanum chromite, $LaCrO_3$, is a p-type semiconductor due to holes in the conduction band of Cr^{3+} ions[9]. Doping either La^{3+} or Cr^{3+} sites with a lower valence ion, in this case Sr^{2+}, results in enhanced conductivity due to formation of Cr^{4+}. The position on which the electron acceptor dopant ion substitutes is determined by its ionic radius according to Pauling's rules[10].

$La_{0.8}Sr_{0.2}CrO_3$ semiconducting metal oxide was purchased as a powder from HUA Associates of Rolla, MO. This material was prepared using a gel-precipitation technique which produces finely dispersed particles of homogeneous composition. The 'as received' powders were screened to +100, 100-200,200-325, 325-400, and -425 mesh portions. Electrodes used for cell tests were prepared from 100-200 mesh powders by dry-pressing in a 1 1/4" die at 8000 psi. The resulting oxide discs were very fragile, thus

a sintering step was necessary to provide enough strength for use in the cell. By trial and error, sintering conditions were found to be 2 hours at 1350°C. This produced a structure with a bulk porosity of approximately 60% and a pore size of about 30 μm.

When used as a cathode material excellent physical and chemical stability was shown, but high ohmic losses through the electrode present inherent system problems. An anode was manufactured from this material and successfully used in the natural gas sweetening application. The electrode polarization, however, was found to be unacceptably high.

Metal Electrodes: Phase diagrams may be constructed for metal-sulfur-oxygen systems based on analysis of the Gibb's free energy of all stable phases within the system at a given temperature[11]. From these diagrams, the phase in thermodynamic equilibrium with the process gas stream can be determined.

For metal-sulfur-oxygen systems at 650°C, the stable phases will consist of metal, metal sulfide, metal oxide, and metal sulfate components. Weaver performed this analysis for Co, Mo, and Ni[12]. In his analysis, the gas phase activities were assumed to be equal to the partial pressure and solid phase activity was set equal to unity. The chemical reactions between the system compounds were written in terms of S_2 and O_2 activity.

The S_2 and O_2 partial pressures were related to actual stream components using the following equilibrium expressions:

$$H_2 + \frac{1}{2}O_2 \rightleftharpoons H_2O \qquad (22)$$

$$CO + \frac{1}{2}O_2 \rightleftharpoons CO_2 \qquad (23)$$

$$H_2 + \frac{1}{2}S_2 \rightleftharpoons H_2S \qquad (24)$$

All thermodynamic data was taken from Barin and Knacke[13, 14].

While useful in predicting "zero-current" thermodynamic equilibrium phases for metal-sulfur-oxygen systems, the phase diagrams generated by Weaver do not provide a complete picture of the system equilibrium because chemical kinetics, the effects of applied current (and induced potential), and reactions with the electrolyte species were not considered.

Preto has studied Ni-S and Co-S systems in molten LiCl/KCl electrolytes for use in Li-Al/FeS battery cells[15]. He showed that Ni and Co undergo simple oxidation/reduction transitions of the form:

$$M + 2S^{2-} \rightleftharpoons MS + S^{2-} \rightleftharpoons MS_2 \qquad (25)$$

Ingram has studied the oxidation of Ni to NiO within the molten carbonate fuel cell system[16]. He shows oxidation/reduction transitions of the form:

$$M + CO_3^{2-} \rightleftharpoons MO + CO_2 + 2e^- \qquad (26)$$

The potentials at which these reactions occur at 650°C were calculated from published data[13,14] and are presented in Table I.

Co, Co_9S_8, and CoS_2: Cobalt electrodes were converted to the stable metal sulfide phase in situ, similar to the technique used to produce the NiO cathode in a molten carbonate fuel cell. Metal powders (less than 2μm particle size) were purchased from Aldrich Chemical. The cobalt powder was evenly loaded into a 1 1/4" stainless steel die and dry pressed at 8000 psi total static pressure using a hydraulic ram. No sintering step was used in preparation of the metal electrodes due to the oxidation, cracking, and warping which occurred when the metal discs were heated in air.

High purity CoS_2 (particle size average of 75μm) was obtained from Alfa Chemicals and mixed with hydroxyethyl cellulose (HEC) from Union Carbide Corp. Void percentages as high as 60% were obtained using a mixture of 10 weight % HEC and 90 weight % metal-sulfide powder. This mixture was loaded into a 1 1/4" stainless steel die and pressed at 8000 psi using a hydraulic ram. The resulting electrode wafer was then heated at 350°C for 30 minutes to burn out the HEC. This final electrode was then cooled, weighed, and stored for use in the electrochemical cell.

Weaver reported Co-S electrodes as successful cathode materials. He reported Co_9S_8 as the stable phase under coal gas applications and showed by cyclic voltammetry that this compound was electrochemically reduced to Co metal and sulfide ion, providing a catal ::c mechanism for H_2S removal by:

$$Co_9S_8 + 16e^- \rightarrow 9Co + 8S^{2-} \qquad (27)$$

followed by:

$$9\,Co + 8\,H_2S \rightarrow Co_9S_8 + 16\,H_2 \qquad (28)$$

Cobalt cathodes used in several coal gasification experiments provided stoichiomatric carbonate transport across the cell, however removal of H_2S using cobalt metal is still under investigation.

CoS_2 was the material of choice for the anode in natural gas sweetening applications. This material showed excellent stability in the oxidizing enviroment of the cell, as long as the operating current of the cell did not run the anodic overpotential high enough to promote significant oxidation of carbonate. If the anode potenital was run too high during the course of the run, the material would oxidize, loose conductivity, and break-down as an electrode material. CoS_2 was used successfully in runs 37 and 38.

Table I Estimated Phase Transitions - Metal-S-O Systems at 650°C.

Phase Transitions for the Ni-S-O System

Transition Reaction (Oxidation)	Calculated Potential,V
$3Ni + 2S^{2-} \Rightarrow Ni_3S_2 + 4e^-$	0.922
$Ni_3S_2 + S^{2-} \Rightarrow 3NiS + 2e^-$	0.716
$Ni + CO_3^{2-} \Rightarrow NiO + CO_2 + 2e^-$	1.013

Phase Transitions for the Co-S-O System

Transition Reaction (Oxidation)	Calculated Potential,V
$9Co + 8S^{2-} \Rightarrow Co_9S_8 + 16e^-$	-0.018
$Co_9S_8 + 10S^{2-} \Rightarrow 9CoS_2 + 20e^-$	1.189
$Co + CO_3^{2-} \Rightarrow CoO + CO_2 + 2e^-$	1.067
$CoO + CO_3^{2-} \Rightarrow Co_3O_4 + CO_2 + 2e^-$	0.359

Ni and NiO: Ni electrodes were donated to this research by ERC as 8" by 11" sheets (pore size was proprietary, but average porosity was between 75 and 80%). A die was used to cut 1 1/4" electrodes from this sheet. These electrodes were then soaked in 1 M LiOH and then dried. If Ni electrodes were to be used, the electrodes were then loaded into the cell and the run was started. If NiO electrodes were to be used, the electrodes were placed between two sintered Al_2O_3 disks and placed in an oven at 650°C under atmospheric air for at least six hours. Gravimetric analysis of these oxidized electrodes showed that the Ni was at least 96% converted to NiO. This material was successfully used as the starting material for a cathode in run 43 of the natural gas polishing application and runs 47, 48, and 49 of the coal gas polishing application. Lithiated NiO was successfully used as the starting material for the anode in runs 42 and 43 of the natural gas polishing application and runs 47, 48, and 49 of the coal gas polishing application. Lithiated Ni was successfully used as the starting material for a cathode material in run 39 for natural gas polishing application and runs 55, 56, 57, 58, 59, 62, 65, 4, and 5 for coal gas polishing applications. Lithiated Ni was successfully used as the starting material for an anode in runs 39 and 40 for natural gas polishing application and in runs 55, 56, 57, 58, 59, 62, 65, 4, and 5 for coal gas polishing application.

X-ray diffraction of used electrodes from the natural gas polishing studies showed that the equilibrium structures were a mixture of several compounds, primarily Ni and NiO with traces of Ni_3S_2 and NiS present in both the cathode and the anode materials.

The x-ray diffraction scan of the cathode material used in run 39 showed that the equilibrium material was a mixture that was predominantly NiO, with smaller ammounts of Ni, Ni_3S_2, and NiS. The anode material in run 39 was shown to be entirely NiO. The anode material for run 40 was shown to be a mixture of Ni, NiO, and Ni_3S_2. The difference between run 39 and run 40 with respect to the anode was that run 39 removed CO_2 through the carbonate transport reaction:

$$CO_3^{2-} \rightarrow CO_2 + \frac{1}{2}O_2 + 2e^- \qquad (10)$$

O_2 from this reaction would have served to oxidize the initially Ni anode into NiO. In run 40, however, selective removal of H_2S was observed. NiO was present in the anode of run 40 to a lesser extent than run 39, and the presence of Ni_3S_2 is due to transported sulfide/sulfur.

The electrodes used in run 43 started as lithiated NiO. After 222 hours of operation, the cathode was shown to be a mixture of Ni, NiO, and Ni_3S_2, supporting the results obtained in run 39 even though the starting material was NiO rather than Ni. The anode of run 43 started out as pure NiO and remained unchanged even after 222 hours of operation.

X-ray diffraction of the materials used in the coal gas polishing application also showed primarily Ni and NiO with traces of Ni_3S_2 in the electrode materials. Run 49 started with NiO as both the cathode and anode material. After 216 hours of operation, the cathode was entirely Ni. The anode was a mixture of Ni, NiO, and Ni_3S_2.

Further investigation revealed H_2S levels in the coal gasification stream above 100 ppm created a molten electrode material of form Ni_3S_2 . This caused the reaction sites for the reduction of H_2S to diminish completely nullifying the E.M.S. removal capabilities. Alternate cathode materials must be utilized with coal gas streams containing higher than 100 ppm H_2S. Cobalt is the predominent candidate due to previous success in full-cell experiments.

Anode materials which were stable in the oxidizing enviroment of the anode side of the process cell were developed and tested. Ni-O-S and Co-S anode materials allowed operation of the cell with suffi(+(% *25^I^\ nt flux to accomidate the required H_2S removal rates while allowing the cross-cell potenital to remain low enough so that CO_3^{2-} was not preferentially transported across the cell.

Various candidate electrode materials have been tested and compared on the basis of physical and chemical stability, electrical conductivity, and electrochemical performance in an operating cell.

Electrolyte

The composition of the electrolyte present in the membrane of the cell reaches an equilibrium sulfide level based on the following reaction:

$$(Li_{0.62}K_{0.38})_2CO_3 + H_2S <=> (Li_{0.62}K_{0.38})_2S + CO_2 + H_2O \qquad (16)$$

Theoretical compositions are calculated through an analysis of the Gibb's free energy of this reaction yielding the equilibrium constant by:

$$\ln K_a = - \Delta G/RT \qquad (17)$$

with K_a defined as:

$$K_a = P_{CO2}\, P_{H2O}\, a_{M2S} \,/\, P_{H2S}\, a_{M2CO3} \qquad (18)$$

If the activity coefficients of the molten phase constituents (namely the sulfide and carbonate in the electrolyte) are assumed to be unity, then equation (18) becomes:

$$K_a = P_{CO2}\, P_{H2O}\, X_{M2S} \,/\, P_{H2S}\, X_{M2CO3} \qquad (29)$$

with X_{M2S} and X_{M2CO3} defined as the mole fractions of sulfide and carbonate present in the melt such that:

$$X_{M2S} + X_{M2CO3} = 1 \qquad (30)$$

Actual compositions are measured by gravimetric analysis of total sulfur species present after oxidation with hydrogen peroxide. A sample of membrane material is weighed and then dissolved in water. The insoluble matrix materials are filtered and the filtrate is treated with excess hydrogen peroxide which oxidizes all sulfur species to sulfate. It is assumed that only sulfur in the form of sulfide is present in the membrane under run conditions. This solution is then acidified with hydrochloric acid to decompose the carbonate to carbon dioxide and water. The solution is boiled to de-gas the mixture and then barium chloride is added, causing the sulfate to precipitate as barium sulfate. The solution is then filtered, and the precipitate is rinsed, ignited, and weighed. The moles of barium sulfate precipitated is directly related to the moles of sulfide in the electrolyte.

Since the mass of the original sample is known, and the mass of the insolubles is known, then the mass of the soluble electrolyte present in the sample is known by difference. It is assumed that carbonate and sulfide species are the only components of

the electrolyte, thus, the moles of carbonate is related to the moles of sulfide by equation (30). The results of this analysis are presented in Figure 3 for runs 37 through 40. Examination of this data shows that the equilibrium composition of the electrolyte can be closely approximated by the above analysis. The method is subject to a degree of experimental error, and this is shown in the variations between the theoretical and actual results. Still, the method does confirm the assumption of unity activity coefficients of the sulfide and carbonate species in the electrolyte melt.

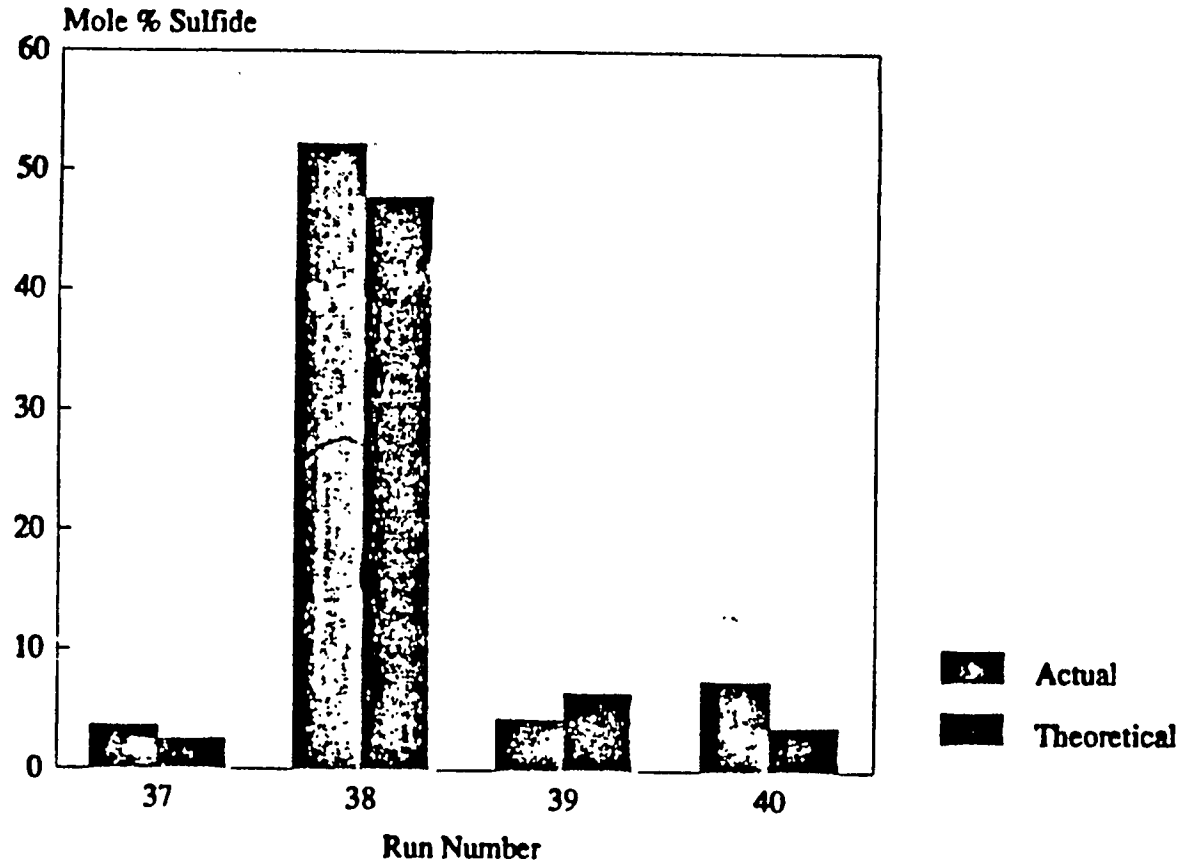

Figure 3 Electrolyte Composition (Actual vs Theorectical Sulfide)

Electrode Analysis: Electrode analysis consists of three phases: (1) solubles analysis, (2) insolubles analysis, and (3) bulk structure analysis. Each phase of the overall electrode analysis proceeds in the following manner.

Solubles Analysis

This phase proceeds in a manner very similar to the technique outlined above for membrane electrolyte analysis. First, the electrode sample is ground and weighed. It is then washed in a water bath where the soluble components are dissolved. The soluble components consist primarily of electrolyte salts which have wicked into the pores of the electrode structure. There may also be some soluble electrode materials in the form of metal sulfates. Dissolved metal sulfates can be tested for by atomic absorption, and access to this test method is currently being arranged. An attempt has also been made at determining the amount of dissolved metal sulfates by precipitation as metal hydroxides but the presence of barium and lithium in the final filtrate solution makes this method questionable as these metal hydroxide species are also insoluble. The results of this testing are discussed for certain experimental runs in the results section of this report.

Insolubles Analysis

This phase of electrode analysis is performed using x-ray diffraction. The results of this testing are discussed for certain experimental runs in the results section of this report.

Bulk Structure Analysis

This phase of electrode analysis is performed using scanning electron microscopy (SEM) techniques. The results of this testing are used intermitently to insure the integrity of materials for the E.M.S.; however, due to the quality of photo-copied S.E.M. pictures inclusion is not possible.

Matrix

Perhaps the most important issue facing the E.M.S. is finding an adequate membrane material. A suitable matrix material must meet three criteria (1) be chemically and electrically stable in the E.M.S. environment, (2) provide a consistent pathway for ionic transfer (small pores to maintain complete electrolyte flooding of the matrix material while wetting the electrode pores with electroyte), and (3) provide a barrier against process gas cross-over from the cathode side of the cell to the anode side in order to deter alternate reactions. Several materials have been invetsigated including MgO, $LiAlO_2$, and yttria-stabilized zirconia.

MCFC membranes: Early experiments used Molten Carbonate Fuel Cell(MCFC) membranes (eutectic Li/K carbonate electrolyte hot pressed within a $LiAlO_2$ matrix in approximately a 50/50 weight ratio) which were donated by GRI. These membranes were placed in the cell and allowed to go to their equilibrium sulfide levels in-situ. Successful H_2S removal has been recorded with the natural gas sweetening applications; therefore application in run 42 for natural gas experimentation utilized this membrane

successfully as shown in Figure 10. Also a GRI membrane with sufficient Li_2S sprinkled onto the membrane to bring it to its equilibrium sulfide level after the electrolyte had melted was successfully used with the coal gas polishing application in run 58, shown in Figure 22.

Density changes inherent with in-situ sulfiding of an initially carbonate electrolyte caused cracks within these membranes after a few hours of operation. The only exception to this was run 42. Since this was a natural gas polishing application, the equilibrium sulfide level was low enough that density change stress within the electrolyte did not appear to damage the membrane. Use of these membranes was discontinued in favor of manufacturing techniques which allowed customization of the electrolyte composition and improved matrix structure capable of handling more thermal and mechanical stress.

Hot Pressing: Several methods for the manufacture of the electrolyte membrane were developed and tested. Previously 'hot-pressing' was used in which powders of matrix material and electrolyte are intimately mixed in a dry atmosphere. They are then measured into a die and pressed into a tile at 5000 psi or greater pressure, 5°C or so below the electrolyte melting point. In the case of the sulfide/carbonate membranes, this temperture is determined from the phase diagram of Babcock[17]. This technique was used with success with application to the natural gas sweetening process. Since the membrane must be able to prevent bulk H_2 cross-over from the cathode to the anode side in order to selectively remove H_2S from the process gas, the technique was

abandoned since it was very difficult to manufacture a membrane without micro-cracks inherent in the structure. The technique involves two thermal cycles (heat-up to press the structure, cool down to release the structure, and heat-up within the cell housings), a sever mechanical shock (removing the heated piston from the die after pressing at elevated temperature), and a single handling step (cleaning the Graphite Foil, used as a die release material to prevent the membrane from bonding to the steel die, from the membrane surfaces) before the membrane can be used. Completely selective removal of H_2S from the process gas stream could not be achieved with this technique.

Sintered Ceramic Matrix: The second technique previously used involves the manufacture of a partially sintered ceramic matrix without electrolyte present and then wicking the molten electrolyte into the matrix voids by capillary action. This created a ceramic matrix with more structural integrity than the hot-pressed structures since the ceramic particles were actually bonded together to form a porous structure. The electrolyte flooded the pores and channels within this structure. This technique was used successfully with natural gas sweetening. Sulfur recovery in the anode sweep tubes was recorded in several experiments.

While the process selectivity was improved over the GRI membranes and the hot-pressed membranes, the membranes were still suseptable to thermal and mechanical stress during manufacture and cell operation. After the partially sintered body was formed, the membrane had to undergo thermal cycle as the electrolyte was melted into the structure and another as the cell was heated to its run temperature. The membrane

was mechanically stressed during handling between the processing steps. This membrane was also sensitive to density changes within the electrolyte. Equilibrium level sulfide electrolyte was wicked into the structures used in several runs under a N_2 blanket to relieve electrolyte density change stress on the membrane.

Zirconia Mats: The third technique recently used involved utilizing woven ZrO_2 textiles purchased from Zircar, Inc. These were pre-made woven ceramic fiber textiles made of Y_2O_3 stabilized ZrO_2. Woven cloth of 30 mil and 15 mil thickness was purchased and used as a matrix material by wicking molten electrolyte into the structure in-situ. This technique was used successfully with natural gas sweetening application and natural gas polishing application.

The average pore size of the zirconia textile structure has a bimodal distribution around 10 μm and 70 μm. While the structure had the ability to withstand thermal and mechanical stresses, the open aspect of the matrix (83% voids) allowed enough H_2 cross-over to keep selectivity low. The situation was improved somewhat when equilibrium level electrolyte was used or when the equilibrium sulfide level was low since the matrix did not have to contend with density stresses within the electrolyte. A denser structure was needed to hold the electrolyte and prevent gas cross-over.

Tape-casting: The fourth technique for membrane manufacture utilized tape-casting technology. By this method, the matrix material, dispersed along with an organic binder in a liquid, was formed into a dried tape along a glass substrate, maintained at

constant thickness by an overhead bird bar. The solvents from the slurry were then dried out and the ceramic/organic tape was the peeled off the surface of the substrate. The flexible 'green' tape was cut to the desired size and laminated under pressure with another flexible 'green' tape of ceramic material until the desired membrane thickness was achieved. The binders are then volatilized out in the process cell in an inert atmosphere or burned out of the cell under pure O_2 and the electrolyte was allowed to soak into the intersitial voids of the matrix powders, forming a membrane 'paste' between the gas diffusion electrodes.

The best results from tape casting were obtained using 'packaged' organic binder/solvent solutions purchased from Metoramics, Inc. By trial and error, the optimum ceramic/binder ratio for tape casting MgO within an their acrylic binder system K565-4 (the exact nature of the polymer is proprietory to Metoramics) was found to be 16.5 wt% MgO (Fisher, 325 mesh). This made a 'green' tape that was 44.4 wt% MgO (18.2 vol%) after solvent evaporation.

This technique for membrane manufacture was used successfully in run 43. Other unsuccessful experimental runs were attempted. After binder burn-out, the membrane was just a layer of powder with no structural integrety at all. The addition of electrolyte turned these powders into an electrolyte paste between the electrodes. As long as there was no gap between the electrode and the edge of the electrode well, tape casting worked well. However, the nature of the bench scale apparatus made it difficult to insure that there was no gaps anywhere around the circumference of the electrode (a perfect fit was required). In order to prevent the Ni/NiO electrodes from warping as

they went to their equilibrium structures, some gap between the electrode edge and the housing well was required. Tape cast membranes would fail at these gaps and allow bulk mixing of the process streams.

In answer to the need for a dense powder membrane with structural integrety, the fourth technique developed for membrane manufacture uses a composite structure in which a mat of woven yttria stabilized zirconia cloth with tape cast MgO 'bubble barriers' on each side of the membrane after the method of Iacovangelo and Karas[18]. The bubble pressure barrier concept provides a layered structure, with two tight matrix layeres on each side of a more open matrix layer. Any gas cross-over would have to find a single path through all three electrolyte filled matrix layers.

Using this concept, tape cast MgO was layered with zirconia cloth to operate successfully in runs 38 and 40 in the natural gas polishing application. Runs 49 and 57 successfully used this layered structure in coal gas polishing application of this technology.

Densified Zirconia: The fifth an final technique for membrane manufacture that was attempted came from the need to have an extremely dense ceramic membrane that still had enough structural integrety to withstand the thermal and mechanical stresses inherent in our experimental apparatus (an ultimately future industrial application). Zirconia cloth was densified with an inert ceramic powder (MgO, ZrO_2, or $LiAlO_2$) by suspending the powders in a slurry with ethanol and then soaking the mat in the slurry while pulling a vacuum on the vessel containing the mat and slurry. This vacuum de-

airs the voids of the mat and aids in the wetting of the woven material with the ceramic slurry. Zircar, Inc., had used similar techniques to create ceramic gas diaphrams with an average pore size of only 0.03 μm[19]. Such a structure would be dense enough to prevent the bulk diffusion of gases through the membrane and both strong and flexible enough to withstand localized density changes in the electrolyte due to carbonate/sulfide equilibrium shifts.

Membranes of this nature were used with success in run 59 (densified with 325 mesh $LiAlO_2$ from Aldrich), 60 (densified with sub-micron ZrO_2 from Zircar), 62 (densified with ZrO_2), and 65 (densifided with ZrO_2) in application of this technology to coal gas polishing.

FULL CELL TESTING

The following is a compilation of the most outstanding experiments done during the funding period. These are based on high removal of H_2S, low polarization, and low carbonate transport compared to sulfide transport. Other runs are entered to give a more detailed analysis of material issues and the thought process in determining the best possible E.M.S. set-up.

Run 38

This experimental run was the second polishing application run and used three mats of ZYW-30A zirconia cloth layered with three cast tapes of MgO ceramic as a membrane material. The MgO was present as a densifier for the membrane matrix to

prevent H_2 cross-over and subsequent transport of CO_2 across the cell. The electrolyte was lithium/potassium carbonate eutectic and was layered into the membrane during set-up. Both the cathode and the anode in this experiment were CoS_2.

A nitrogen sweep was applied to both sides of the cell and the cell was loaded into the furnace for heat-up. The binder from the MgO tapes was volatilized out at 375°C overnight. The pressure on the pneumatic ram was only 2.5 psi during volatilization and was increased to 5 psi once run temperature was reached.

Examination of the data presented in Figure 4 shows that the densification of the matrix appears to have worked. Completely selective removal of H_2S from the process gas was achieved. The overpotential data presented in Figure 5 shows that the 1 volt cross-cell potential threshold was never crossed during the period of time that this data was taken. No elemental sulfur was collected; since the concentration of H_2S was so low, a negligible amount of sulfur would have been produced. The cell ran for 130 hours and was shut down due to break-down of the anode, probably due to the slow oxidation of CoS_2 at higher potentials. With transport of CO_2 at higher potentials, O_2 would also have been produced, reacting with the CoS_2 to form cobalt oxide species and sulfur dioxide. Since cobalt oxide is not conductive, this would have driven the anodic overpotential higher and thus made the situation worse, increasing the rate of cobalt oxidation. This situation was observed, with rapid decay of the cobalt disulfide anode once CO_2 transport started and a possible sulfur dioxide peak appearing in the anode sweep gas chromatograph (the signal was retained too long in the column to have been H_2S or COS).

An analysis of the membrane electrolyte from this run showed a sulfide level of 52.2 mole% and a carbonate level of 47.8 mole% (see Figure 3) with 58.2 wt% insolubles. This compares with theoretical values of 45.7 mole% sulfide and 54.3 mole% carbonate (in equilibrium with 0.963% CO_2, 0.212% H_2S, and 3.2% H_2O). Dissolved $CoSO_4$ was subtracted from the total sulfur results by precipitating Co from the filtrate.

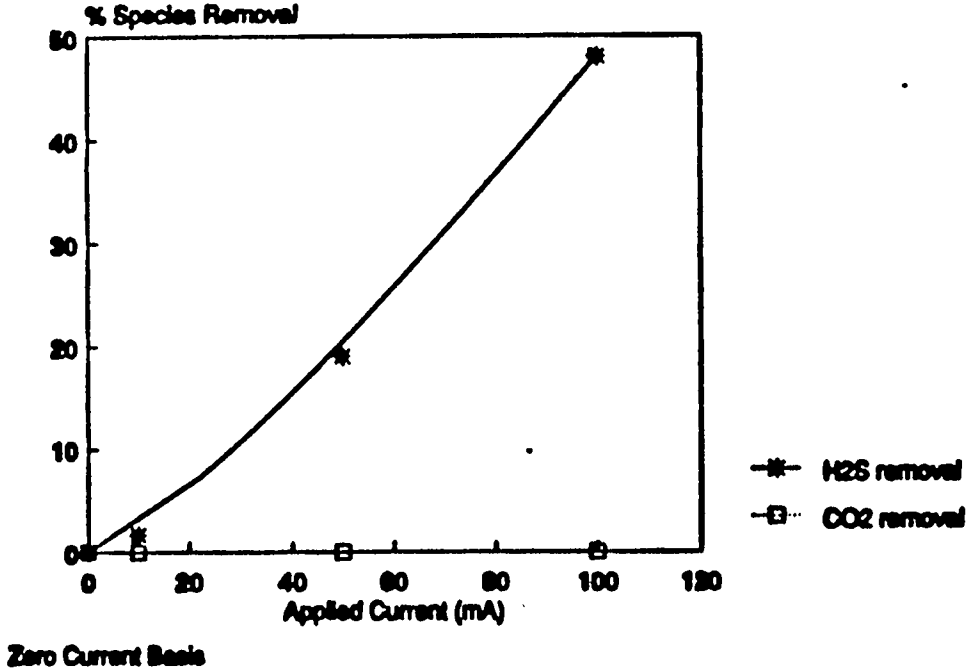

Figure 4 Run 38: Species Removal vs Applied Current

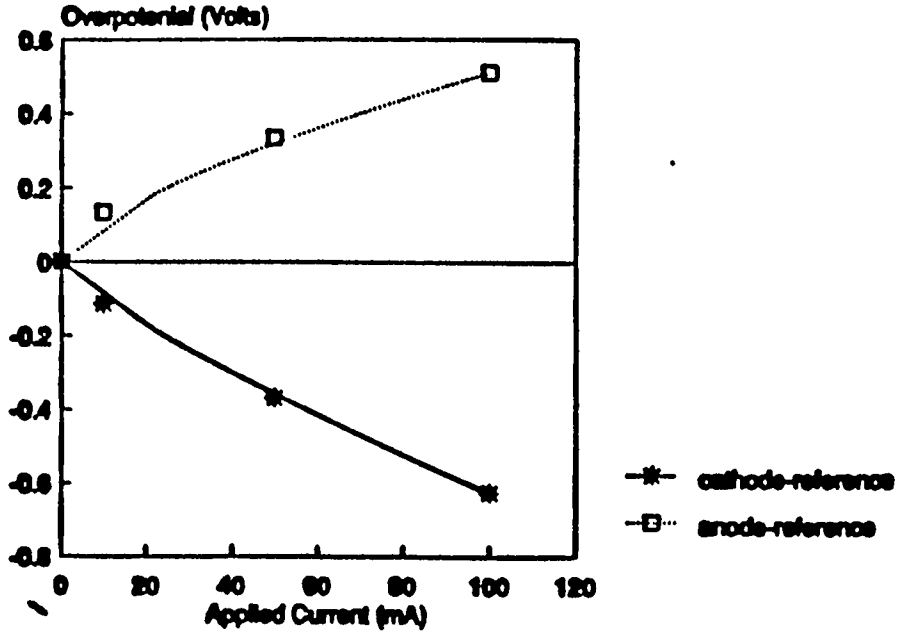

Figure 5 Run 38: Overpotential vs Applied Current

The composition of the Co precipitate from run 38 was verified by ashing to Co_2O_4. The Co precipitates (assumed to be $Co_2O_3*3H_2O$) were taken and ashed at a temperature of 850° C. This resulted in a black-purple substance with a recorded weight change which corresponded closely to the predicted change for $Co_2O_3*3H_2O$ going to Co_2O_4.

Run 40

This experimental run used a layered membrane structure similar to that used by run 38, except that the layers of ZYW-30A were contacting the wet seal areas instead of the cast MgO tape. Aluminum foil gaskets were also cut and laid into the wet seal area between the membrane and the MACOR housings. This was done in an attempt to improve the wet seal of the cell by intimately binding the membrane structure to the MACOR housings with a layer of $LiAlO_2$ formed in-situ. During heat-up to run temperature, the aluminum was converted to Al_2O_3 and then to $LiAlO_2$ through a subsequent reaction with Li_2CO_3:

$$Li_2CO_3 + Al_2O_3 <=> 2LiAlO_2 + CO_2 \qquad (31)$$

This run used carbon at the cathode and Ni (converted to NiO in-situ) at the anode. The choice of carbon was made in an attempt to isolate electrochemical H_2S removal by working around the "sulfide sink" presented by allowing an Ni electrode form metal sulfide species in-situ. The process gas for this run had a composition of 98 ppm H_2S, 1.45% CO_2, 3.9% H_2O, and balance CH_4.

Initially, cell seals were excellent. No cell cross-flow was detected and the cell was capable of pushing several inches of water back pressure. However, approximately 23 hours into the run a malfunction in the temperature controller allowed the cell to cool off to room temperature. N_2 was started to both cathode and anode sides of the cell as soon as the fault was detected and the controller was repaired. Unfortunately, the membrane was slightly damaged during the cool-down from run temperature. The $LiAlO_2$ gaskets lost integrity and began to leak. Cathode side to anode side bulk cross-flow was also detected. Current collector / electrode / membrane contact was also damaged as cross-cell resistances went from 0.9Ω to 4.0Ω. The cell would still pass current however, and cross-flow could be limited to cathode to anode side flow by decreasing the anode sweep flow rate. H_2S levels in the process gas were brought as low as 2 ppm (below GC analytical limits) (see Figure 6) over the course of the run with application of as little as 5 mA (cathode flow rate = 450 cc/min) with cross-cell potentials of only around 0.8 volts (see Figure 7) and no detectable CO_2 removal.

After 135 hours of operation, the cell was shut down for post-mortem analysis. The carbon cathode, while still operational, had degraded and was showing obvious signs of H_2O vapor erosion. The current collector on the anode side had also dissolved which explained the poor performance of the anode late in the run. A yellow tint was observed covering an area on the anode side wet seal were the seal had failed and was allowing sweep gas to be blown into the furnace.

Post-mortem analysis of the membrane showed an actual sulfide level of 7.5 mole% and a carbonate level of 92.3 mole% with 60.1 wt% insolubles present.

Theoretical analysis predicted a sulfide level of 3.7 mole% and a carbonate level of 96.3 mole%(see Figure 3).

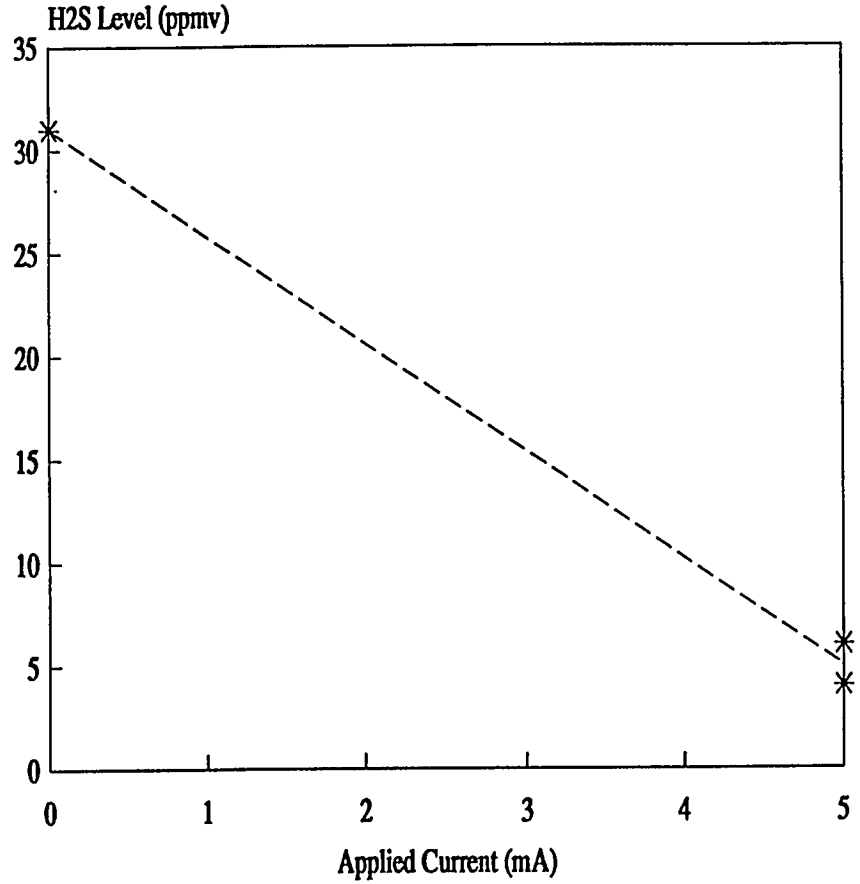

Inlet: 98 ppmv H2S
Cathode Flow = 225 cc/min

Figure 6 Run 40: Species Removal vs Applied Current

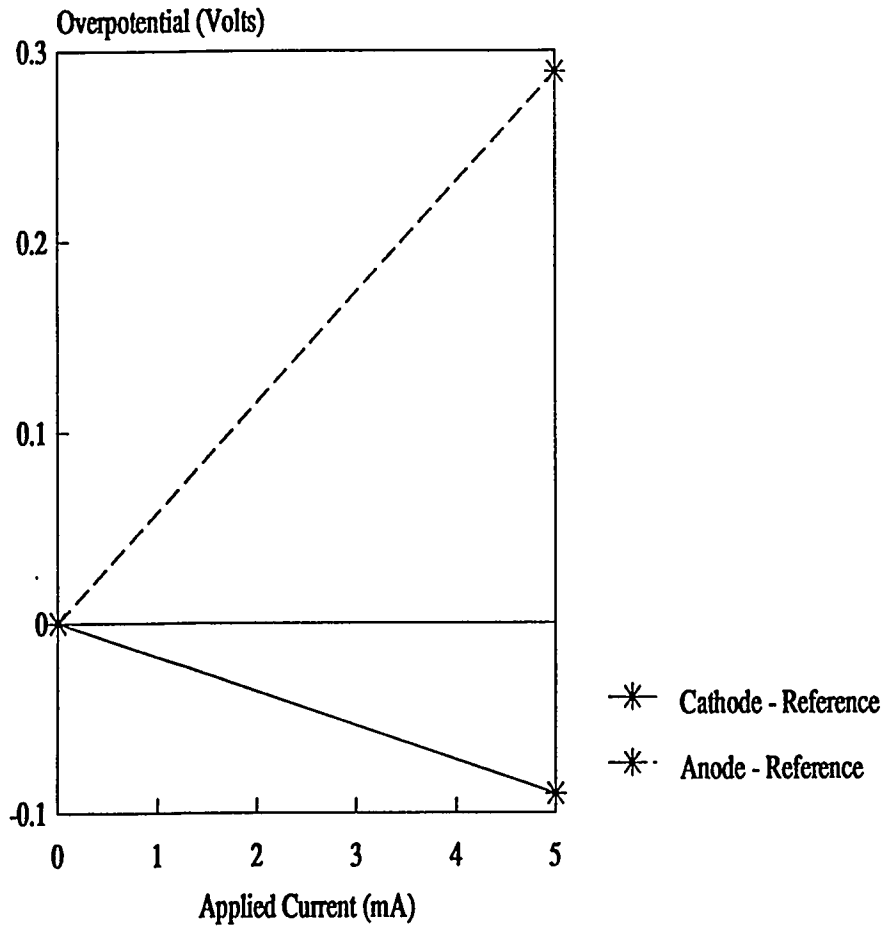

Figure 7 Run 40: Overpotential vs Applied Current

An analysis of the anode showed that the structure was only 62.9% flooded. The electrolyte which was wetting the pores of the electrode had an approximate composition of 4.8 mole% sulfide and 95.2 mole% carbonate. An analysis for dissolved $NiSO_4$ was not performed. Examination of the x-ray data presented in Figure 8 shows that the primary insoluble species are Ni and NiO, as expected in this run environment. However, when the scale is decreased as in Figure 9, Ni_3S_2 is seen to be present.

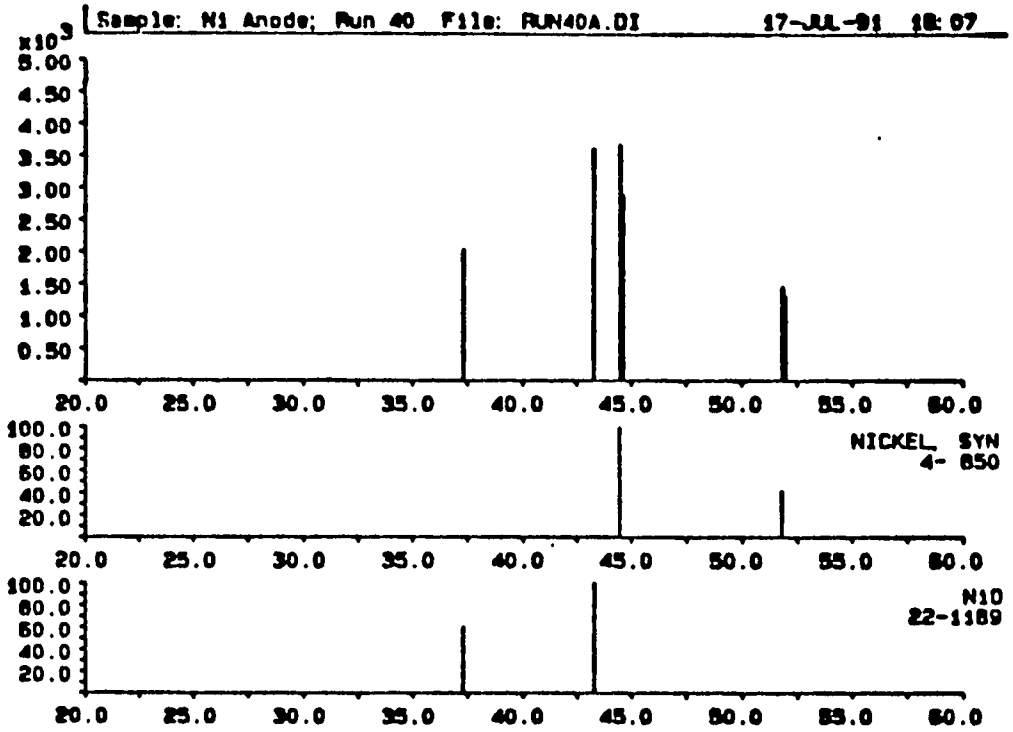

Figure 8 Run 40: Anode X-Ray Diffraction Pattern

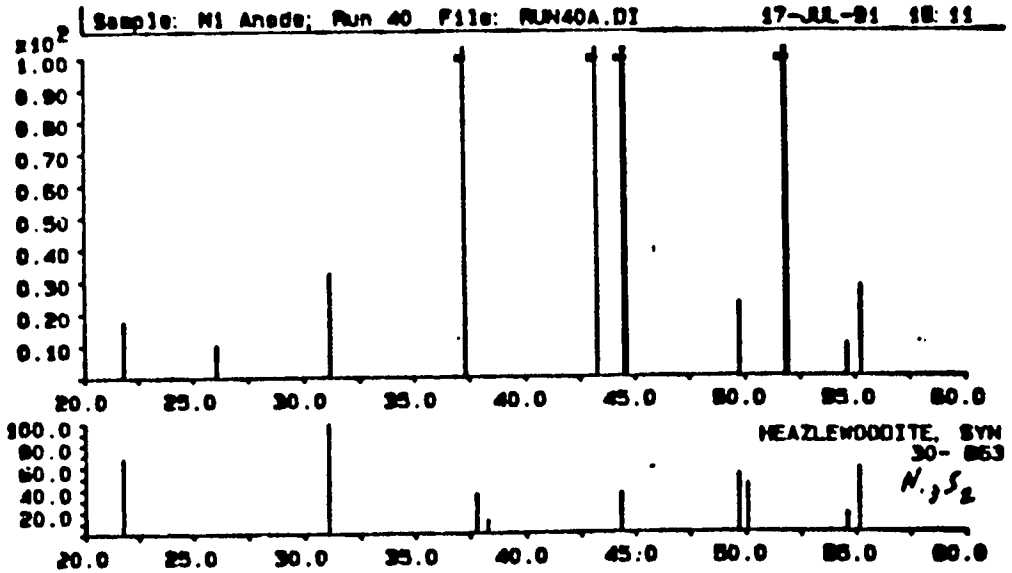

Figure 9 Run 40: Anode X-Ray Diffraction Patterns (Detail)

Run 42

This attempt at using MCFC tiles as membrane materials was more successful. Once again, the tile had $LiAlO_2$ as the matrix material with eutectic composition Li_2CO_3 and K_2CO_3 as the electrolyte. The cathode was carbon and the anode was lithiated NiO. Carbon was used as the cathode material in an atempt to eliminate the sulfide capacitance effects as Ni is converted to NiS or Ni_3S_2 (as in Run 40). The NiO anode was manufactured by soaking Ni electrode material from ERC in 1M LiOH and then heating to 650°C overnight. Weight analysis of the resulting electrode showed greater than 98% conversion of Ni to NiO. The process gas for this run, a simulated natural gas, had a composition of 1.44% CO_2, 97 ppm H_2S, 4.4% H_2O, and the balance CH_4.

Completely selective removals of H_2S as high as 98% (97 ppm down to less than 2 ppm) were observed with negligible cross-cell potential and 2.5 mA applied to the cell (0.32 mA/cm^2) at a process flow rate of 200 cc/min. This corresponds to 98% current efficiency. At higher process flow rates 75.2% removal of H_2S (97 ppm down to 24 ppm) with 5 mA applied to the cell (current density of .64 mA/cm^2) and a process flow rate of 450 cc/min was observed. This current density should have given 88% removal. This corresponds to a current efficiency of 85%. Figure 10 shows the H_2S removal vs applied current.

An analysis of the electrolyte from this run showed the sulfide level at 6.7% and the carbonate level at 93.3%. This corresponds to predicted values of 2.8% sulfide and 97.2% carbonate. This discrepancy between the predicted values and the actual values can be explained by the presence of an unknown slag found in the crucible after ashing

to recover the $BaSO_4$; the $BaSO_4$ precipitate was not adequately washed during the filtering process. X-ray analysis of the membrane material shows only $LiAlO_2$ and the hydrated forms $LiOH*2Al(OH)_3*xH_2O$ and $Li_2Al_2O_4*xH_2O$ present. Evidently, the low sulfide levels were not sufficient to cause attack of the $LiAlO_2$ matrix. The hydrated species of $LiAlO_2$ were no doubt formed when the membrane material was washed overnight in water to dissolve the electrolyte species out of the matrix. X-ray analysis results are presented graphically in Figure 11.

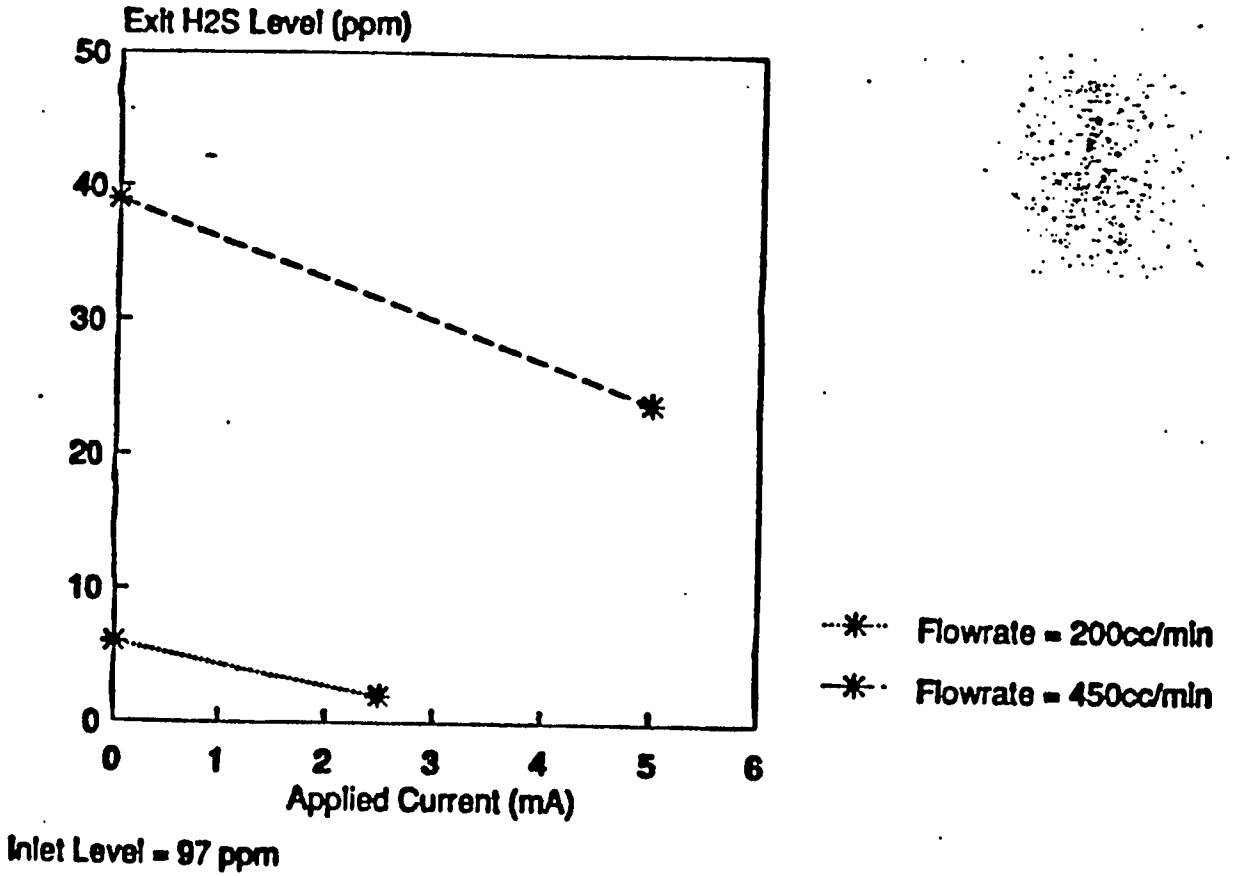

Figure 10 Run 42: H_2S Level vs Applied Current

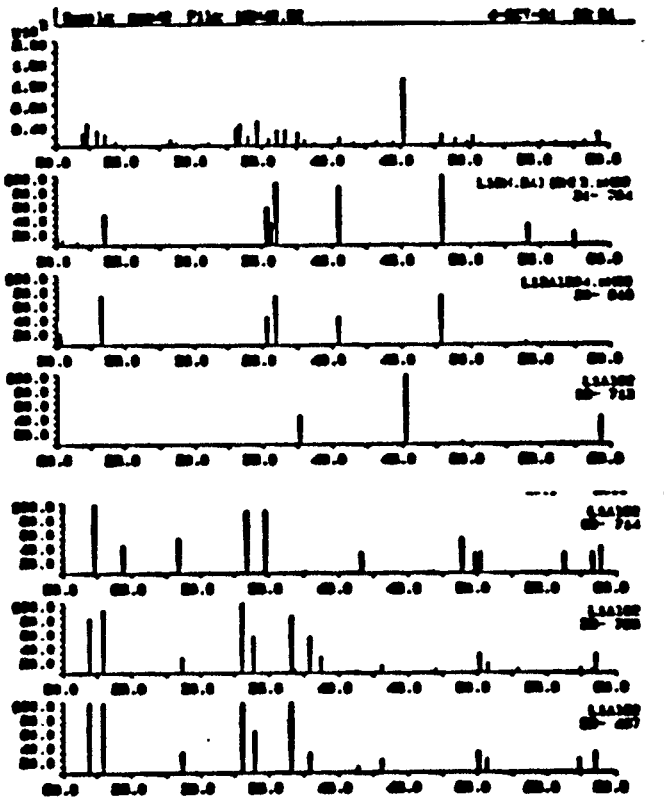

Figure 11 Run 42: Membrane Matrix X-Ray Diffraction Pattern

Run 43

This experimental run was the first successful run which used a completely tape cast membrane MgO matrix. The electrolyte was eutectic potassium/lithium carbonate which was added after the binder material was burned out. Both the cathode and the anode in this experiment started out as lithiated NiO. The process gas for this experiment started out as 1.4% CO_2, 3.9% H_2O, balance methane. Later in the run, 1.38% CO_2, 92 ppm H_2S, 3.9% H_2O, balance methane was used.

The ceramic membrane was manufactured by mixing 16.5 grams MgO, 83.3 grams Metoramics K565-4 Acrylic Binder System (24.9 wt% acrylic polymer), 1 gm Metoramics M-1111 releasing agent, and 1 gm Metoramics M-1114 surfactant. The exact composition of these tape casting agents are proprietary to Metoramics. These were mixed in a ball mill overnight and poured out onto M-1111 coated glass. Air drafts across the surface of the cast were prevented by placing a cardboard sheet over the cast with a 4mm thick spacing between the surface of the cast and the cardboard sheet. This allowed uniform evaporation of the solvents from the cast since the convective effects of room air were minimized. The resulting tape was 42.1 wt% MgO with the remainder acrylic binders. When the binders were burned away, this corresponded to 88.1 vol% free volume.

Three inch diameter, 0.5mm thick membranes were cut from the tape and three of these were layered in the cell. Pure O_2 was blown across the cathode and anode sides of the cell and the assembly was heated to 375°C overnight. The next day, after smoking from the burning binder material was no longer observed, fuel gas (1.40 % CO_2, 3.9% H_2O, balance CH_4) was started to the cathode side of the cell and N_2 was started to the

anode. Electrolyte was added, 20.8 grams, through the reference electrode hole in the top of the cell assembly. Only 17.3 grams were required based on the free volume of the membrane, but more was added to compensate for electrode wetting, wet seal formation with the MACOR housings, and spillage during the adding process.

Upon adding electrolyte to the cell, cross-cell resistance dropped from infinite to 0.35 ohms. Initial tests of the cell performance were centered around CO_2 transport. With applied currents of 400 mA (50.5 mA/cm^2) CO_2 levels dropped from 1.4% to 0.6% (57.1% removal). CO_2 removal data is presented in Figure 12. This corresponds to a current efficiency of only 52%. Since the cross-cell potential was stable at only -1.36 volts, an alternative current path was probably present. Since the CO_2 present in the anode corresponds to the CO_2 removed from the anode to within 75%, there must be transport present by a species that we are not presently analyzing for. This may possibly be explained by the following mechanism:

Cathode:
$$H_2O + Ni \Rightarrow NiO + H_2 \quad (32)$$
$$NiO + 2e^- \Rightarrow Ni + O^{2-} \quad (33)$$

Overall Cathode:
$$H_2O + 2e^- \Rightarrow H_2 + O^{2-} \quad (34)$$

Anode:
$$O^{2-} \Rightarrow 1/2O_2 + 2e^- \quad (35)$$

These two half cell reactions sum to the same overall cell reaction as that for carbonate transport:

$$H_2O \Rightarrow H_2 + 1/2O_2 \quad (36)$$

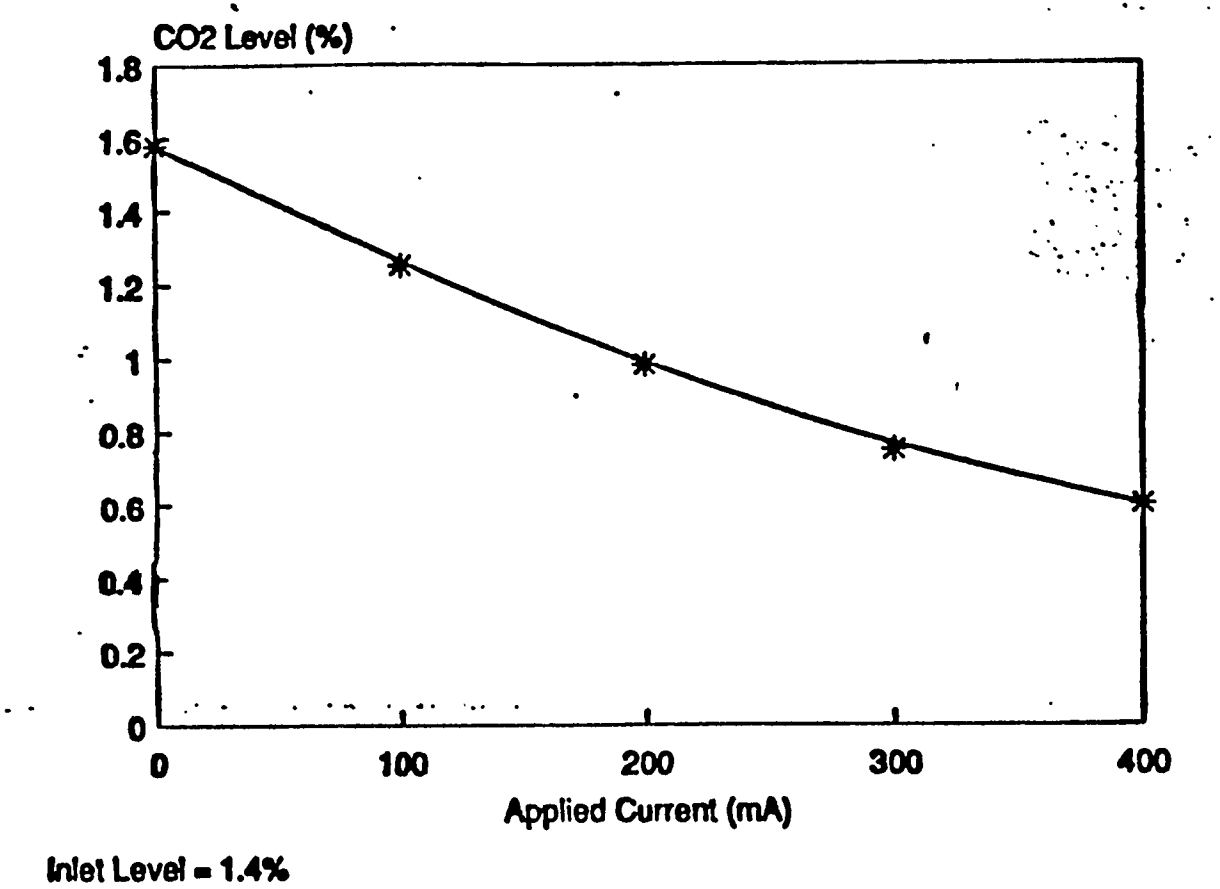

Figure 12 Run 43: CO_2 Level vs Applied Current

The only question is that the O^{2-} ion is highly basic and should react with CO_2 to form CO_3^{2-}. If this were the case, CO_2 would be removed in amounts closer to stoichiometric. This has not been observed. Possible explanations for this lack of CO_2 transport is that the reduction of NiO to Ni in equation (4) takes place below the electrode/electrolyte interface and thus the O^{2-} ion is not exposed to sufficient CO_2 to form appreciable quantities of CO_3^{2-}. Thermodynamic analysis shows that reaction (4) takes place at a standard potential of only -1.596 volts with respect to the O_2/CO_2 reference electrode. Reaction (6) takes place at a standard potential of only 0.773 Volts with respect to the reference electrode (around the same potential as the oxidation of sulfide). Thus the electrochemical potentials for the above mechanism are on the proper order of magnitude.

H_2S was then fed into the system gas by bleeding in a contaminated gas stream to obtain a final gas composition of 1.38% CO_2, 92 ppm H_2S, 3.9% H_2O, and the balance CH_4. Removal was demonstrated to a level of less than 2 ppm with an applied current of 5 mA (current density of 0.63 mA/cm^2) and a process stream flowrate of 415 cc/min. H_2S removal data is presented in Figure 13. This corresponds to 100% current efficiency. It should be noted that nearly 5 days exposure to the H_2S contaminated stream was required to sufficiently sulfide the electrolyte so that any effect with current at all could be seen; current was applied for 24 hours before a sufficient sulfide gradient within the membrane was established to bring cathode process gas concentrations below 2 ppm. At these gas phase concentration levels, the equilibrium sulfide concentration of the

membrane is very slow to be reached as the molar flowrate of sulfide in the gas phase is very small. Cross-cell potentials hovered around -0.650 Volts.

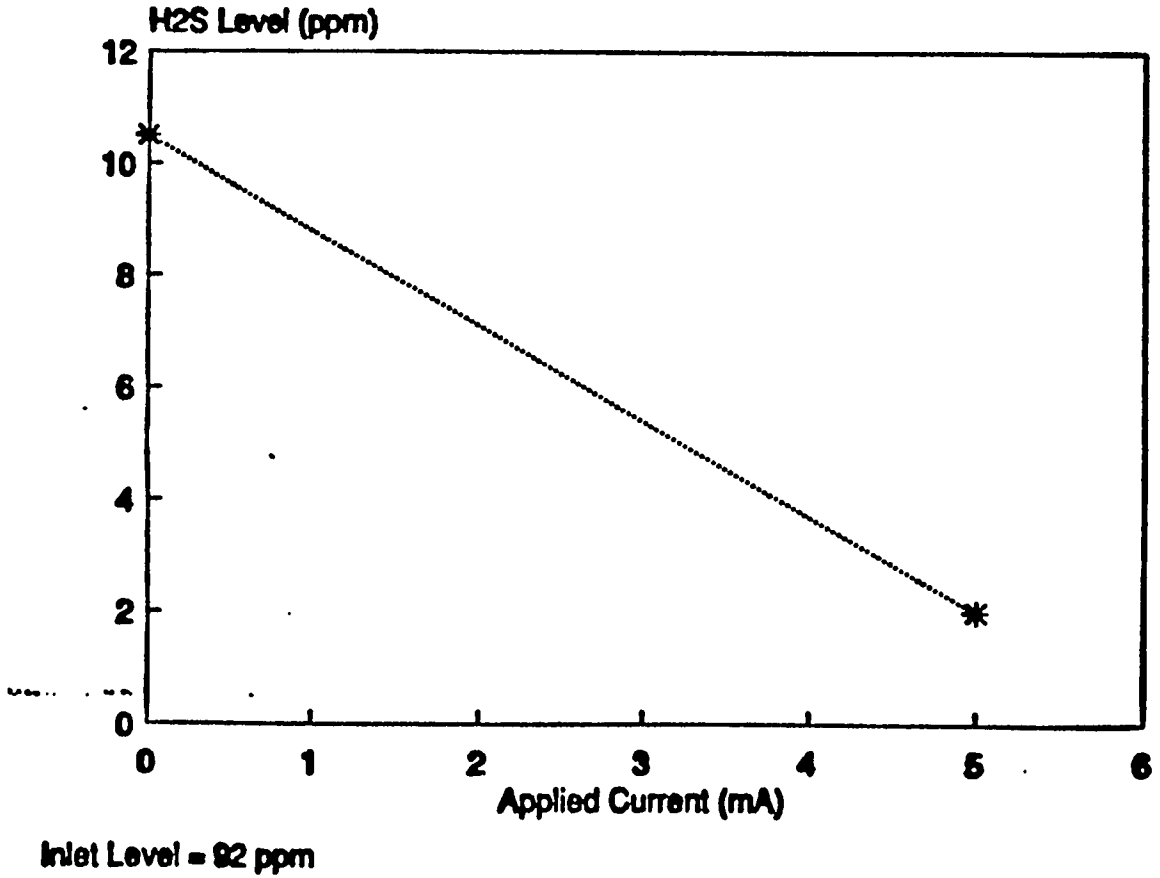

Figure 13 Run 43: H_2S Level vs Applied Current

The cell was shut down after 222 hours of operation when gas supplies ran out. X-ray analysis of the electrode materials showed that the cathode was a mixture of Ni, NiO, Ni_3S_2, and NiS. Cathode X-ray data is presented in Figure 14. The presence of both Ni and NiO in the cathode suggests possible support for the above current transport mechanism through the O^{2-} ion at higher cross-cell potentials. The anode was almost entirely NiO with some traces of Ni present. X-ray data for the anode is presented in Figure 15. Post-run examination of the anode exit gas-flow tube showed a brownish-yellow coating of the interior wall of the tube at a position just outside of the cell furnace. This is the location that condensing sulfur would be expected to collect. The coloration and location of this tube discoloration suggests that it is amorphous sulfur.

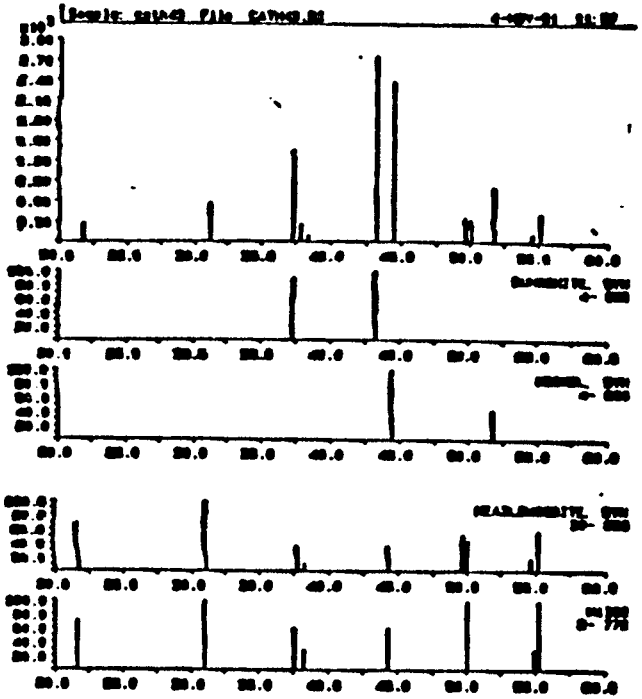

Figure 14 Run 43: Cathode X-Ray Diffraction Pattern

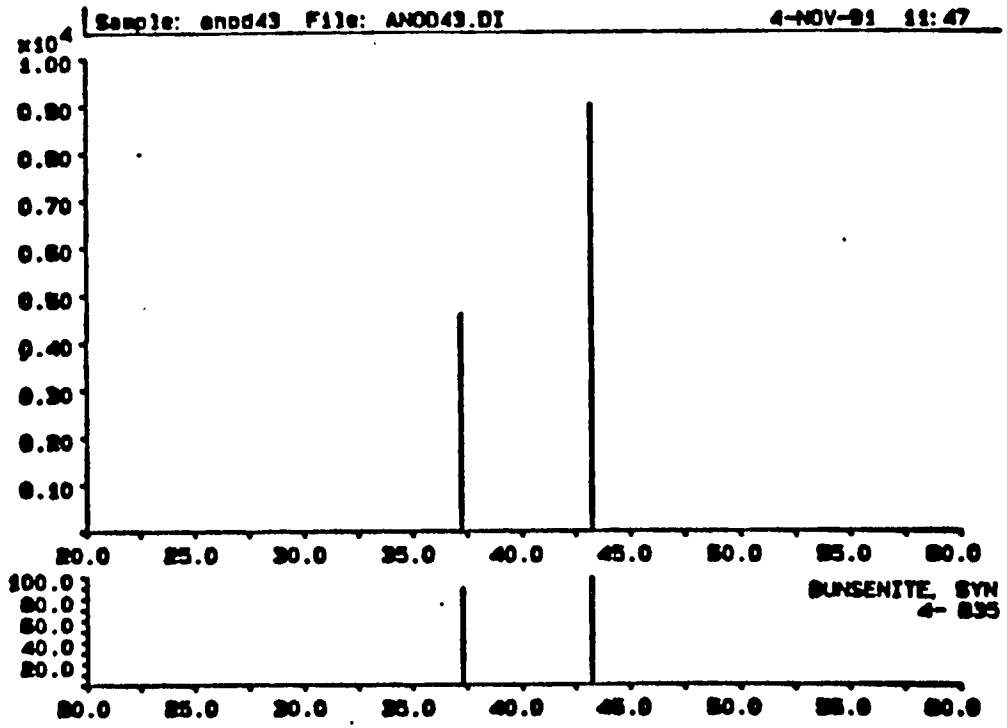

Figure 15 Run 43: Anode X-Ray Diffraction Pattern

Run 49

This was the fifth experimental run using coal gas. It used two tapes of MgO and one mat of zirconia cloth as the membrane matrix material. The electrodes were both lithiated NiO. The acrylic binders in the tapes of MgO were burned out under an O_2 atmosphere and the Li/K eutectic-composition electrolyte was added with the cell at run temperature. MACOR machinable ceramic housings were used instead of stainless steel housings. The inlet gases were passed through a stainless steel shift reactor to allow then to come to their equilibrium composition before passing through the cell.

This experimental run was divided into three sections: the first confirmed ionic transport through the membrane by removal of CO_2 (and H_2O) from the syn-gas at 625°C (Run 49A), the second was an attempt at removal of H_2S from the syn-gas at 625°C (run 49B), and the third was an attempt at removal of H_2S from the syn-gas at 700°C (Run 49C). The results of these studies are presented below:

Run 49A

CO_2 removal from the process gas as a function of applied current was recorded and is presented in Table 2. Examination of this data shows that the removal of CO_2 from the cathode side of the cell and production of CO_2 at the anode side of the cell is stoichiometric across the range of applied currents examined.

Fuel gas flow was set at 75 cc/min and N_2 sweep was set at 63 cc/min. Seals were good and no cross-flow between the two process streams was observed.

Table II.
Run 49A Recorded Data.

Applied Current (mA)	Actual Cathode CO_2 Out	Calc. Cathode CO_2 Out	Actual Anode CO_2 Out	Calc. Anode CO_2 Out
0	17.8%	17.8%	0.0%	0.0%
100	16.8%	16.8%	1.8%	1.2%
200	15.8%	15.7%	2.8%	2.4%
300	15.2%	14.7%	3.8%	3.7%

This data shows that the cell was functioning properly with respect to ionic transport of carbonate through the electrolyte.

After 2.65 hours with current applied, cross-flow between the cathode and the anode was observed, indicating that the ceramic matrix was damaged. Over the next 13.25 hours, 10.5 grams of electrolyte were added to the cell in order to stop this cross-flow by flooding any matrix cracks with electrolyte. Cross-flow between the two process streams was stopped in this manner and H_2S removal with applied current was then examined.

Run 49B

After 22.3 hours exposure to fuel gas at 625°C, an exit H_2S composition of 27.7 ppm was recorded. A current of 5 mA was applied to the cell (0.63 mA/cm^2, superficial electrode area = 7.92 cm^2). After 27.7 hours with applied current, no significant removal of H_2S was observed. Examination of the limiting current densities at these run conditions shows that at 625°C the gas phase limiting current density is only 1.1 mA/cm^2

while the membrane limiting current density is only 1.4 mA/cm^2. This membrane limiting current density assumes as electrolyte diffusivity of 10^{-5} cm^2/sec. Once membrane porosity and tortuosity are taken into account, this estimate is in all probability too large. As an 'order-of-magnitude' estimate, however, it does show that the transport through the membrane is on the same order as the transport through the gas phase. It is probable that at these temperatures, the membrane cannot support the necessary flux of sulfide ion to significantly affect the exit H_2S concentration.

Run 49C

Cell temperature was increased to 700°C. At this temperature, analysis of limiting current densities within the system shows that the gas phase limiting current density is 1.15 mA/cm^2 while the membrane limiting current density is 3.29 mA/cm^2. This shows that even if the electrolyte diffusivity estimate is in error, the membrane flux is three times greater at this temperature than at 625°C. H_2S removal at a variety of flowrates was observed and is tabulated in Table 3. The overpotentials reported here have not been corrected for IR loss. The measured cross-cell resistance by current interrupt was observed to be only around 1Ω. With the maximum current applied to the cell only 20 mA, this corresponds to only 20 mV of ohmic loss. This is negligible compared to the overall cross-cell potential, which includes concentration effects, and potentials required to drive the electrochemical reactions.

Table III.
Run 49C Recorded Data.

Time	Applied Current (mA)	Cathode H_2S Out (ppm)	Cathode - Reference Overpotential	Anode - Reference Overpotential
Cathode flow = 88 cc/min				
17:21 (2/16)	0	85.0	0.0	0.0
18:15	5	26.7	-0.007	0.159
19:48	5	16.0	-0.006	0.127
21:30	0	89.5	0.0	0.0
8:46 (2/17)	0	89.5	0.0	0.0
10:00	5	20.0	-0.030	0.149
12:02	1.2	42.0	N/A	N/A
12:35	2	51.5	-0.017	0.030
13:00	2	47.5	N/A	N/A
13:15	2	53.0	N/A	N/A
13:34	20	29.5	N/A	N/A
14:20	20	9.7	N/A	N/A
14:47	15	18.5	-0.023	0.099
15:07	10	25	-0.022	0.050
15:48	20	15.5	-0.033	0.106

Table III (con.)
Run 49C Recorded Data.

Time	Applied Current (mA)	Cathode H_2S Out (ppm)	Cathode - Reference Overpotential	Anode - Reference Overpotential
Cathode Flow = 210 cc/min				
17:10	0	57	0.0	0.0
18:05	5	35.5	-0.014	0.127
19:00	5	30.6	N/A	N/A
20:09	10	31.5	-0.008	0.213
10:51 (2/18)	0	75.5	0.0	0.0
11:34	5	38.5	0.0	0.184
12:01	5	32	0.003	0.253
12:58	5	30	0.011	0.280
14:23	5	28.5	0.017	0.299
Cathode Flow = 400 cc/min				
21:15	0	59.4	0.0	0.0
21:40	5	48.7	-0.093	0.004
21:55	5	44.5	-0.088	0.055
22:24	5	39.7	-0.081	0.099
22:48	5	39.7	-0.082	0.117
10:31 (2/19)	0	73	0.0	0.0
14:14	10	49	-0.007	0.150
14:55	10	37.3	0.002	0.280
15:34	10	38	0.007	0.293
16:16	15	37.5	0.009	0.333
17:08	15	38.3	0.014	0.343
17:55	20	38.7	0.012	0.326
Cathode Flow = 600 cc/min				
12:00 (2/20)	0	68	0.0	0.0
12:44	10	42	-0.001	0.208
13:15	10	43.3	0.0	0.273
13:45	10	48.3	0.006	0.249
14:30	20	46	0.001	0.318
15:00	20	40	0.003	0.310
15:30	20	45.3	0.003	0.365

The above data are presented graphically in Figures 16 through 19. The H_2S exit composition is plotted against run event for the 88 cc/min data in Figure 16. Note that initially, the membrane was showing process stream cross-flow. 1.5 grams of electrolyte were added to stop the cross flow and 5 mA were applied to the cell. This current level corresponds to five times the theoretical current required for complete H_2S removal. After driving the H_2S down to 16 ppm (81.2% removal, zero current basis) the current was turned off. The exit H_2S level returned to 89.5 ppm. The lowest level to which the H_2S level was driven was 9.7 ppm (89.1% removal, zero current basis). This data shows good response of the system to applied current. The overpotential to accomplish this removal is shown by Figure 20 to be negligible.

The H_2S removal versus run event for the 210 cc/min data is shown in Figure 17. This data still shows good response of the system to applied current. More electrolyte had to be added to repair membrane damage, and thus the initial exit H_2S cathode level with no current applied is down to 57 ppm. This is due to a build-up of carbonate caused by excess electrolyte which had been added to the system.

The data taken at a flowrate of 400 cc/min is presented in Figure 18 and the data taken at 600 cc/min is presented in Figure 19. Comparison of this data with the overpotential results presented in Figure 20 shows that the efficiency of the system dropped off with time. At several points through the run, as marked on Figures 16 through 19, electrolyte was added to stop cross-over between the cathode side of the cell and the anode side. The increase in anodic overpotential shows that this excess electrolyte had flooded the anode, thus decreasing the reactive surface area from the

interfacial area of the electrolyte wetting the walls of the electrode capillaries to the superficial area of the electrode when the pores were fully flooded. This was verified in the post-mortem analysis of the cell when the assembly was taken apart and the components examined. The anode flooded because it is physically on the bottom of the assembly.

A total of 18.7 grams of electrolyte was added to the membrane during the course of the run in addition to the 11 grams that were initially added to fill the ceramic matrix of the membrane. Post-mortem examination of the membrane showed a small fracture in the matrix around the edge of the electrodes. This fracture would be temporarily flooded with electrolyte to form a gas impermeable barrier. However, aggressive attack by the electrolyte on the MACOR housings would deplete the membrane of electrolyte and lead to gas cross-flow. This problem can be overcome by the use of stainless steel housings, which are more resistant to electrolyte attack. The cell was terminated due to flooding of the anode and poor membrane integrity after 216 hours of operation.

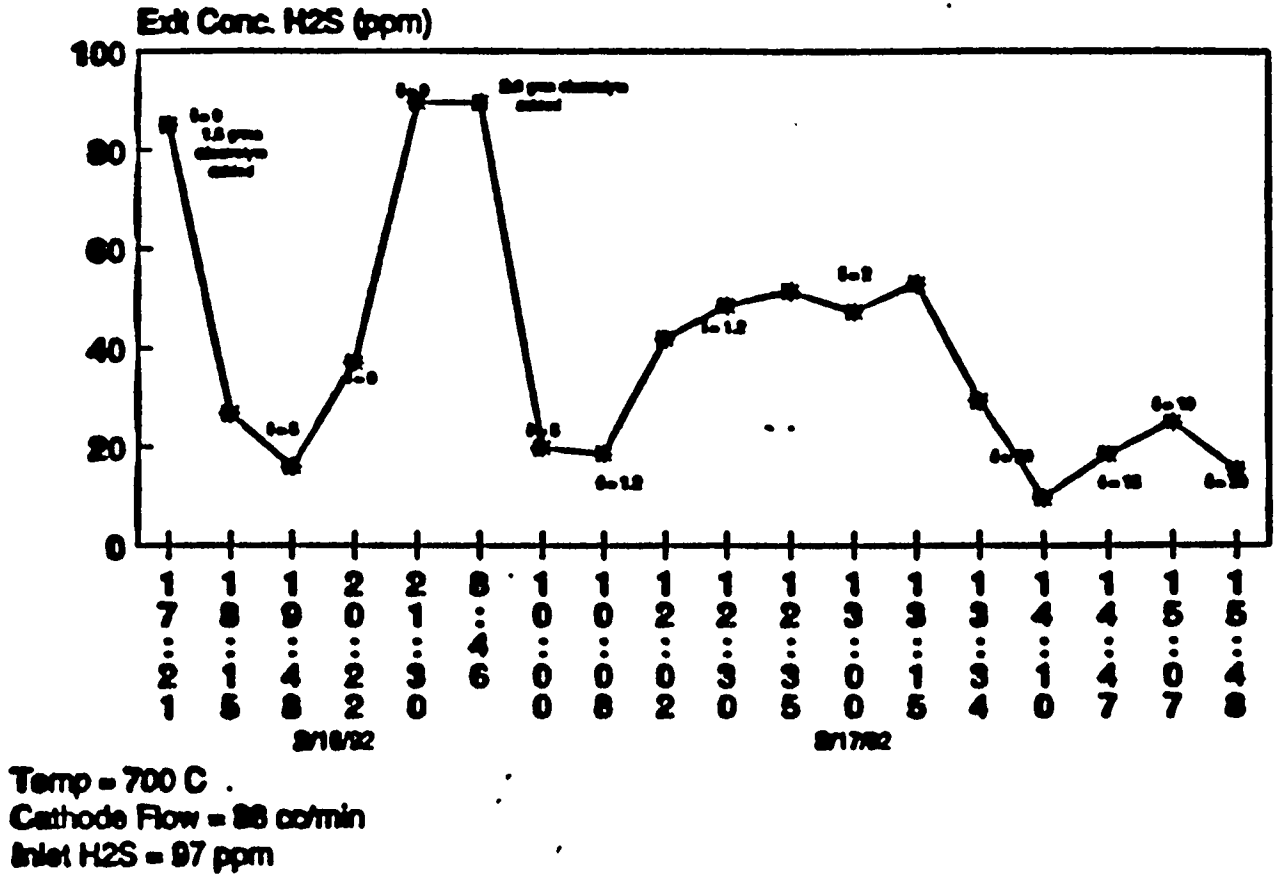

Figure 16 Run 49C: H_2S Concentration vs Applied Current and Time
88 cc/min

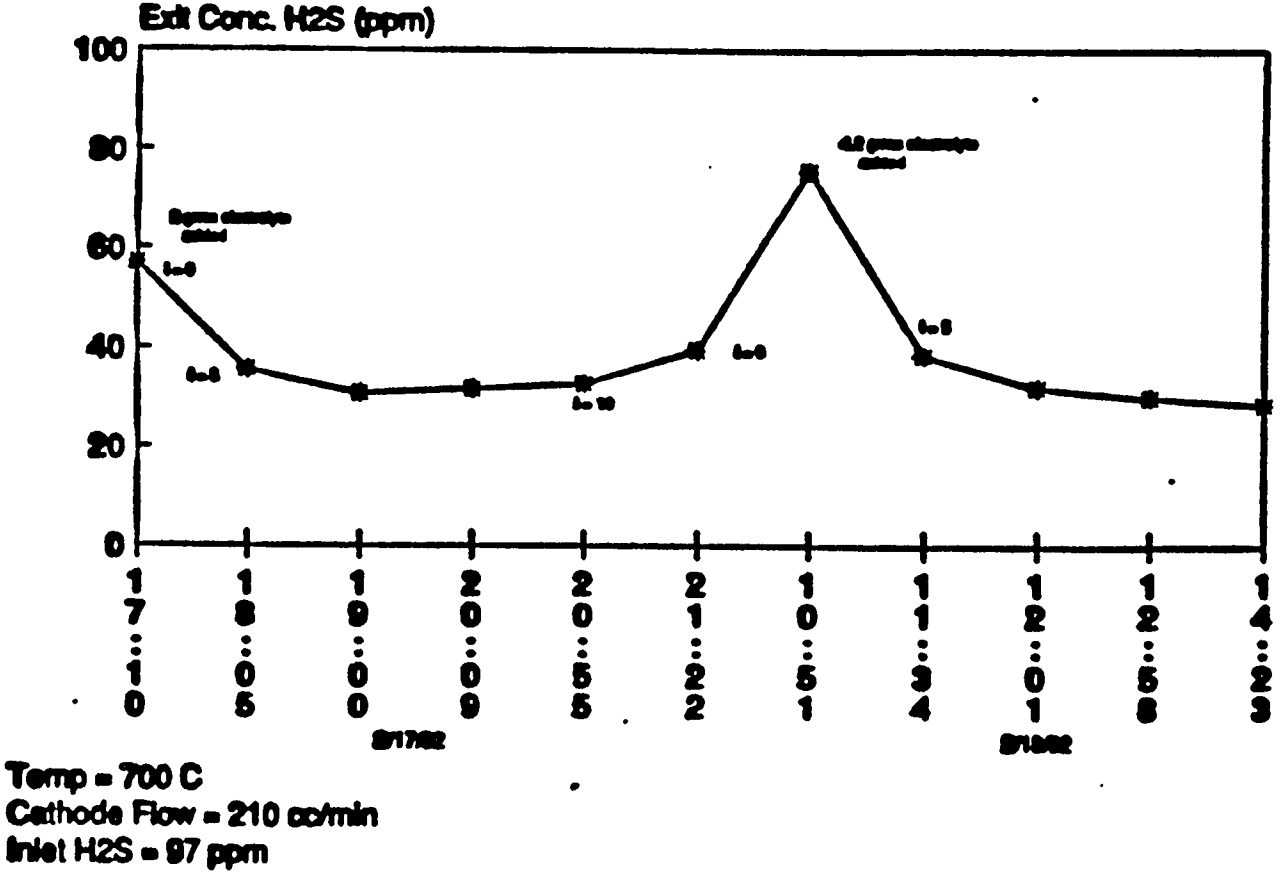

Figure 17 Run 49C: H_2S Concentration vs Applied Current and Time, 210 cc/min

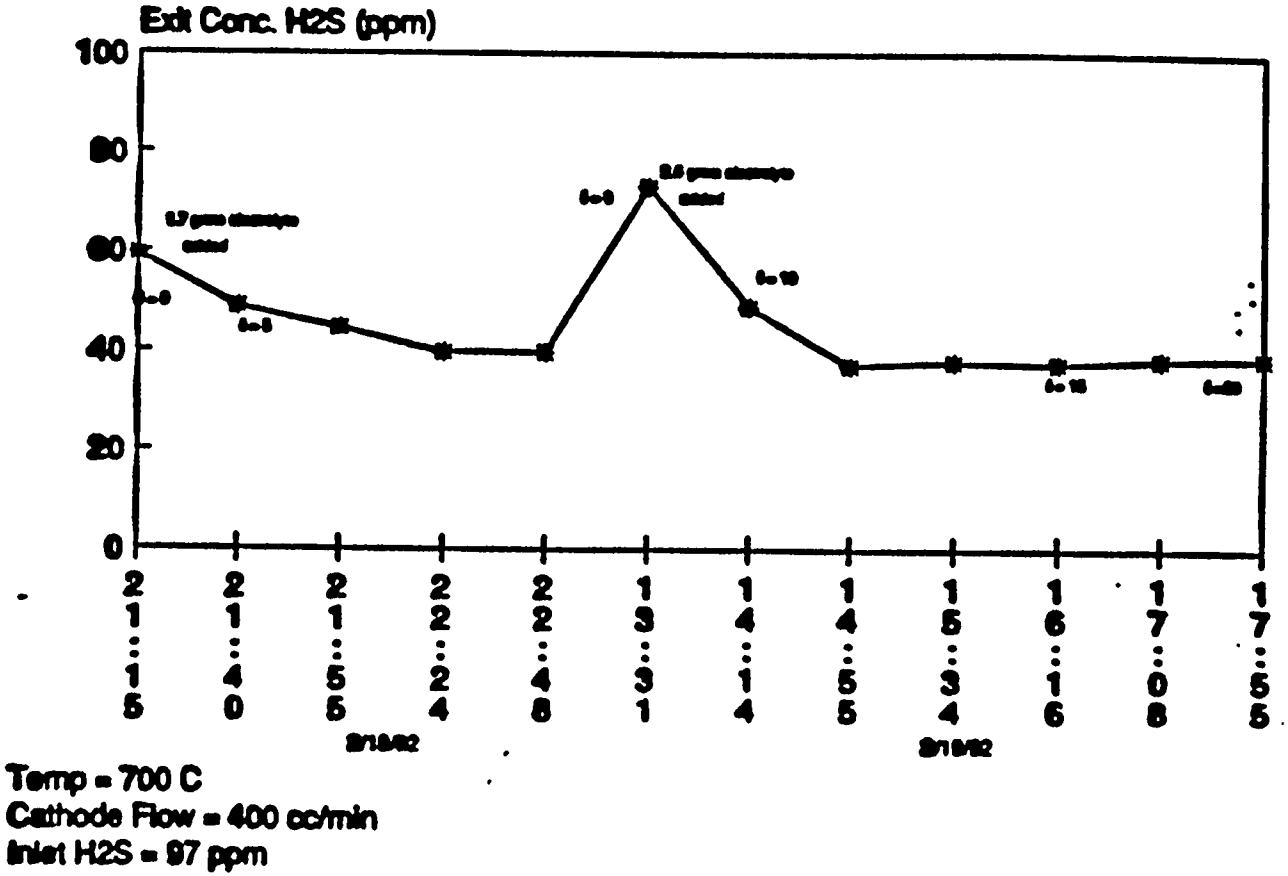

Figure 18 Run 49C: H_2S Concentration vs Applied Current and Time, 400 cc/min

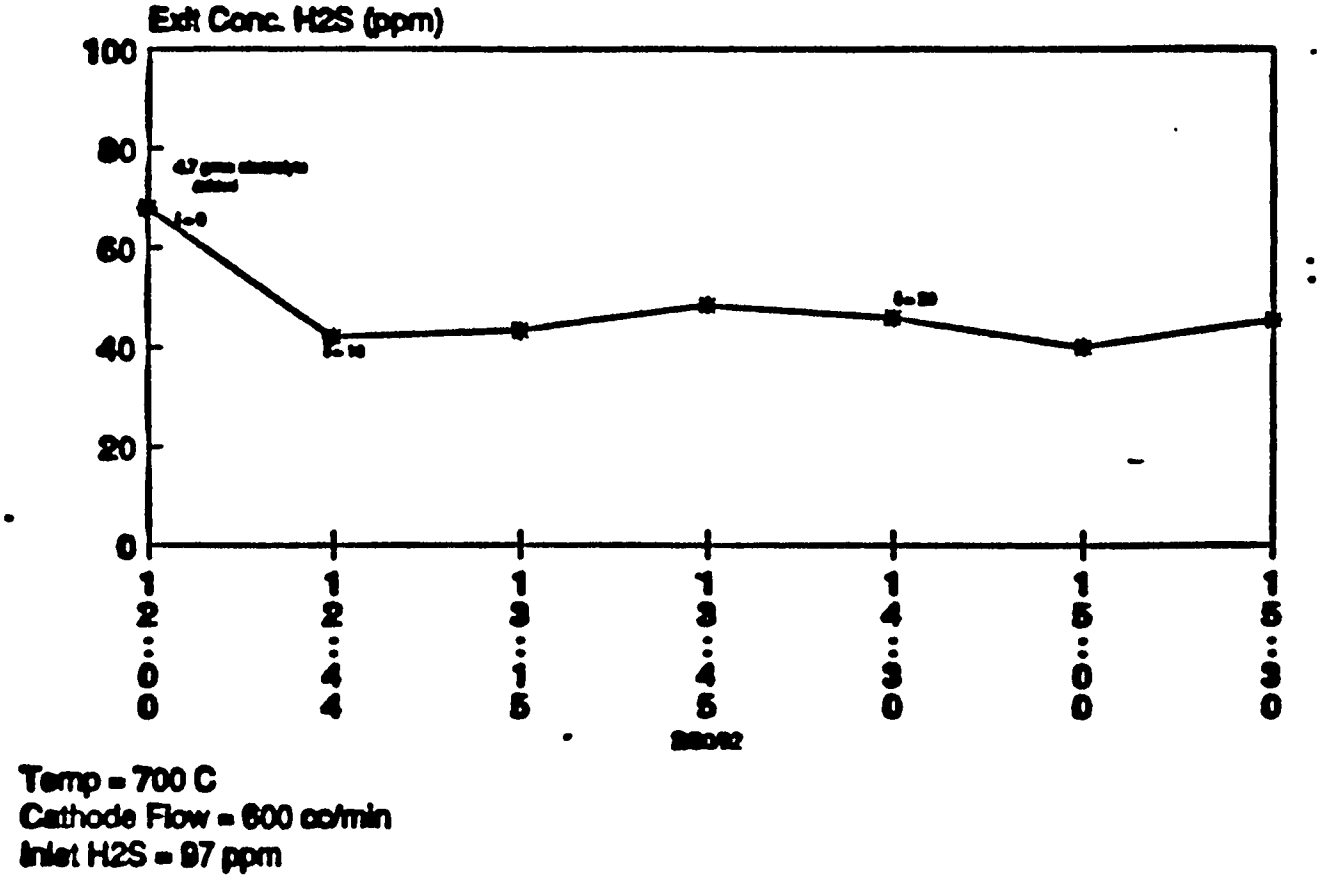

Figure 19 Run 49C: H_2S Concentration vs Applied Current and Time, 600 cc/min

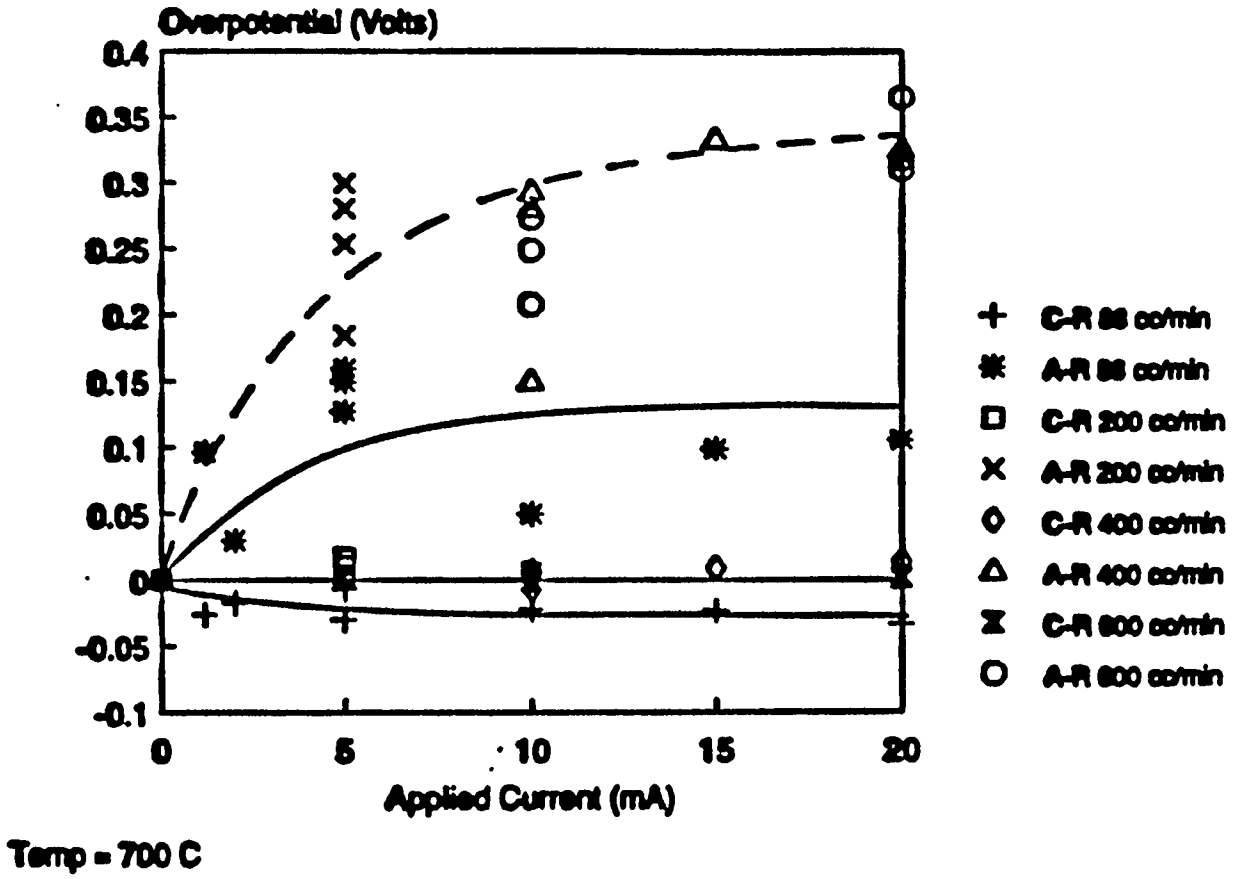

Figure 20 Run 49C: Overpotential vs Applied Current and Time, Various Flow Rates

Run 57

Both electrodes in this experiment were lithiated Ni. The membrane was two tapes of MgO with two mats of zirconia cloth. One of the zirconia mats was cut with a wick extending out of the cell and resting in an electrolyte reservoir. This was to provide a continuous supply of electrolyte to the membrane in the event of electrolyte evaporation/reaction with the cell materials. The electrolyte loaded into the cell was 0.8 mole% sulfide in a carbonate supporting electrolyte. Eutectic carbonate electrolyte was loaded into the reservoir. The cell housings were 316 stainless steel painted with aluminum.

After binder burn-out and the cell had reached run temperature, fuel gas of final composition 14.4%CO_2, 45.1% CO, 6.2% H_2O, 34.2% H_2, and 113 ppmv H_2S was fed to the cell. This gives an equilibrium sulfide level in the electrolyte of 0.63 mole% sulfide. The gas phase limiting current density under these conditions was estimated to be 1.28 mA/cm^2 and the membrane limiting current density was estimated at 1.97 mA/cm^2.

H_2S removal data is presented in Figure 21. Removal of H_2S below 2 ppmv (GC detector limit) was recorded with only 5 mA (0.63 mA/cm^2) applied to the cell and a cross cell potential of only -275 mV (cathode to anode). Upon shutting off applied current, exit H_2S levels only returned to 24 ppm (113 ppm entering the cell). The electrolyte reservoir was removed since it was a potential carbonate sink for reaction with H_2S in the gas. Cell cross flow started soon after this and the cell was shut down. Apparently, electrolyte was wicked out of the membrane onto the surface of the steel housings thereby depleting the membrane of electrolyte and allowing gas cross-over.

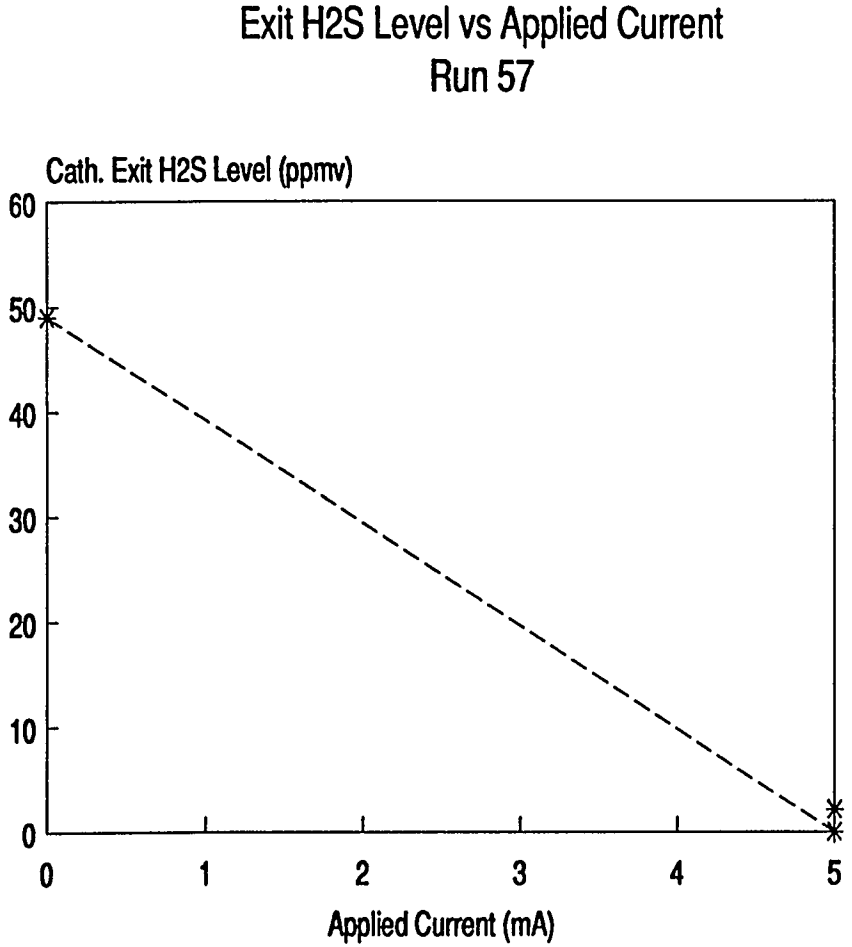

Inlet H2S = 110 ppmv
Cathode Flow = 230 cc/min
Temp = 700 C

Figure 21 Run 57: H_2S Removal vs Applied Current

Run 58

This experimental run also used lithiated Ni electrodes. In this experiment, the membrane was a hot pressed Molten Carbonate Fuel Cell (MCFC) membrane provided by Gas Research Institute (GRI). This structure is a 50/50 weight mixture of $LiAlO_2$ and eutectic Li/K carbonate. The housings were MACOR (with a stainless steel coil in the feed gas line to act as a shift reactor) and aluminum foil gaskets were used. Excess Li_2CO_3 (for reaction with the Al gaskets in conversion to $LiAlO_2$) was sprinkled on the membrane surface with enough Li_2S to bring the electrolyte to 0.8 mole% sulfide.

After the electrolyte was molten, fuel gas with composition 17.3% CO_2, 42.2% CO, 3.3% H_2O, 37.1% H_2, (after shift reaction) and 117 ppmv H_2S was fed to the cell. This gives an equilibrium sulfide level of 0.65 mole%. The calculated gas phase limiting current density at this temperature was found to be 1.31 mA/cm^2 and the membrane limiting current density was estimated to be 1.53 mA/cm^2.

H_2S removal data (see Figure 22), anodic CO_2 production data (see Figure 23), and cross-cell potential data (see Figure 24) was taken. Examination of Figure 22 shows the most dramatic H_2S reduction takes place at currents less than 10 mA (1.23 mA/cm^2). Beyond this, diffusion of H_2 across the cell decreases H_2S current efficiencies in favor of CO_2 production with applied current. Cross-cell potentials were very high at large applied currents (> 500 mA). This was due to concentration effects as the cathode gas was depleted of H_2O by the carbonate transport reaction. H_2S levels were driven as low as 6 ppmv even with H_2 cross-over.

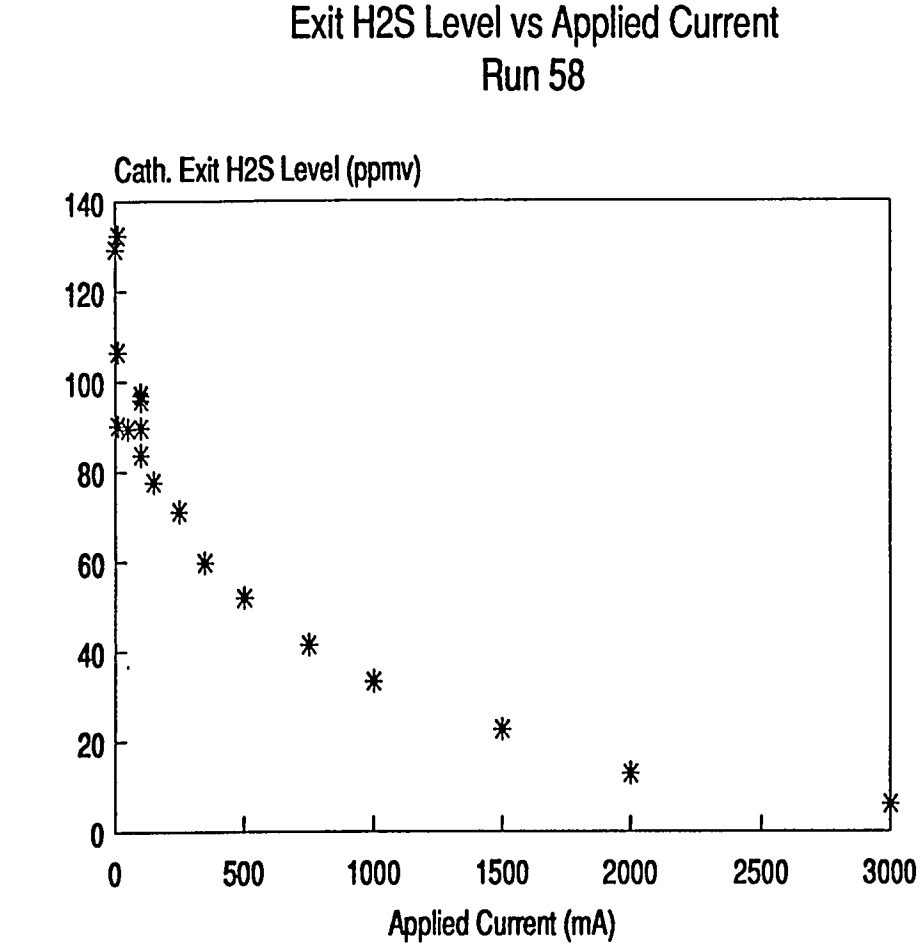

Figure 22 Run 58: H_2S Removal vs Applied Current

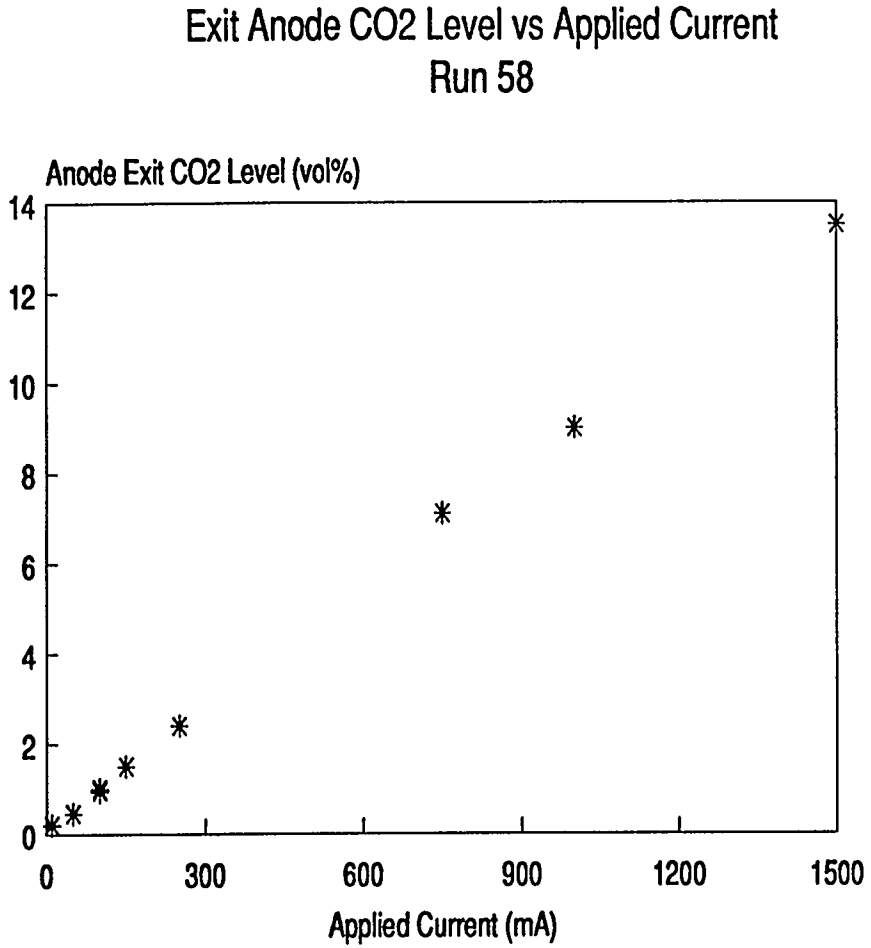

Inlet CO2 = 0 vol%
Anode Flow = 175 cc/min
Temp 700 C

Figure 23 CO_2 Removal vs Applied Current

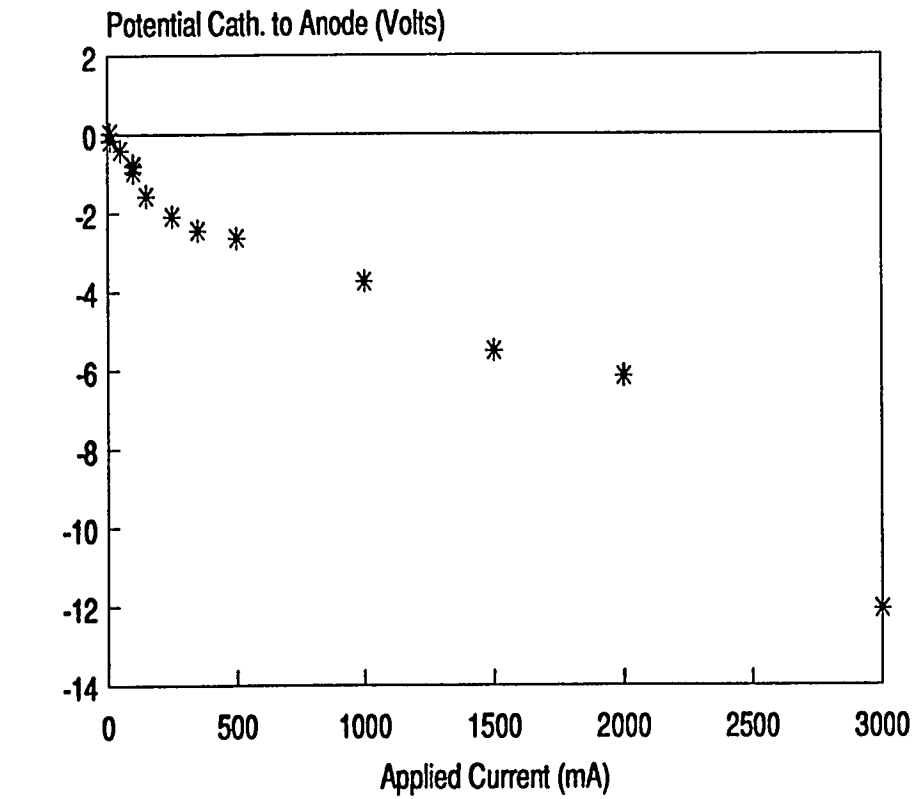

Cathode Flow = 200 cc/min
Anode Flow = 175 cc/min
Temp = 700 C

Figure 24 Run 58: Overpotential vs Applied Current

Run 62

This experimental run used a zirconia mat densified to 64 void %. Only enough electrolyte was added to wet the membrane, extra electrolyte was slowly added after the cell had reached run temperature to react with the Al gaskets.

Once the electrolyte had melted, fuel gas of composition 14.4% CO_2, 45.1% CO, 6.2% H_2O, 34.2% H_2 (after the shift reaction at 700°C) with 120.4 ppmv H_2S. H_2S removal data was taken at 216 cc/min and a temperature of 700°C. At this temperature and gas composition, the equilibrium sulfide level in the electrolyte is calculated to be 0.68%. The gas phase limiting current density is 1.33 mA/cm^2 and the membrane limiting current density is 2.10 mA/cm^2. A second set of H_2S removal data was taken at a flow of 100 cc/min and a temperature of 750°C (gas composition 13.6% CO_2, 45.8% CO, 6.9% H_2O, 33.4% H_2 with 93.6 ppmv H_2S) (see Figures 25 and 26). At this temperature and gas composition, the membrane equilibrium sulfide level was estimated to be 0.91 mole% sulfide. The gas phase limiting current density was estimated to be 1.15 mA/cm^2 and the membrane limiting current density 2.82 mA/cm^2. Anodic CO_2 production was also monitored (see Figures 27 and 28) and cross-cell potentials were recorded for 100 cc/min and run temperature of 750°C (see Figures 29). Comparison of Figures 25 and 26 shows that H_2S removal efficiency is improved by lower flow rates (higher residence time) and higher temperatures (higher limiting current densities).

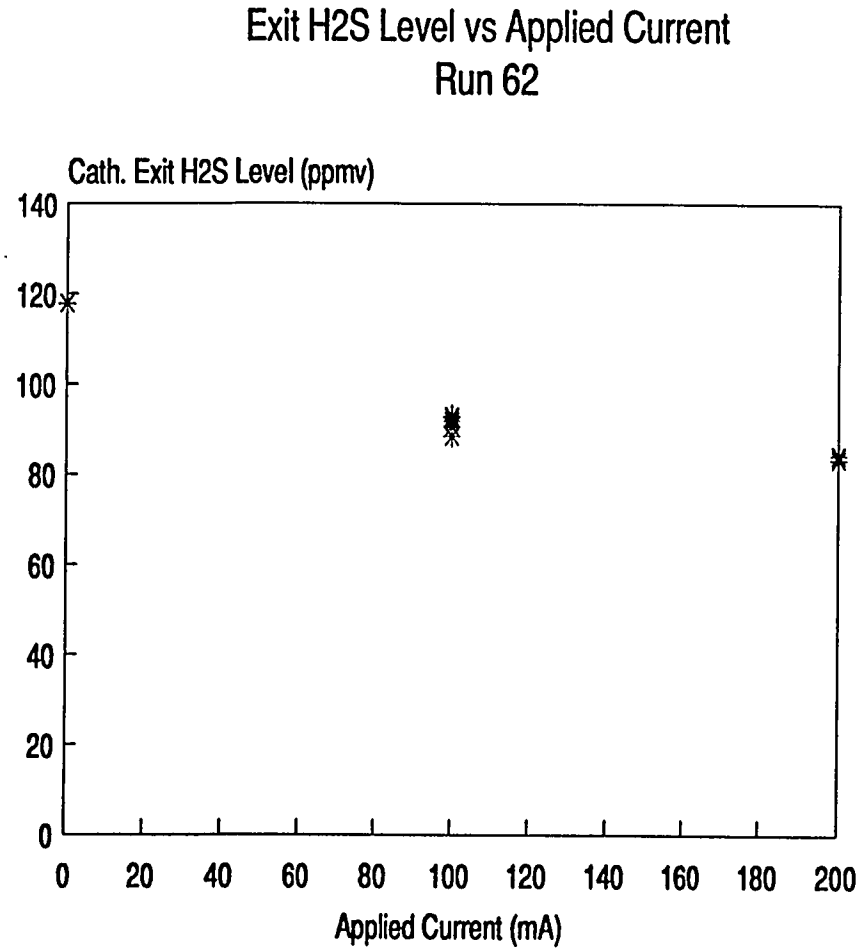

Inlet H2S Level = 120.4 ppmv
Cathode Flow = 216 cc/min
Anode Flow = 42 cc/min

Figure 25 Run 62: H_2S Removal vs Applied Current

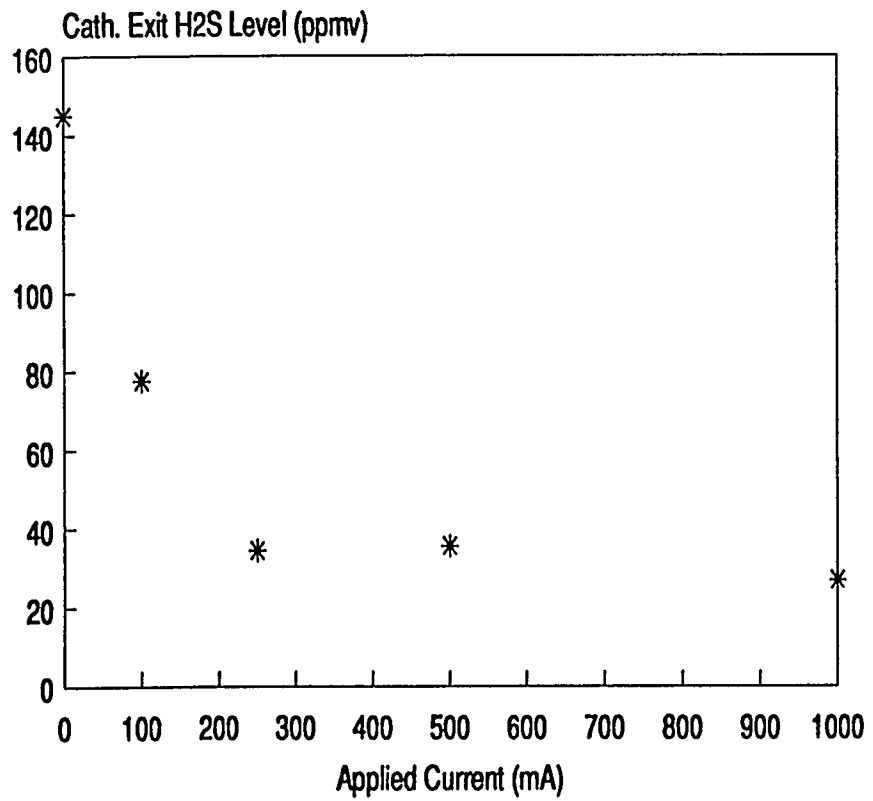

Inlet H2S Level = 93.6 ppmv
Cathode Flow = 100 cc/min
Temp = 750 C

Figure 26 Run 62: H_2S Removal vs Applied Current

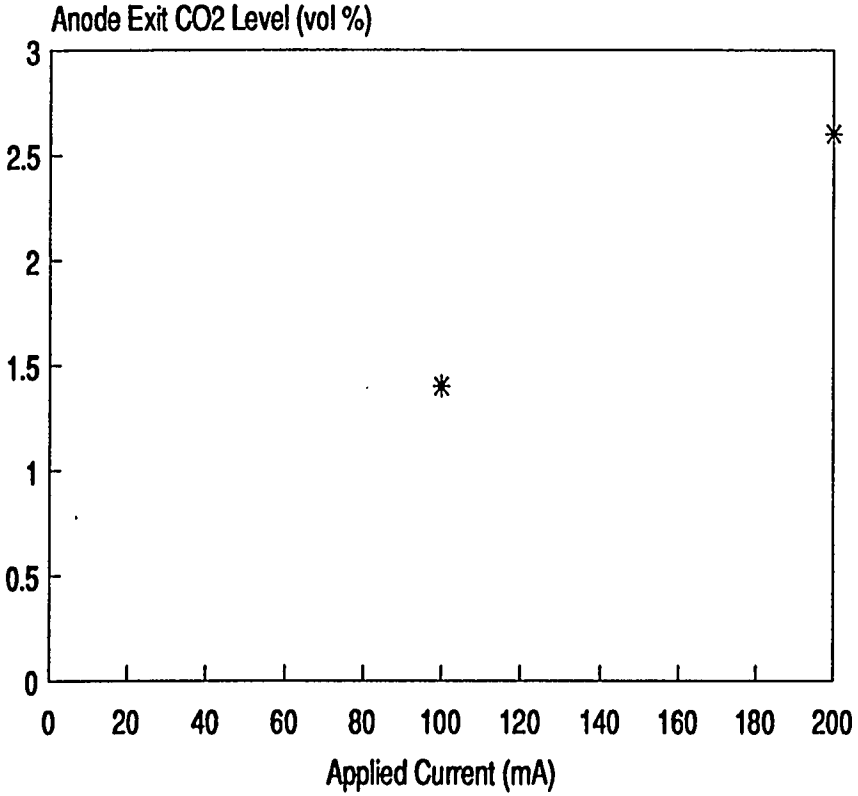

Inlet CO2 Level = 0%
Anode Flow = 42 cc/min
Temp = 700 C

Figure 27 Run 62: CO_2 Removal vs Applied Current

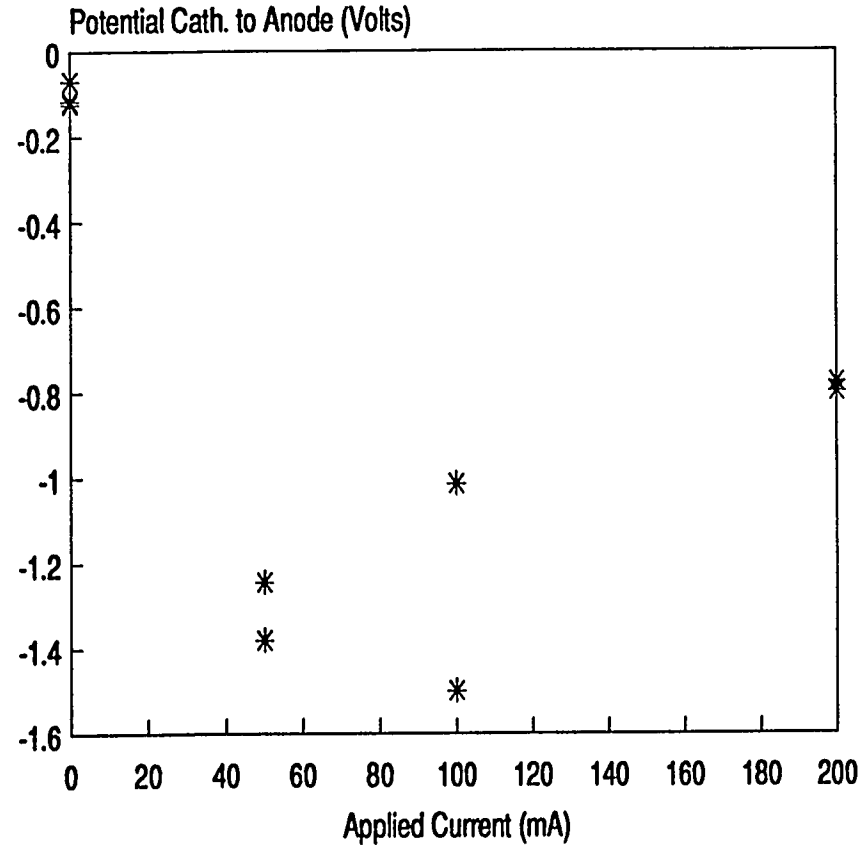

Cathode Flow = 100 cc/min
Anode Flow = 100 cc/min
Temp = 650 C

Figure 28 Run 62: CO_2 Removal vs Applied Current

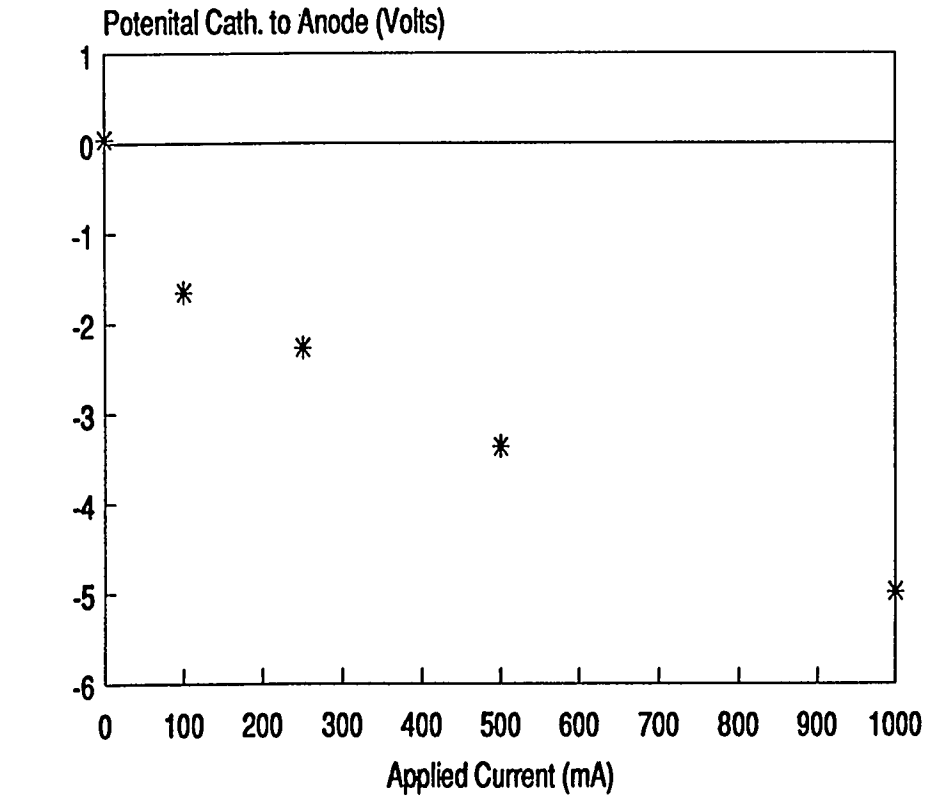

Cathode Flow = 100 cc/min
Anode Flow = 58 cc/min
Temp = 750 C

Figure 29 Run 62: Cross-cell Polarization

Run 65

This experimental run used 1 mat of 30 mil zirconia cloth which was rigidized to 60.8% and two tapes of MgO/ZrO_2 in vinyl binder. The electrolyte was eutectic carbonate and was added to the cell as a pressed disk. the electrodes were lithiated Ni. The housings were MACOR and Al foil gaskets were used. The run temperature was 650°C.

After binder burnout and electrolyte melting, fuel gas of composition 15.2% CO_2, 44.2% CO, 5.4% H_2O, 35.0% H_2 with 18.8 ppmv H_2S was put through the cell. This gas composition and temperature gives an equilibrium membrane sulfide level of 0.06 mole% sulfide. The gas phase limiting current density is estimated to be 0.18 mA/cm^2 and the membrane limiting current density is 0.34 mA/cm^2.

H_2S removal data was taken at cathodic flow rates of 200 cc/min and 100 cc/min (see Figures 30 and 31). Cell polarization data was also take at these flow rates (see Figures 32 and 33). Anodic CO_2 production data was also taken at cathodic flow of 100 cc/min (see Figure 34).

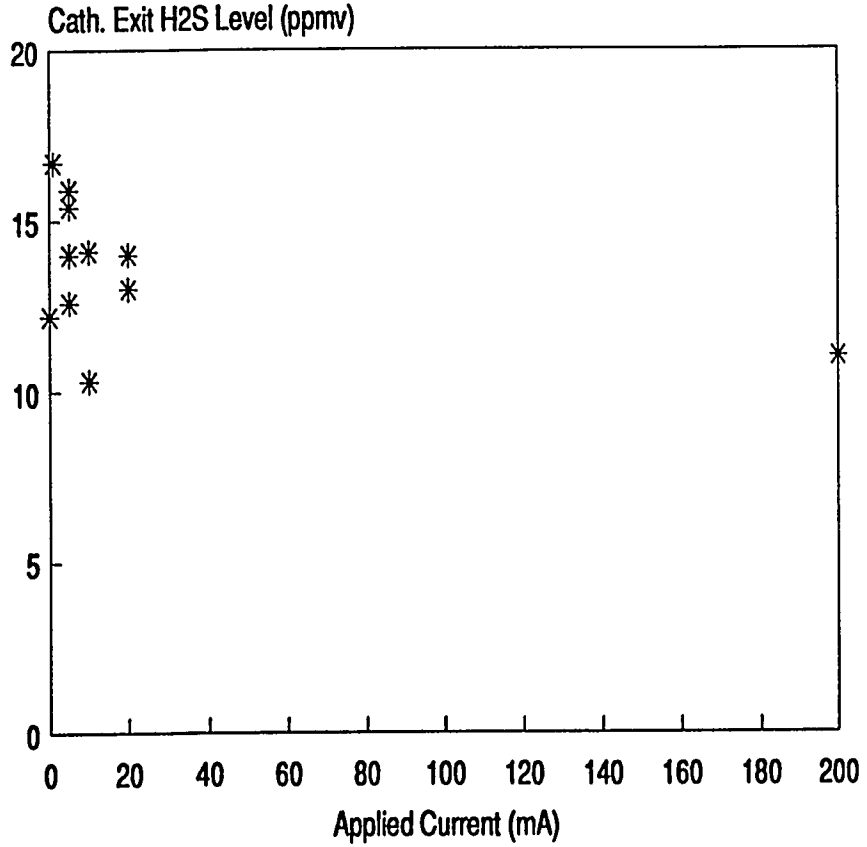

Inlet H2S Level = 18.8 ppmv
Cathode Flow = 200 cc/min
Temp = 650 C

Figure 30 Run 65: H_2S Removal vs Applied Current

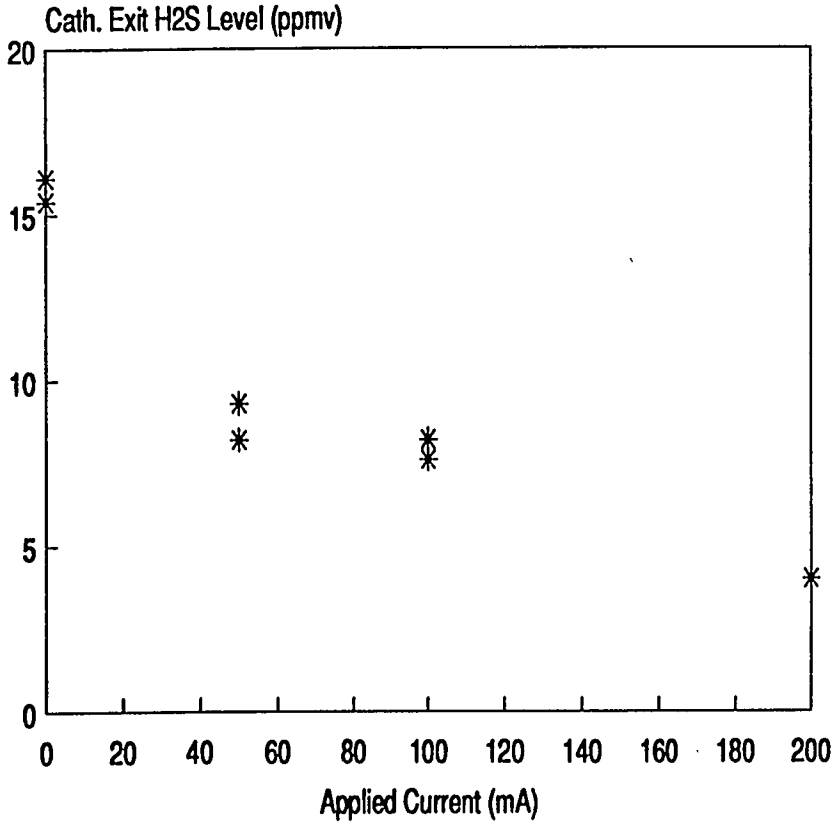

Inlet H2S = 27 ppmv
Cathode Flow = 100 cc/min
Temp = 650 C

Figure 31 Run 65: H_2S Removal vs Applied Current

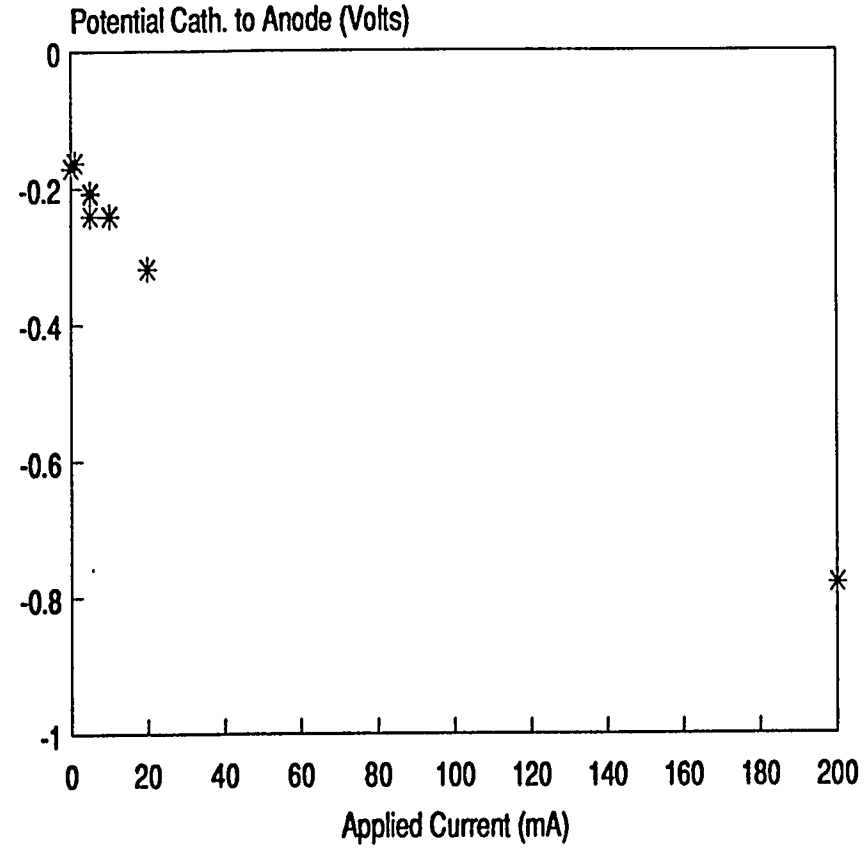

Cathode Flow = 200 cc/min
Anode Flow = 100 cc/min
Temp = 650 C

Figure 32 Run 65: Cross-cell Polarization

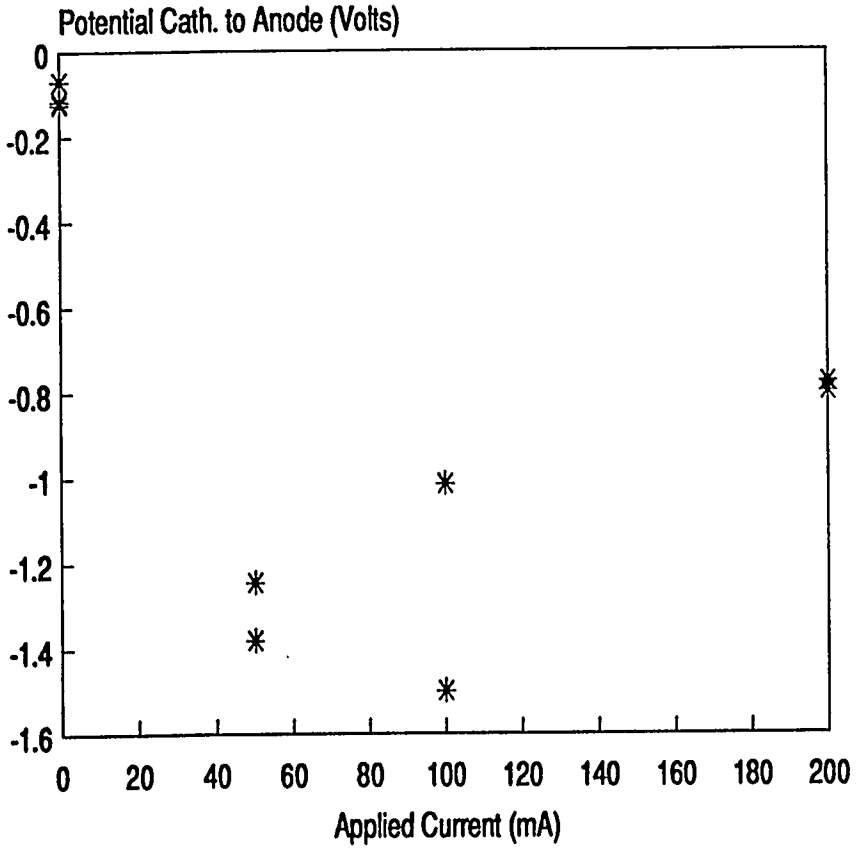

Cathode Flow = 100 cc/min
Anode Flow = 100 cc/min
Temp = 650 C

Figure 33 Run 65: Cross-cell Polarization

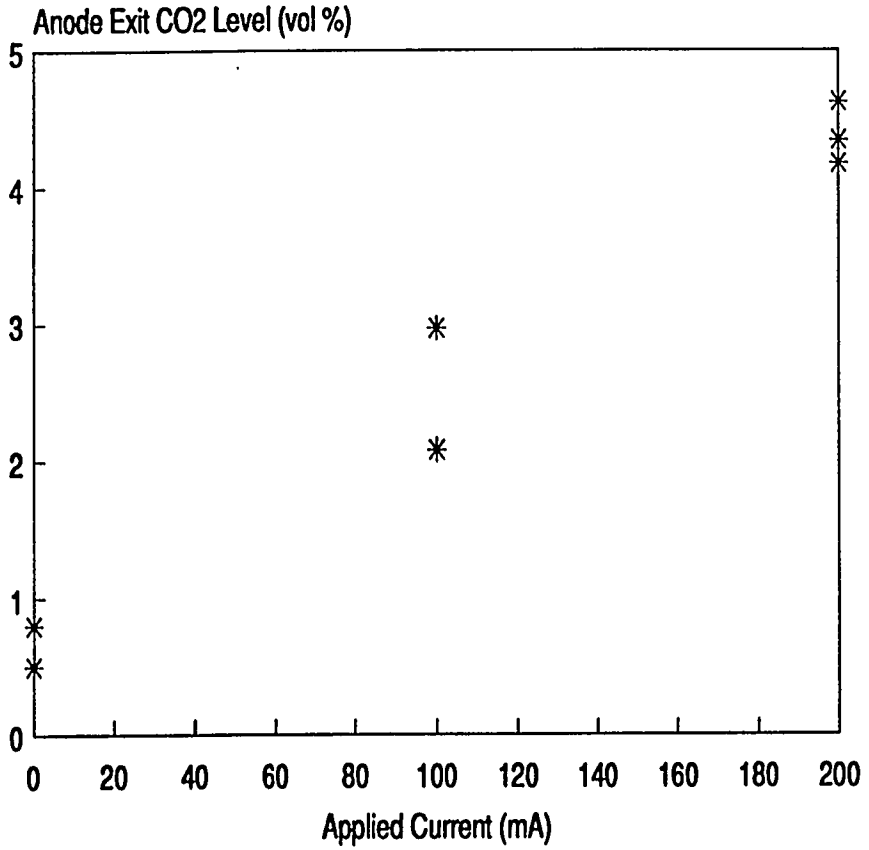

Inlet CO2 Level = 0 %
Anode Flow = 100 cc/min
Temp = 650 C

Figure 34 Run 34: Exit CO_2 Level vs Applied Current

Run 4

A rigid Zirconia mat worked in this experiment. The mat began as a weave of zirconia cloth, then hardened with the zirconia rigidizer, accomplished in a similar fashion as aforementioned. Housing materials were MACOR (machineable ceramic) with lithiated Ni electrodes and seals created from oxidation of aluminum. Seal formation created the opportunity to test carbonate transport through the E.M.S system with cathodic reduction (equation 7) and anodic reduction (equation 10) corresponding to 100% tranport with applied current. The temperature and flow rate were maintained at 650^{0}C and 215 cc/min respectively. Once efficient carbonate transport showed the system operable application of H_2S followed; inlet H_2S was held between 6 and 20 ppm H_2S. As much as 94% removal with applied current was seen in this experiment as shown. Exit H_2S and applied current vs potential difference (cathode to anode) are shown in figures 35 & 36. The results of both run 4 & 5 are tabulated in Table 4. The experiment was shut down due to hydrogen cross-over. Run #4 lasted 163 hours.

Cross-cell Potential vs H2S Removal

Run #4

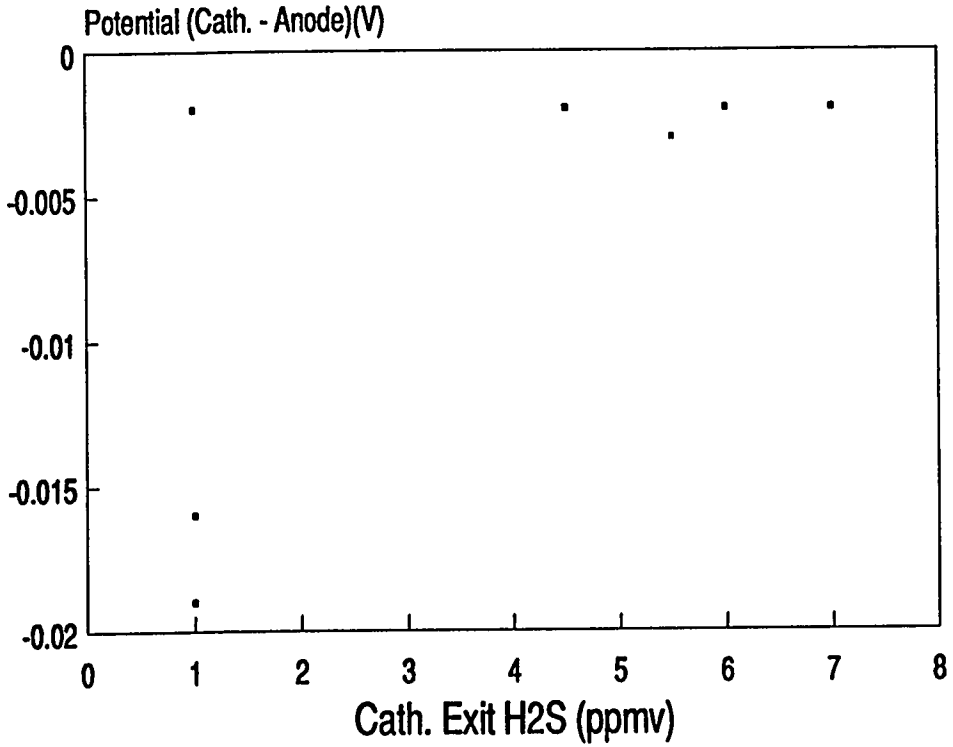

Temp. = 650 C
Flow Rate = 215 cc/min
Inlet H2S = 10 ppmv

Figure 35 Cross-cell Potential vs H_2S Removal

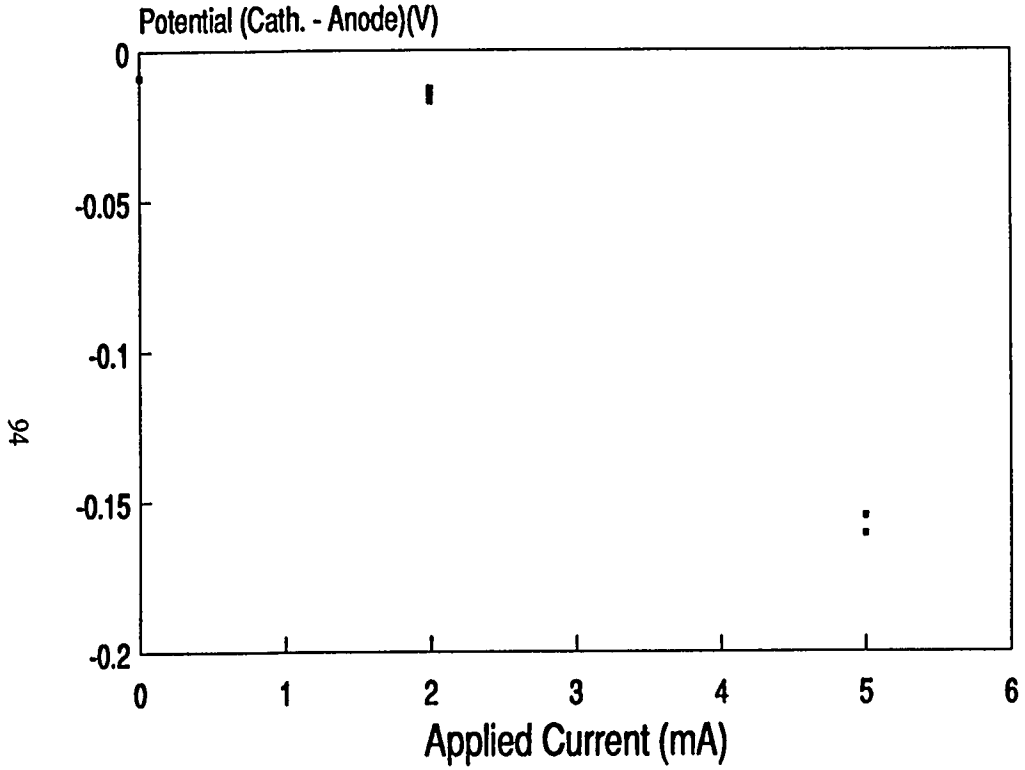

Figure 36 Cross-cell Potential vs Applied Current

Run 5

A manufactured Zircar membrane provided the medium for electrolyte support. Other materials were identical to Run 4. The manufactured membrane is advantagous, due to uniform porosity (66%) and reduced warping. Once efficient carbonate transport occurred, H_2S was applied to the cell and held at a concentration of 20 ppm. Flow rates varied from 200 cc/min - 800 cc/min at constant temperature (650° C). Removals over 90% were recorded with applied current. Exit H_2S and applied current vs cross-cell potential (cathode-anode) are shown in figures 37 & 38. The cell was shut down after 208 hours, due to an increase in membrane thickness, limiting sulfide migration.

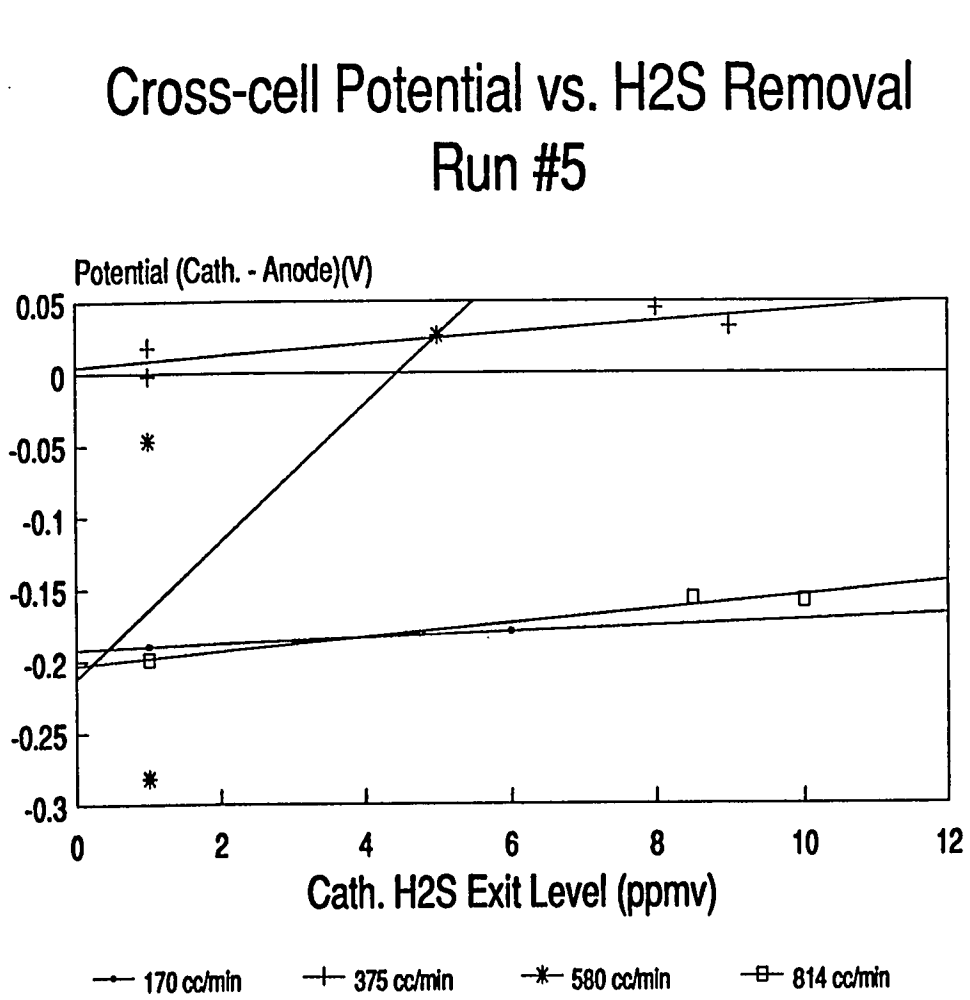

Inlet H2S = 20 ppmv
Temp. = 650 C

Figure 37 Cross-cell Potential vs H_2S Removal

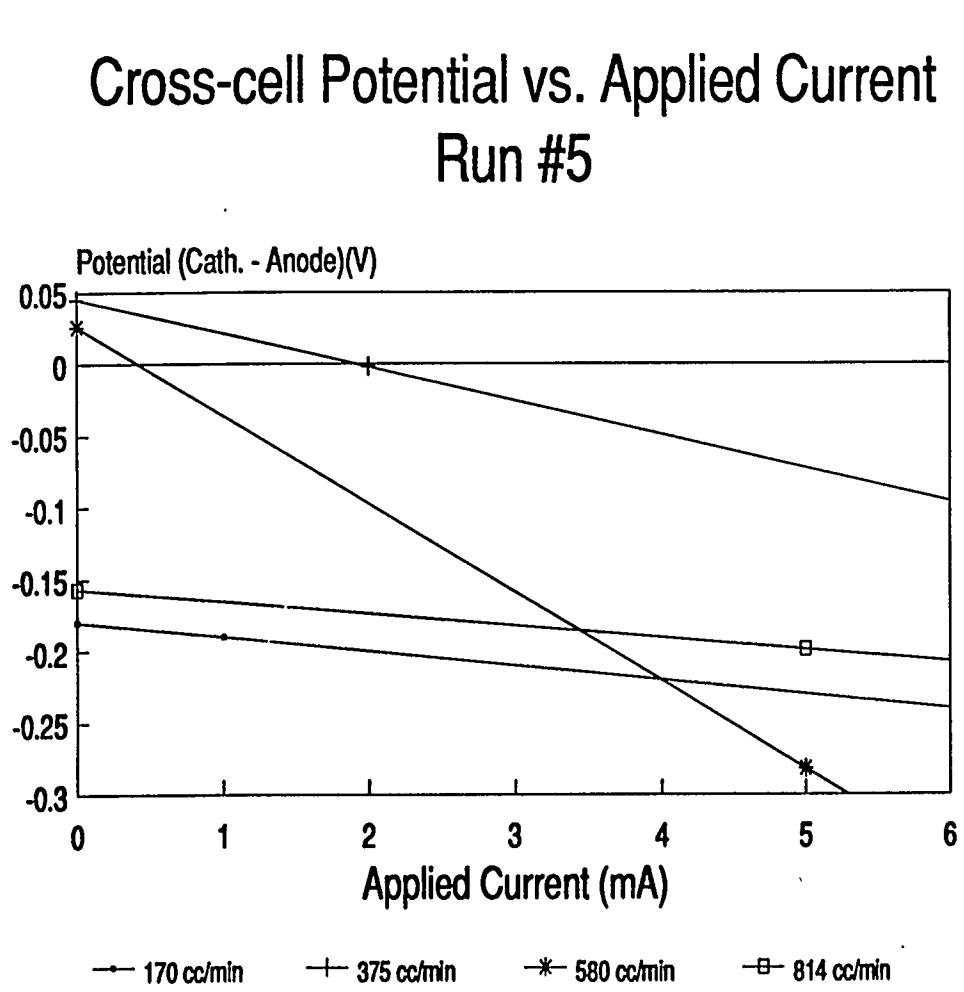

Inlet H2S = 20 ppmv
Temp. = 650 C

Figure 38 Cross-cell Potential vs Applied Current

Table IV. Experimental Results for Runs #4 & #5

Temp. (°C)	Flow-Rate (cc/min)	Residence Time (sec.)	Inlet H_2S (ppm)	Exit H_2S (@ I_{app})	I_{app} (mA)	E_{c-a} (Volts)
650	170	0.197	25	1	1	-0.190
	225	0.146	8.5	1	2	-0.013
	375	0.089	22	1	2	-0.003
	580	0.058	20	1	5	-0.047
	814	0.041	22	1	5	-0.199

CONCLUSIONS

The most important issue facing the removal of H_2S by the Electrochemical Membrane Separator is finding/developing an adequate matrix material that simultaneously sustains an ionic pathway and hinders process-gas cross-over. Exploration of various matrix materials and manufacturing techniques revealed a variety of possibilities for the electrochemical separation cell; matrices of densified zirconia provided the best results in full-cell experimentation.

Anodes of lithiated Ni converted to NiO in-situ performed effectively with similar usefulness at the cathode; however, H_2S levels > 100 ppm requires an alternate cathode material due to the conversion of NiO to a molten nickel sulfide. Recent experiments using cobalt cathodes have been successful.

High temperature removal of over 90% H_2S utilized the aforementioned membrane and electrode materials attaining the removals with high current efficiencies and low polarizations, creating a low overall power requirement.

SO_2 REMOVAL

SO_2 removal is carried out through electrochemical steps, in combination with a number of chemical steps. The overall reaction involves the selective removal of SO_x from the cathodic (reducing) side of the membrane, and the generation of SO_3 and some O_2 at the anodic (oxidizing) side. This SO_3 and oxygen can be concentrated to produce a stream for use in production of a high purity oleum. This reaction takes place over a molten salt electrolyte consisting of 90 wt% $K_2S_2O_7$ and 10 wt% V_2O_5 at 400° C.

The chemical reactions of $K_2S_2O_7$ melts over varying temperatures were analyzed by Flood *et. al.*[20,21]. Their experiments, carried out with SO_3, SO_2, and O_2, determined that two chemical equilibriums existed. The first was an equilibrium imposed with SO_3:

$$M_2SO_4 + SO_3 \rightleftharpoons M_2S_2O_7 \qquad (37)$$

with stability of the melt being the highest when M=K. The second equilibrium of importance was with SO_2 and O_2 present:

$$SO_2 + \tfrac{1}{2}O_2 + K_2SO_4 \rightleftharpoons K_2S_2O_7 \qquad (38)$$

Flood then made an estimation for the ratio of liquidus activity coefficients based upon variations from Nernstian effects in electrolyte of known composition and at constant temperature and partial pressures. There is suggestion of an eutectic melt at approximately 400° C, with a sulfate solubility of approximately 3-5wt% in pyrosulfate.

Boreskov *et. a.*[22] further attempted to study $K_2S_2O_7$ in conjunction with V_2O_5 under oxygen at various temperatures, but could not decipher the reactions from 400-500° C. He did, however, suspect the formation of a $K_2S_2O_7$-V_2O_5 compound.

Fang and Rapp *et. al.*[23,24,25] found that at a platinum electrode at 900° C, pyrosulfate reduction in a sulfate melt would require one electron, and be reduced according to:

$$S_2O_7^{2-} + e^- \rightleftharpoons SO_4^{2-} + SO_3^- \qquad (39)$$

The SO_3^- ion would not be stable in the melt, and could react with itself to form the bisulfite ion, or with one electron, to form the sulfite ion. They further determined that neither the sulfite nor bisulfite ions would be stable in the melt, but would chemically react as

$$S_2O_6^{2-} \rightleftharpoons 2SO_2 + O_2^{2-} \qquad (40)$$

and

$$SO_3^{2-} \rightleftharpoons SO_2 + O^{2-} \qquad (41)$$

Franke[26] and Scott[27] completely decoded the reactions in the electrolyte through use of techniques including cyclic voltammetry, equilibrium potential techniques, X-ray diffraction, and effluent analysis. Performed upon potassium pyrosulfate ($K_2S_2O_7$) with variations in the gas composition as well as the salt itself, their analysis determined the dominant reactions.

Simulated exit gas is first introduced ex-situ to Pt or an acid catalyst such as Haldor-Topsoe VK-38 where all SO_2 is converted to SO_3 according to

$$\text{(42)} \quad SO_2 + \tfrac{1}{2}O_2 \rightarrow SO_3$$

This SO_3 stream enters the cell, and is then passed over the cathodic side of the cell as seen in Figure 39.

Two electrons are supplied to the cathode to reduce pyrosulfate according to

$$2S_2O_7^{2-} + 2e^- \rightarrow 2SO_2 + 2SO_4^{2-} + O_2^{2-} \qquad (43)$$

It is important to note that the reduction of pyrosulfate involves the *production* of two moles SO_2. SO_2 present can react with the superoxide ion to generate the sulfite ion:

$$SO_2 + O_2^{2-} \rightarrow SO_4^{2-} \qquad (44)$$

SO_2 may also combine with the sulfate ion, forming the unstable bisulfate ion. Bisulfate will then rapidly decompose to form sulfur trioxide and the sulfite ion:

$$2SO_2 + 2SO_4^{2-} \rightarrow 2S_2O_6^{2-} \rightarrow 2SO_3 + 2SO_3^{2-} \qquad (45)$$

Sulfite ion, unstable in the melt, reacts with any dissolved oxygen in the system:

$$2SO_3^{2-} + O_2 \rightarrow 2SO_4^{2-} \qquad (46)$$

The SO_3, flowing over the cathodic surface, will react with sulfate ions present to reform the favored pyrosulfate ion according to:

$$2SO_3 + 2SO_4^{2-} \rightleftharpoons 2S_2O_7^{2-} \qquad (47)$$

If the preoxidation reaction of Equation (42) is considered, the summation of the reactions leaves the overall cathodic reaction as:

$$SO_2 + O_2 + 2e^- \rightarrow SO_4^{2-} \quad (48)$$

This reaction was confirmed by Townley[28] to remove one mole of SO_2 for every two electrons supplied. Salzano and Newman[29] demonstrated that a similar equilibrium could exist:

$$SO_3 + \tfrac{1}{2}O_2 + 2e^- \rightarrow SO_4^{2-} \quad (49)$$

Equation (49) is the sum of the above reactions without the preoxidation reactor taken into account and will be more indicative of the physical electrochemical cell, and the measurements thereof.

At the anode, the thermodynamically favored oxidation of the sulfate ion will take place according to:

$$SO_4^{2-} \rightarrow 2e^- + \tfrac{1}{2}O_2 + SO_3 \quad (50)$$

The sum of Equations (49) and (50) yield the overall cell reaction for the removal of SO_3 as:

$$(SO_3 + \tfrac{1}{2}O_2)_{cathode} \rightarrow (SO_3 + \tfrac{1}{2}O_2)_{anode} \quad (51)$$

The potential, if calculated from a cathodic stream of 3000 ppm SO_3 and 3.0 mole% O_2 concentrated to a stream of 66.7 mol% SO_3 and 33.3 mole% O_2 would be -192 mV at 400° C.

Two reactions of importance are the sum of Equations (45) and (46), and the chemical equilibrium of Equation (47). Summing the reactions yields the overall step in Equation (52). This step is catalyzed in situ by V_2O_5 present in the $K_2S_2O_7$ in

$$SO_2 + \frac{1}{2}O_2 \rightarrow SO_3 \qquad (52)$$

quantities up to 10 wt.%. V_2O_5 is used often as a catalytic oxidant for sulfuric acid production in oxygenated systems. Flood and Kleppa[30] studied the equilibrium reaction of SO_2/SO_3 over vanadia. They found evidence of vanadia complexing when characterizing the reaction. Maximum catalytic effect was found to take place at 530° C, the decomposition temperature of $VOSO_4$.

Franke found that the addition of V_2O_5 to the melt resulted in a two-step chemical oxidation:

$$2SO_2 + 2\,[K_2O\text{-}V_2O_5\text{-}2SO_3] \rightleftharpoons 2\,[K_2O\text{-}V_2O_4\text{-}3SO_3] \qquad (53)$$

$$O_2 + 2\,[K_2O\text{-}V_2O_4\text{-}3SO_3] \rightleftharpoons 2\,[K_2O\text{-}V_2O_5\text{-}2SO_3] + 2SO_3 \qquad (54)$$

The vanadia complex may also take part in either the storing of excess SO_3

$$[K_2O\text{-}V_2O_5\text{-}2SO_3] + 2SO_3 \rightleftharpoons [K_2O\text{-}V_2O_5\text{-}4SO_3] \qquad (55)$$

or an electrochemical reaction

$$[K_2O\text{-}V_2O_5\text{-}4SO_3] + 2e^- \rightleftharpoons [K_2O\text{-}V_2O_4\text{-}3SO_3] + SO_4^{2-} \qquad (56)$$

Karydis *et. al.*[31,32] studied the equilibrium chemistry of $V_2O_5/K_2S_2O_7$ in $SO_3/SO_2/N_2$ atmospheres, and concluded that an equilibrium existed as

$$(VO)_2O(SO_4)_2^{4-} + SO_2 \rightleftharpoons 2VO(SO_4)_2^{2-} + SO_3 \qquad (57)$$

Estimation of liquid and solid temperatures led to the construction of a phase diagram for low loadings of V_2O_5 in pyrosulfate.

The chemical equilibrium established in Equation (47) shows the dependence of the concentration of sulfate in the melt on the partial pressure of SO_3 over the melt. At just over 400° C, the equilibrium will be established between sulfate and pyrosulfate. At 400° C, however, there is a limited solubility of sulfate in pyrosulfate of 4 wt%.

The removal is accompished through the use of a ceramic matrix sandwiched by two porous gas diffusion electrodes, and impregnated with a molten salt electrolyte. As seen in Figure 40. The housings are constructed of 316LSS, with the electrode area encompasing approximately 20 cm^2 and membrane diameters of 7.62 cm. The 316LSS housings form a passivating layer, while still allowing current flow to the surface of the imbeded electrodes.

In accordance with the goals of the research, electrode and matrix materials were tested for performance and stability in this complicated system. This work and additional work with the electrolyte over the research period is detailed, followed by the resulting full cell tests of the integrated system.

Electrochemical Flue Gas Clean-Up

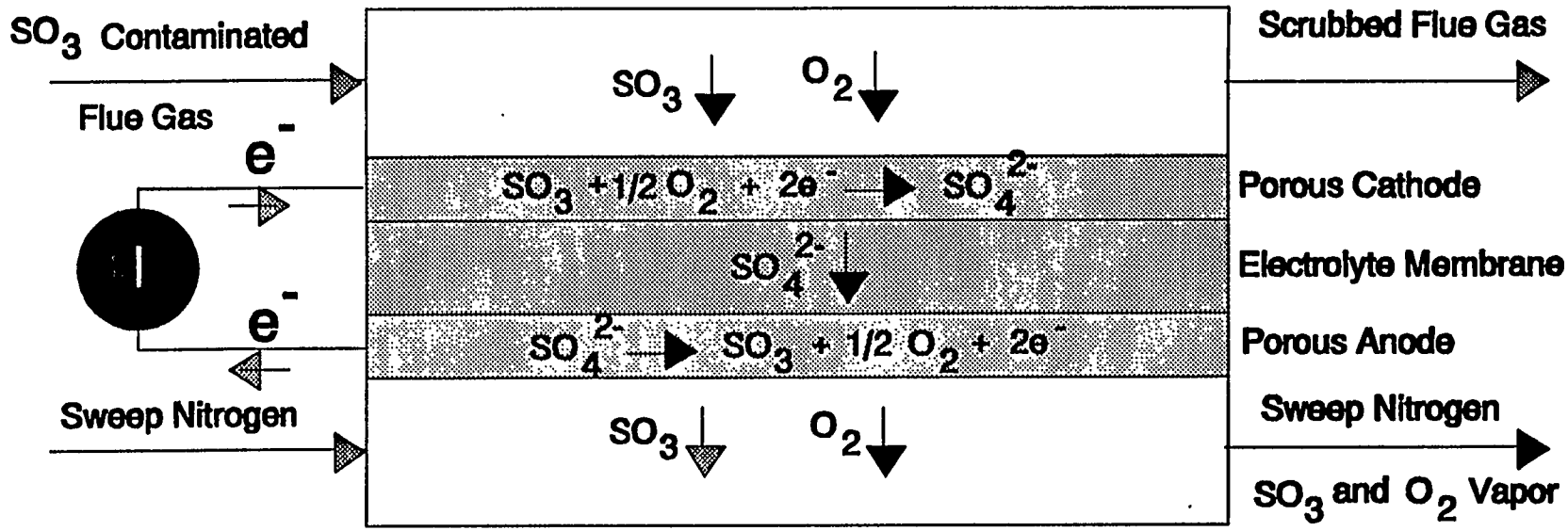

Figure 39: Conceptual cell configuration. T=400° C.

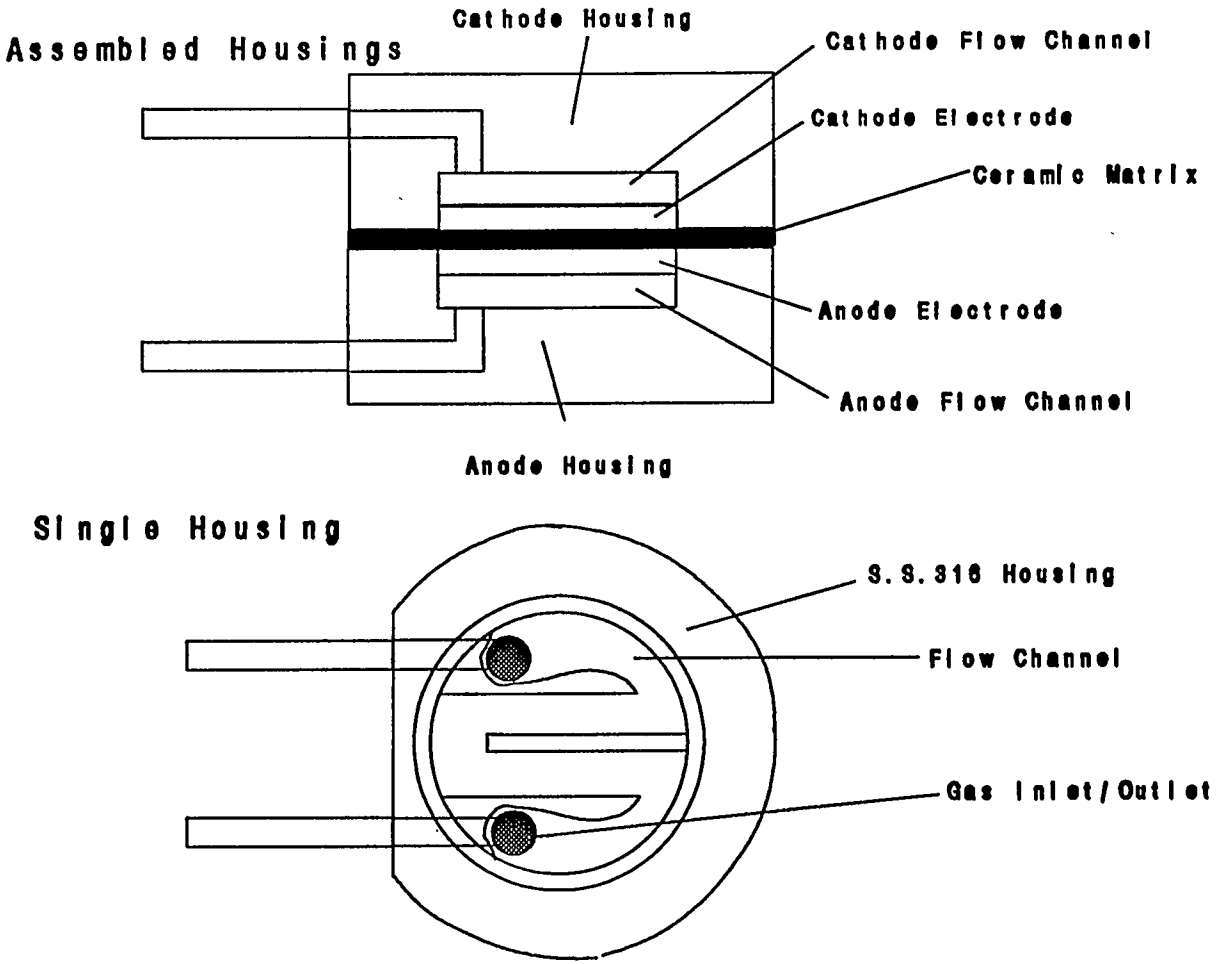

Figure 40: Bench scale full system test apparatus.

MATERIALS

There are a number of factors crucial to component development addressed throughout the following research. The first is the question of chemical and electrochemical stability. If either one of these tests if failed, the component will most certainly degrade, affecting total cell performance. Another aspect is the ability of the materials to be formed into the correct geometry. Costly material handling processes would negate the commercial viability of the system.

A last important factor is that of pore size matching between the porous electrode and the ceramic matrix. Impregnated electrolyte must be maintained in the ceramic matrix through capillary action, while still wetting the pores of the gas-diffusion electrode (see Figure 41). If the pores of the electrode are small enough to pull electrolyte from the matrix through capillary action, current and ion migration paths will be disrupted, as well as possible destruction of the wet seal formed by the matrix when wet with electrolyte. In addition, with electrolyte now flooding the porous electrode, the great advantage of increased transfer area will be lost as a smaller surface is presented to the gas flowing past the electrode, resulting in decaying performance.

These factors were kept in mind as the components of the full cell removal system were tested.

Electrodes

Many metals were investigated as electrodes, including stainless steels (SS 304, 347 and 430), oxidation-resistant alloys (Haynes 188 and Hastelloy-X) and nickel or lithiated nickel oxide. These materials were tested because they are commercially available in fibrous mesh form. Testing included cyclic voltammetry (CV) for corrosion resistance in the molten pyrosulfate ($K_2S_2O_7$) and longer duration stability tests, where samples were exposed to the molten salt and weight changes determined. The lithiated nickel oxide (a common molten carbonate fuel cell cathode material) was manufactured by soaking nickel mesh in 1M LiOH and heating to 600° C to form the lithiated nickel oxide. This structure was confirmed by X-ray powder diffraction, with the remaining phase being unoxidized nickel.

Of all the materials examined, lithiated nickel oxide appears to be the best. A CV on clean nickel wire showed a distinct oxidation peak, corresponding to the formation of NiO. After testing, the wire had gained an oxide coating on the area exposed to the melt. A CV on lithiated NiO mesh showed no oxidation peak. This test showed the electrochemical corrosion did not occur, but gave no conclusions as to chemical corrosion. Stability tests showed the formation of small amounts of $NiSO_4$, a corrosion product. This product is non-conductive, but no decrease in performance was seen during CVs and full cell tests (described below). The sulfates may be due to corrosion of either NiO or exposed Ni surfaces. Further evaluation continues on lithiated nickel oxide, but its polarization performance, with any membrane structure, is much better than the previously used perovskite electrodes, $La_{0.8}Sr_{0.2}CoO_3$ or $La_{0.8}Sr_{0.2}CuO_3$. Much of this improvement is due to the higher porosity (95%) and lower surface area

enhancement (actual = 12x superficial) compared with the perovskites (55% porous, 200x surface area enhancement). These factors reduce the possibility of electrode pore flooding.

Constant-current experiments with sufficient gas flow showed that the $La_{0.8}Sr_{0.2}CuO_3$, as an anode, decreases in polarization performance over time, whereas the lithiated NiO maintains, if not improves, its polarization performance. (Compare Figure 42 and Figure 43). After these experiments, the current polarity was switched, making the NiO the anode and the Cu-based perovskite the cathode. Figure 44 shows that the lithiated NiO electrode performs much better than the Cu-based perovskite as a cathode. Even as an anode, the lithiated NiO performs well.

It has been surmised by past researchers that the doping of the NiO lattice with the Li^+ ion results in a p-type semiconductor according to the Equation (58), which utilizes Kröger-Vink notation.

$$Li^{+} \rightarrow Li_{Ni}' + V_O^{\bullet\bullet} \qquad (58)$$

The equation shows that the proposed Li doped NiO lattice would conduct via holes, making it a p-type semi-conductor. This semiconductor should have the property of increasing conductivity with increasing temperature. It has been suggested, however, that the actual mechanism of conduction in the material is polaron conduction. This proposed type of conduction occurs when ions of the same type, but with valences differing by one, occupy adjacent lattice sites. The application of energy allows the change in valence of these adjacent states. In this case, the Ni ion may would be

present, after doping, in the Ni^{+2} and Ni^{+3} state within the lattice. The Ni^{+3} would exist to offset the charge imbalance imposed by the doping of the lattice with the Li^{+1} ion. Thermal excitation would allow the transfer of electrons from the Ni^{+2} ions to the Ni^{+3} ions. The concentration of carriers is dependant only upon the dopant level in the NiO, but the mobility of the electrons is dependant on the temperature and activation energy. A polaron-conducting material will thus show a similar dependance to temperature as a p-type or n-type semiconductor. In addition, the doping level for polarons will tend to be on the order of percent levels, whereas the doping level for a semiconductor can be on the order of parts per million. The formula for the doping of NiO with Li would be $Li_xNi_{1-x}O$.

Two lithiated NiO materials were studied; a proprietary nickel electrode from Energy Research Corporation (ERC) and a nickel mesh from National Standard (Fibrex). The Fibrex material is a sintered mesh of nickel fibers, each 25 microns nominal diameter, with powdered nickel carbonyl added to increase the structural strength of the bonds. The mesh is available in a variety of powder loadings, which has the effect of reducing the porosity of the mesh, while increasing the exposed surface area. The ERC electrode is a sintered nickel body made from particle precursors, producing an electrode with small pores. Since this material is proprietary in nature, only the relative effects of electrolyte wetting will be discussed.

National Standard Fibrex nickel electrodes were analyzed with X-ray powder diffraction to confirm the phases present after oxidation and exposure to electrolyte. After oxidizing the Ni electrodes in air at 600° C for 24 hours, the only NiO (Bunsenite)

was observed. A piece of lithiated NiO was treated in $K_2S_2O_7$ for 24 hours to determine chemical stability. The major phases were $LiNiO_2$ and NiO, with some $K_2Ni_2(SO_4)_3$. The $K_2Ni_2(SO_4)_3$ is a reaction product, most likely caused by reaction with exposed Ni on the surface. When the NiO is formed, the material goes through a 19% volume expansion (119% original size). Since the metal and the oxide have different thermal expansions, it is possible that cracks form in the oxide surface upon cooling, creating bare Ni surfaces prone to attack by $K_2S_2O_7$. X-ray powder diffraction analysis of used lithiated NiO electrodes was conducted. There were several phases present, predominately $LiNiO_2$, with some NiO and $K_2Ni_2(SO_4)_3$. The sulfate phase was present in approximately the same proportion as found in the stability tests mentioned above. No significant decrease in conductivity was found at the end of the run, even though non-conductive sulfates were present. It is unclear whether the sulfates result from corrosion of exposed Ni or SO_3 attack of NiO. The thermal expansion coefficients of Ni and NiO are very different, so that upon heating, some of the NiO may have separated, leaving Ni fibers exposed.

Ni electrodes from the Energy Research Corporation (ERC) were also tested. This proprietary material was lithiated and oxidized, at different temperatures, to determine the effect of oxidation temperature on room temperature conductivity (see Table V). At the lower temperatures, the surface exposed to air was darker than the underside, showing a possible limitation towards oxidation. All samples warped, due to either residual stress relief during heating or a loss of ductility in the oxidized area. The room

temperature resistances are tabulated below and show a strong dependence on firing temperature. All electrodes used in full cell tests were prepared at 575° C.

After electrode chemical stability tests proved successful, research progressed to characterize the surface and its interaction with the molten electrolyte. Figure 45 shows two scanning electron micrographs of the electrode material after its use in a full cell study. The electrode material is in the lithiated and oxidized state. The micrograph on the left displays the surface exposed to gas after use. The other micrograph exhibits the same surface after the electrode has been thoroughly washed. The effect of washing shows these electrodes to retain a large amount of electrolyte in the micropores, a symptom of electrode flooding. Many of the larger pores which run throughout the electrode are filled with electrolyte, reducing the surface area available for the removal of gaseous species. These SEMs confirm the behavior of the full cell during the run.

Figure 46 displays two SEMs of the raw mesh (50% fiber, 50% powder and 86% porous) at two different magnifications. The scan on the left, at 40x, shows the network of fibers with the powder covering the majority of the surface and providing an extensive network of macropores. The SEM on the right, at 3000x, provides a closer look at the micropores in the structure. The smooth nodules of nickel powder supply pores in the range of 1 to 10 microns, with very open gas flow passages between the micropores.

After treatment with LiOH, drying and subsequent oxidation of the Fibrex mesh, the surface of the nodules becomes coarse and the average pore size shrinks by about 20%. This shrinkage is caused by an expansion of the nickel as oxidation occurs (+19%

volume change from Ni to NiO). Figure 47 shows the pores to range from 1 to 7 microns.

Porosity experiments were then performed on five samples of both Fibrex and ERC electrodes, according to ASTM Standard Designation C 373-72. The results of the Fibrex electrodes are shown in Figure 49, along with the formulae used. The electrodes were heated to 150° C for 30 minutes to obtain the dry weight, boiled in water for 5 hours and then let sit overnight to obtain 25° C water. The saturated specimens were then carefully weighed, according to the standard, to obtain the saturated and suspended weights. These numbers are accurate to within 2%.

Mercury intrusion porosimetry was performed on the ERC and Fibrex electrode materials. The details of the ERC material will not be shown. A plot of volume % v. pore radius, Figure 50, shows that the vast majority (87%) of the pores are greater than 1 micron in diameter ($r = 0.55\mu$). Some of compiled data, Table VI, also showed that 57% of the pores were $\geq 4\ \mu$ in diameter, resulting in a good match with the electrolyte membrane structure.

Finally, the electrode resistance was measured while the electrode was subjected to temperature cycling. The electrode was attached to gold and platinum leads on either side, and the resistance between these leads measured. Corrections were made for the resistance of the leads, but not for the subsequent oxidation of the alligator clips used. It can be seen in Figure 51 that there is an initial large drop in resistance with increasing temperature. This is believed to be the effect of incomplete lithiation, with completion occurring in the first cycle. The resistance then follows the same curve, but tends to rise

slightly. This is believed to be the effect of oxidation of the stainless steel alligator clips used in connection. P-type semiconducting behavior is exhibited, with a resistance of approximately 1 Ω at 400° C.

Table V: Variation of lithiated NiO resistance with firing temperature and time.

Firing Temperature, and Time	Upper Surface Resistance (Room T)	Lower Surface Resistance (Room T)
500° C; 24 hrs.	220 Ω	1770 Ω
550° C; 12 hrs.	145 Ω	600 Ω
600° C; 2 hrs.	5 - 10 Ω	4 - 10 Ω
600° C; 2 hrs.	7 - 16 Ω	1.4 - 3 Ω

Table VI. Data for Mercury Porosimetry of Fibrex 50/50 mat.

Pore Radius, μm	Pore Diameter, μm	Intruded Volume, cc/g	% Volume Intruded
4.727	9.454	0.0139	3.8
1.947	3.894	0.2069	56.63
1.241	2.482	0.2579	70.58
0.8944	1.7888	0.2883	78.89
0.6942	1.3884	0.3052	83.52
0.5546	1.1092	0.3177	86.93
0.4554	0.9108	0.3264	89.33
0.3878	0.7756	0.3319	90.84

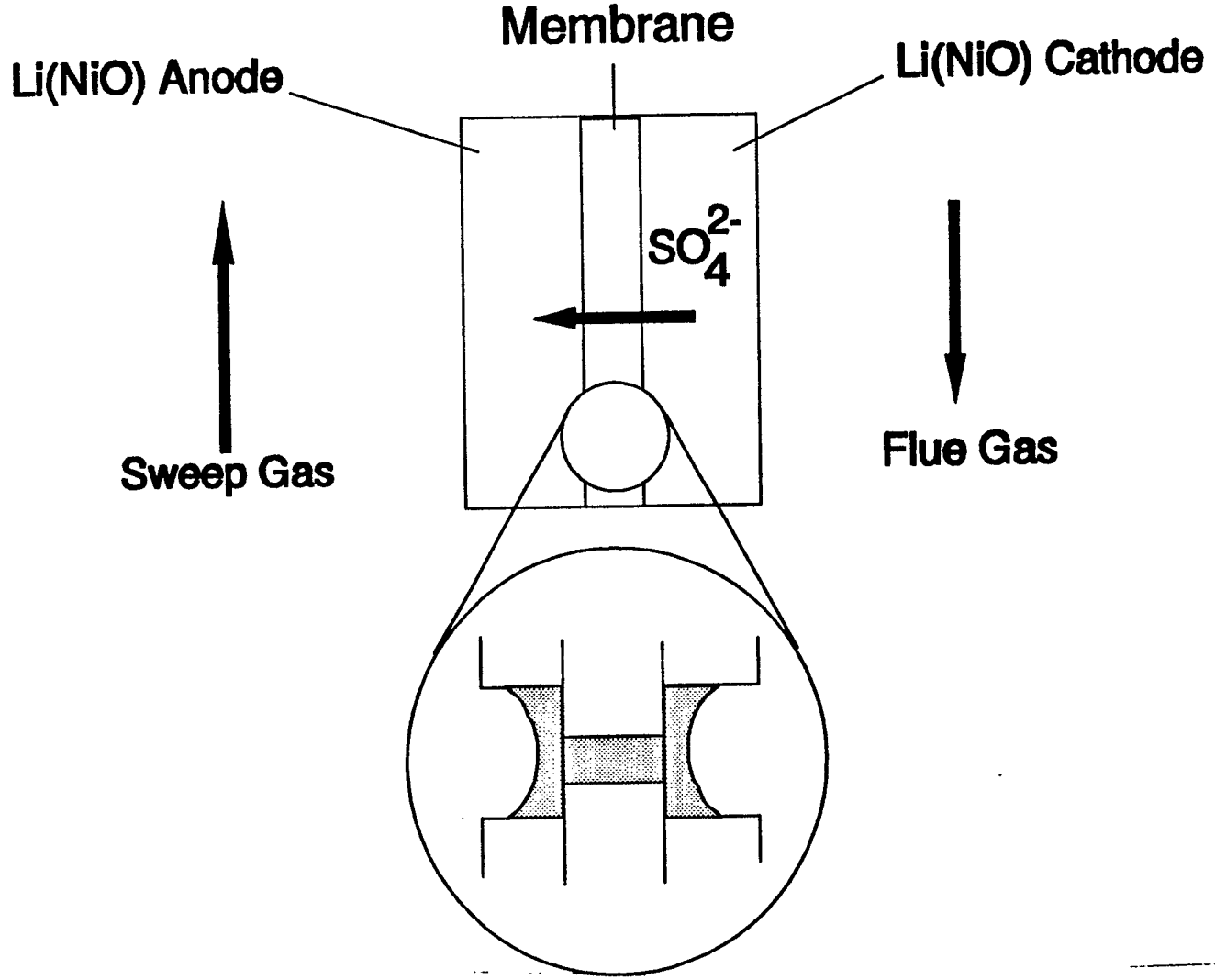

Figure 41: Pore wetting model desired in full cell removal systems.

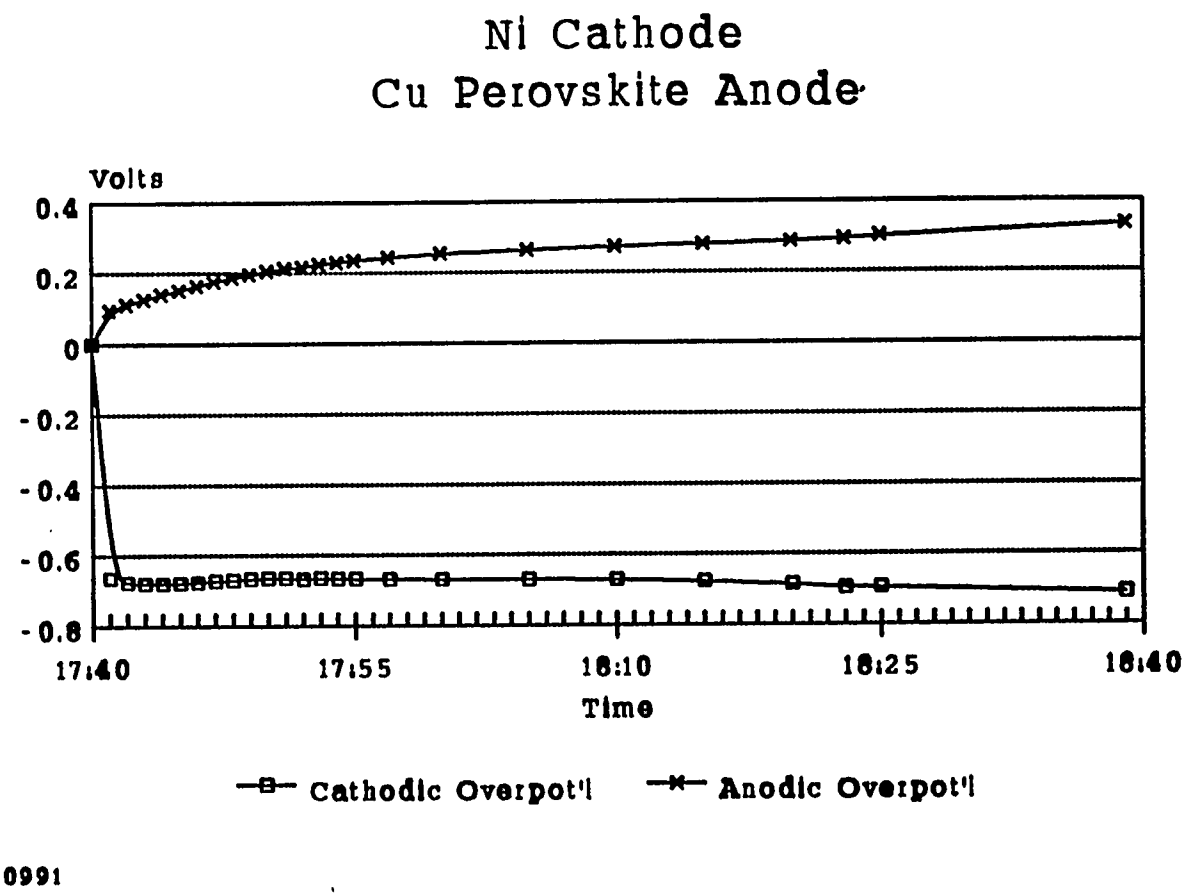

Figure 42. Cell electrode overpotentials at 400° C, 10 mA.

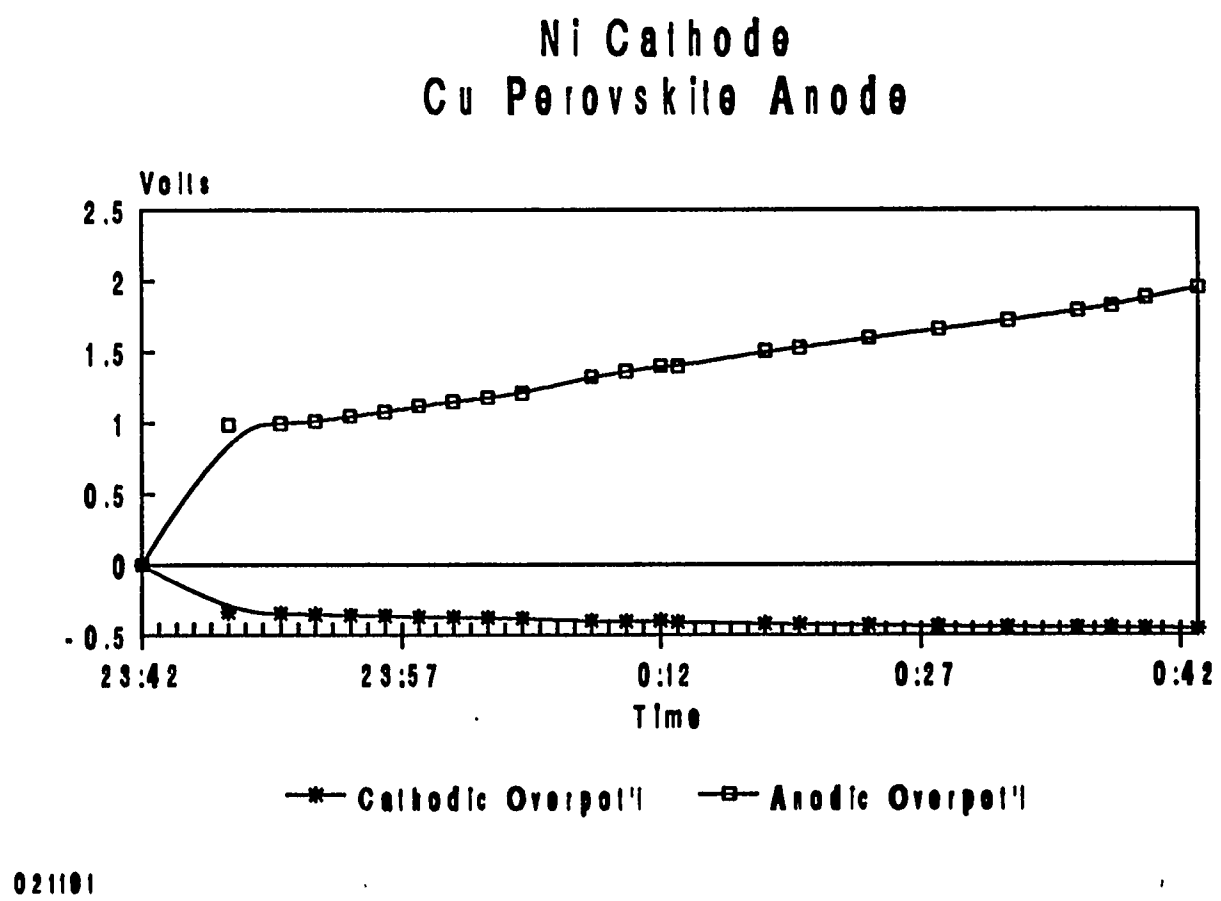

Figure 43. Cell electrode overpotentials at 400° C, 10 mA.

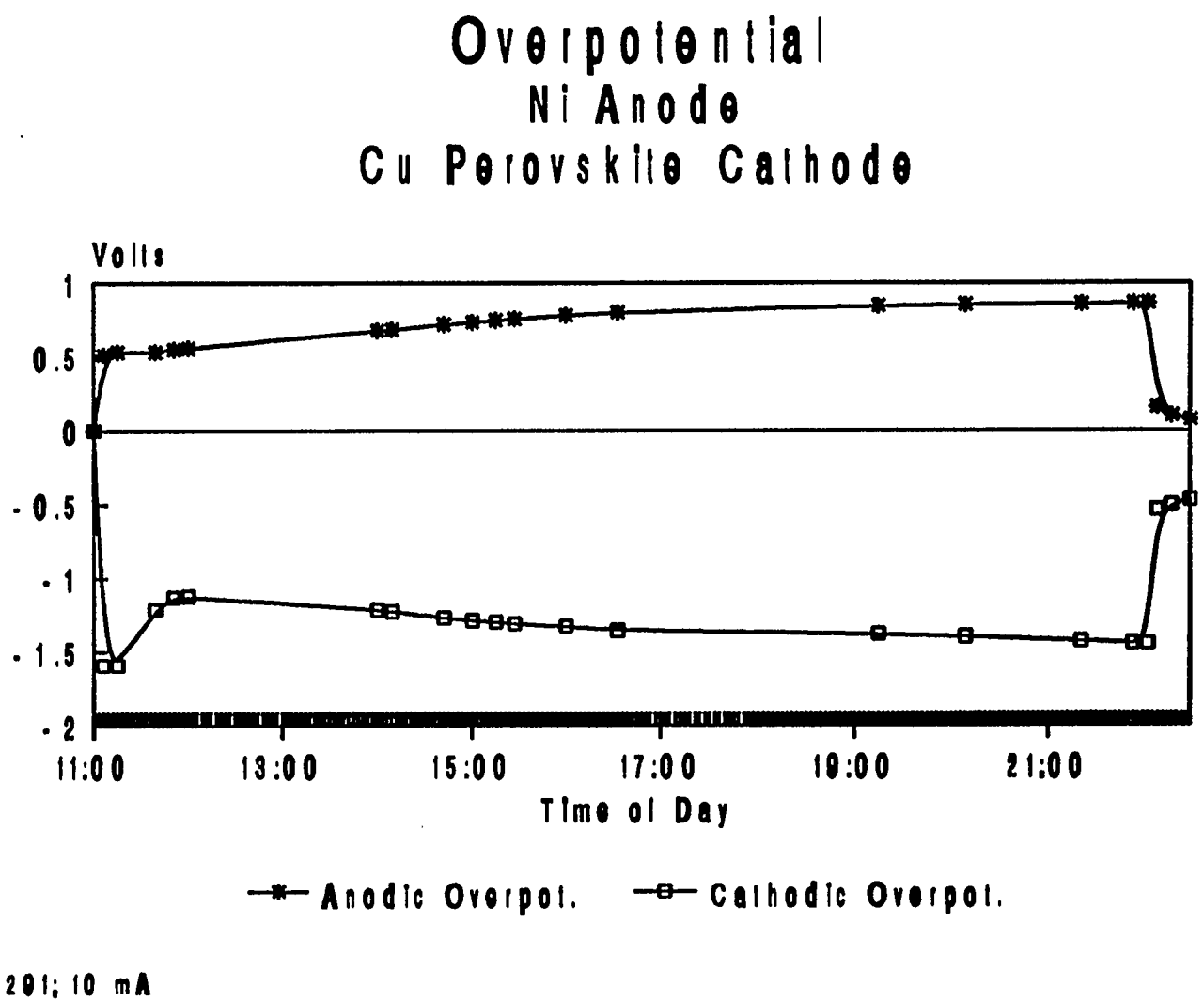

Figure 44. Polarization for cell electrodes at 400° C, 10 mA applied current. 76 ml/min of 0.3% SO_2, 3% O_2 in N_2.

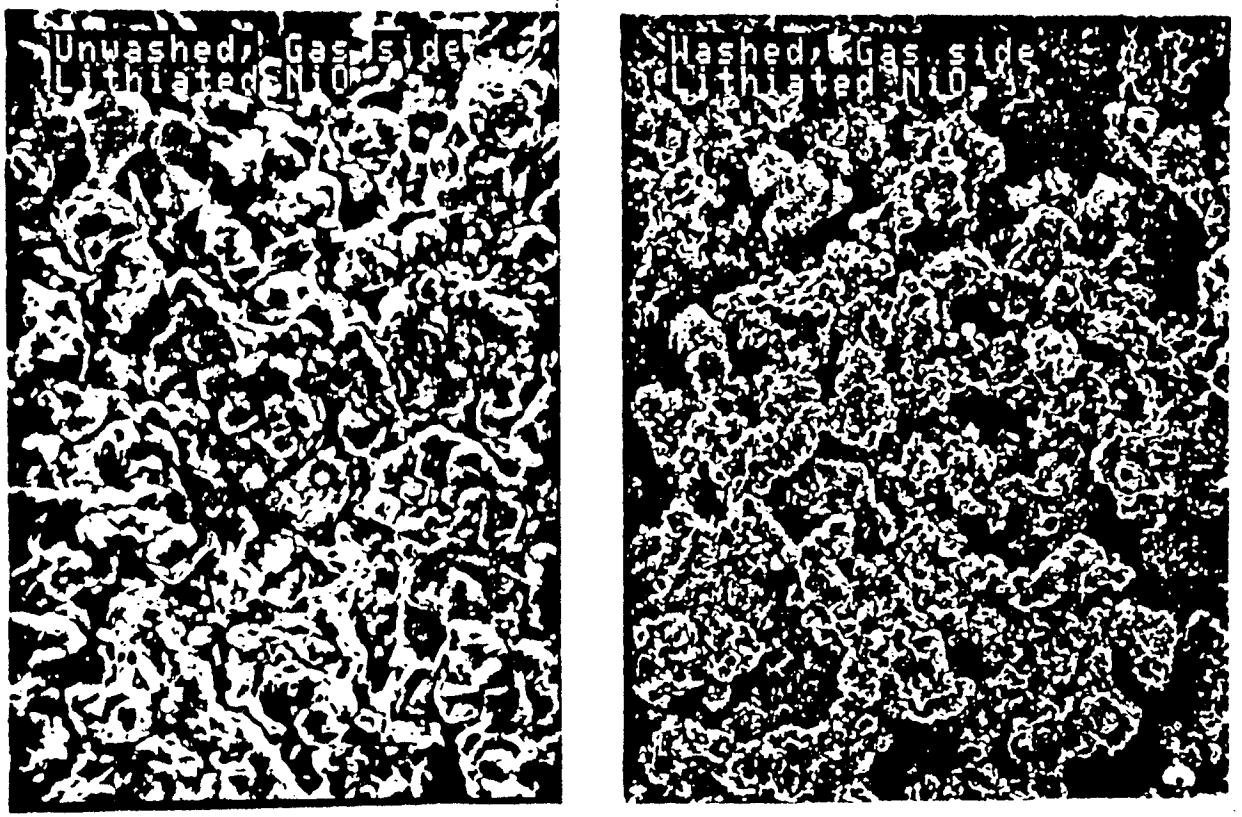

Figure 45. SEMs of ERC electrodes after use in the cell; unwashed (left) and washed (right). Both micrographs at same magnification.

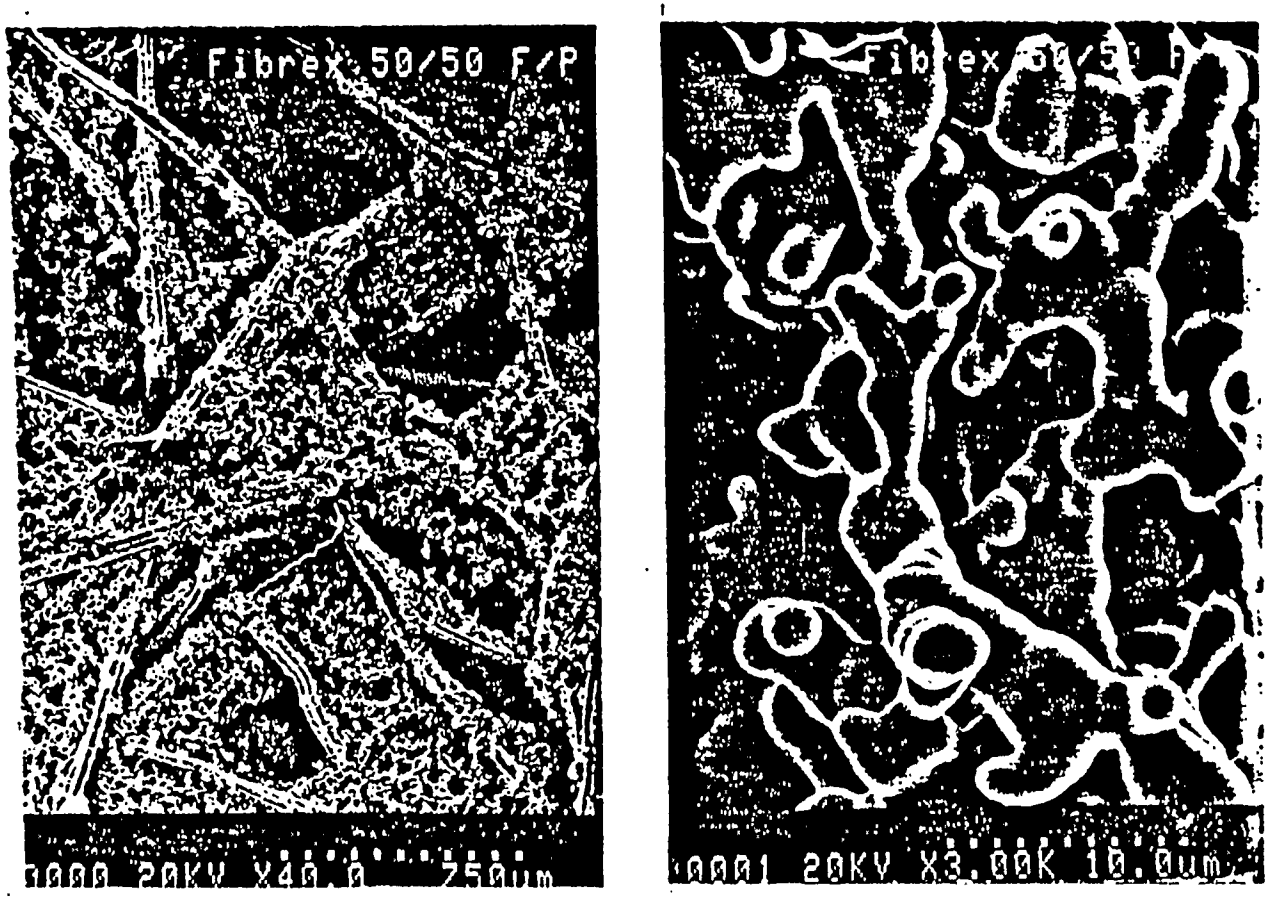

Figure 46. SEMs of Fibrex mesh, 50/50 : fiber/powder. Left, 40x; right, 3000x.

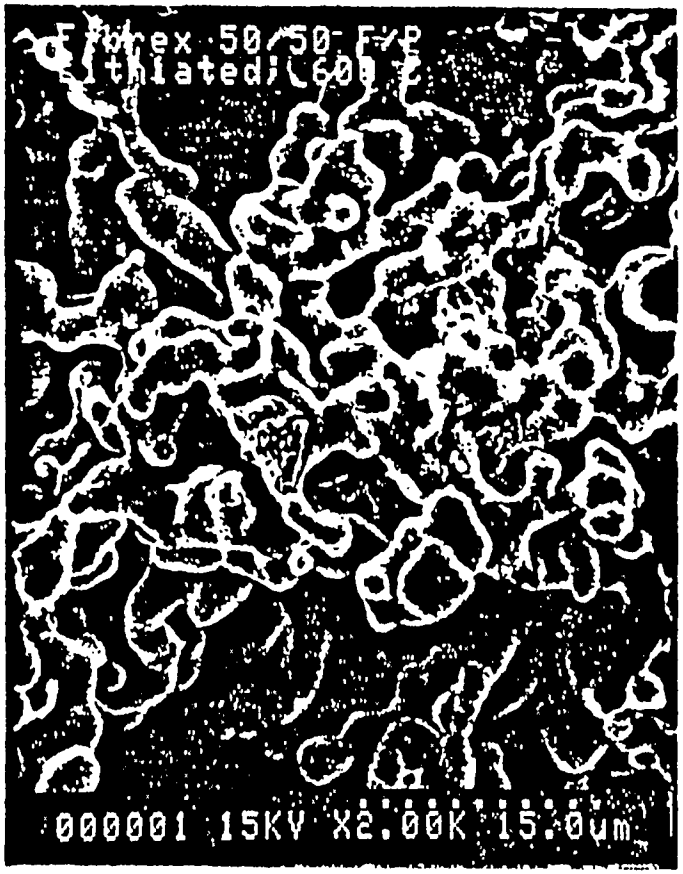

Figure 47. SEM of lithiated and oxidized 50/50 Fibrex Mesh.

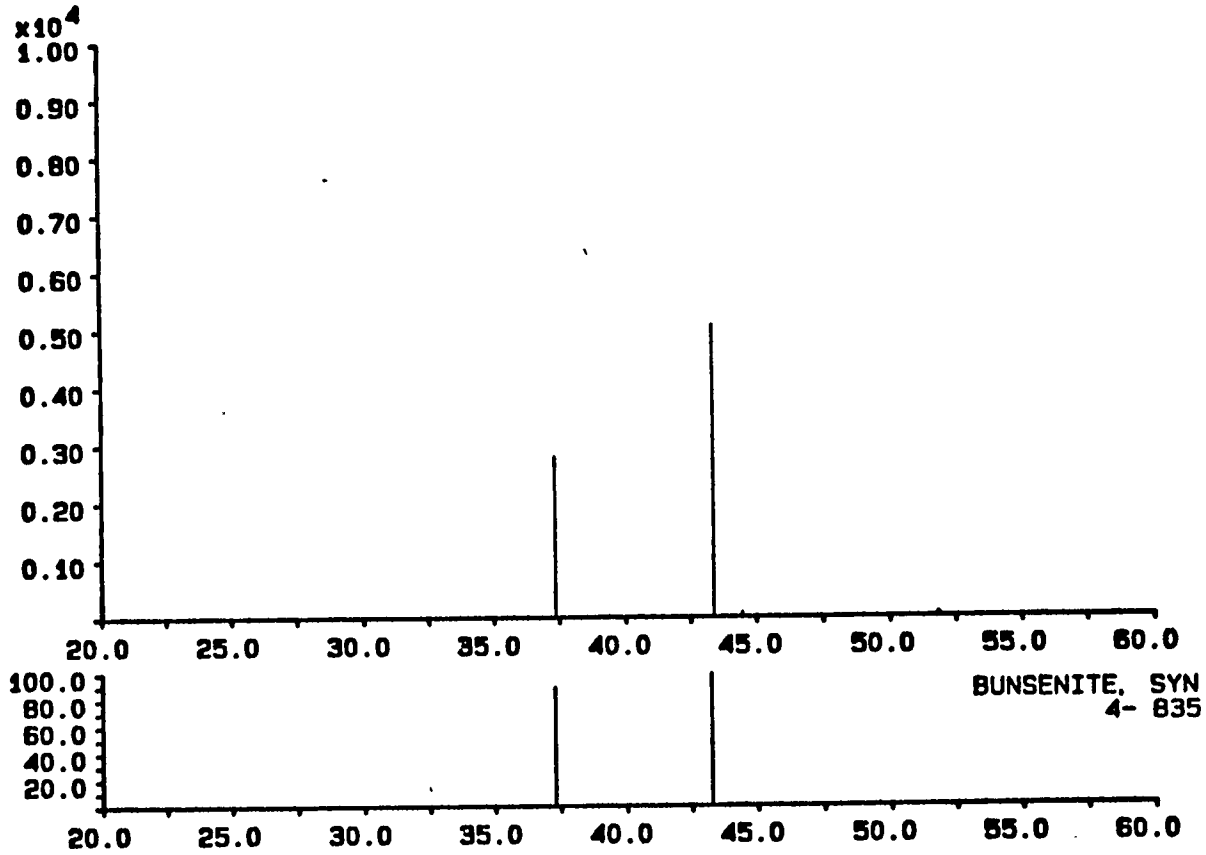

Figure 48: X-ray of oxidized and then lithiated ERC electrode.

Starting porosity of 86% (Fibrex)

January 13, 1993	Sample number-->	1	2	3	4	5	Averages	Standard Deviation
Measurement	Formula							
Dry Weight, g	D	1.466	1.674	1.945	1.152	2.045	1.656	0.324
Saturated Weight, g	M	2.644	2.967	3.585	2.159	3.698	3.011	0.577
Suspended Weight, g	S	1.274	1.454	1.661	1.013	1.792	1.439	0.277
		T(water)= 25C		density= 1 g/cc				
Exterior Volume, cc	V=M-S	1.370	1.513	1.924	1.146	1.906	1.572	0.304
Volume of open pores, cc	M-D	1.178	1.293	1.640	1.007	1.653	1.354	0.255
Volume of Impervious Portions, cc	D-S	0.192	0.220	0.284	0.139	0.253	0.218	0.050
Apparent Porosity, %	P=(M-D)/V*100	85.99%	85.46%	85.24%	87.87%	86.73%	86.26%	0.96%
Water Absorption, %	A=(M-D)/D*100	80.35%	77.24%	84.32%	87.41%	80.83%	82.03%	3.50%
Apparent Specific Gravity	T=D/(D-S)	7.635	7.609	6.849	8.288	8.083	7.693	0.496
Bulk Density, g/cc	B=D/V	1.070	1.106	1.011	1.005	1.073	1.053	0.039

Figure 49: Results of porosity standard on lithiated NiO electrodes (Fibrex).

Sample ID..... fibrex50 Filename..... DEN1.PRD
Instrument..... Autoscan 33 1X 0 - 33000 PSIG
Sample Description..... Fibrex 50/50; Lithiated 575C
Mercury Contact Angle.. 135.00 ° Mercury Surf Tension... 484.0 erg/cm
Sample Weight..... 0.8336 g Bulk Sample Volume..... 1.0000 cc
Minimum Delta Volume... 0.000 % FS

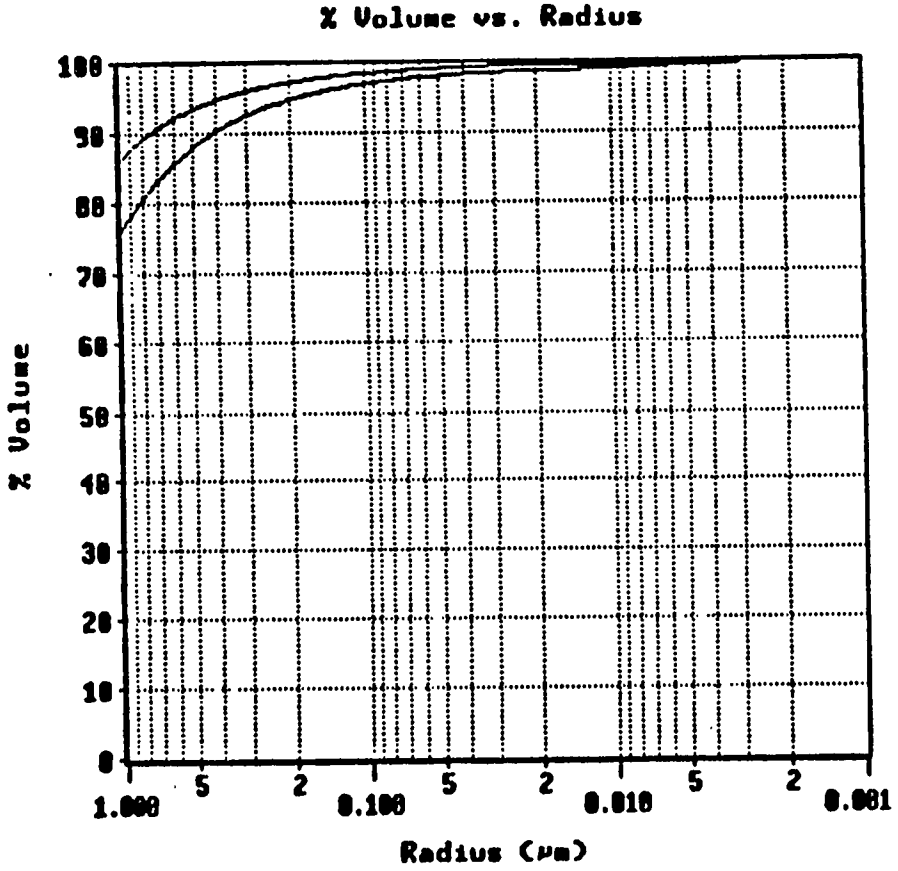

Figure 50. Mercury Porosimetry Curve for Lithiated and Oxidized Fibrex 50/50 mat.

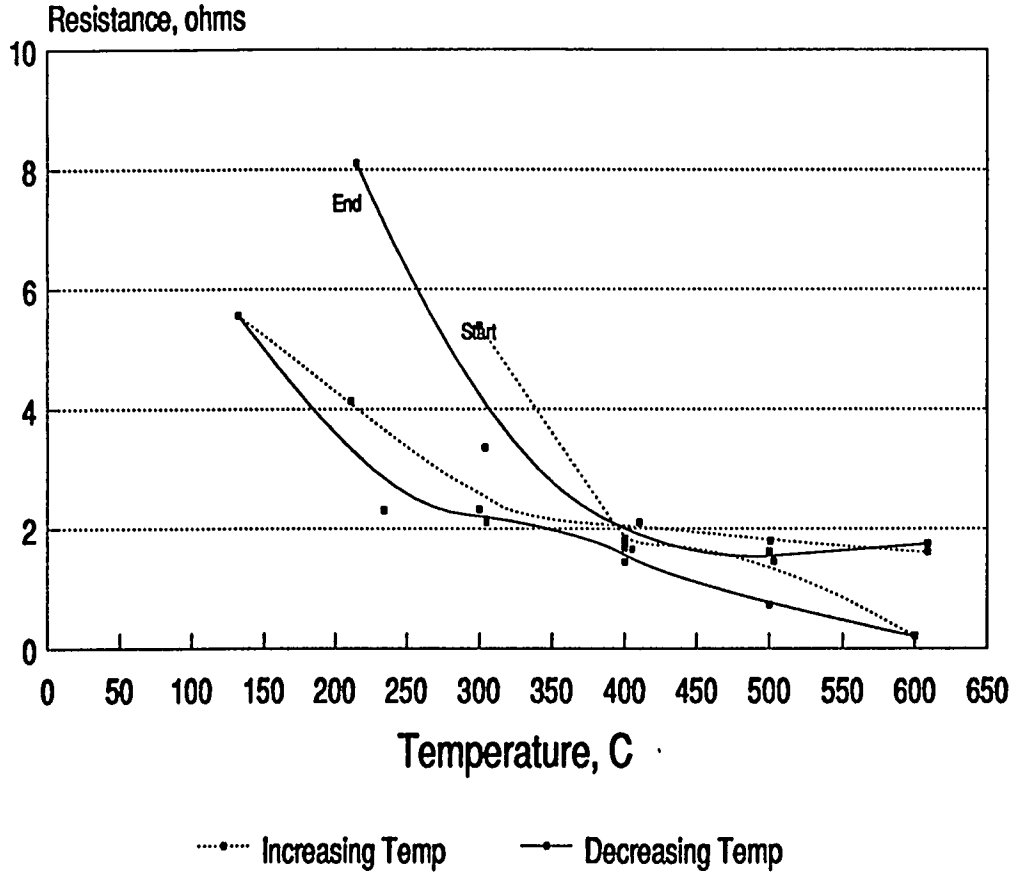

Figure 51: Cyclic resistance of a p-type semiconductor, LiNiO, with temperature.

Electrolyte Management

It is suspected that the 'in situ' introduction of electrolyte will lead to excellent gas seals in full scale testing of the SO_x removal cell. A search began for a method of management allowing the placement of electrolyte in the cell prior to binder burnout and cell heating. The presence of the electrolyte stabilizes the ceramic matrix, making it less susceptible to thermal and mechanical shock than an un-impregnated matrix.

The first attempt at this management was the tape casting of the electrolyte in a 78 vol% mixture with a polyvinyl binder. The result was an inhomogeneous mixture that yielded varying tapes. The slurry itself also presented difficulties, forming a jelly-like substance that was unmanageable. Only additional solvent allowed the mixture to be poured and cast.

A second attempt to tape cast the electrolyte in a 55.6 vol% mixture with the polyvinyl was made. The slurry was again unmanageable, and only the addition of 30 ml solvent (doubling the total volume) after 24 hours of milling allowed recovery of the slurry. The resulting tape cracked and adhered to the casting surface.

Attempts were then made to cold and hot press disks of pure electrolyte. The cold-press was carried out with 2.5 g electrolyte at 1050 psig for 5 minutes. The resulting disk was fragile and crumbled to the touch. Subsequent attempts at pressures of 1680 psig and 10 minutes produced the same results.

The hot press technique is somewhat arbitrary in this application. The presence of bisulfates in the pyrosulfate exposed to humidity greatly reduced the melting point; while bisulfates will melt and decompose to pyrosulfate upon heating, that melting is

not desirable in the hot pressing process. Hot pressing requires compression of the material at a point 10-15° C below its melting point. If that melting point is not well known, the procedure will tend to be ineffective. The melting point of the electrolyte was determined to be approximately 300-350° C, and a pressing temperature of 275° C was chosen. Three times, the die was baked in the oven for 5-10 minutes, and then pressed at 1050 psig for 1 minute. The resulting disk, while showing a slightly stronger mechanical strength than the cold pressed disk, still fell apart during handling.

A polymer was then used in conjunction with the electrolyte in the pressing. Polyethylene oxide was first milled with electrolyte for a minimum of 1/2 hour before placement between two cut aluminum foil circles in the pressing die. The die was then alternated between an oven and the press, for various numbers of cycles and at various temperatures. Pressing occurred at 1900 psig in all cases. This technique was tried with two different molecular weights of polyethylene oxide: 900,000 and 100,000. The results are shown in Table VII. Also shown in Table VII are the results of the use of hydroxyethyl cellulose, courtesy Union Carbide, in a combination with the electrolyte. The hydroxyethyl cellulose has been shown to burn out completely at a temperature of 350°C.

X-ray diffraction performed on an 80wt% electrolyte 20wt% hydroxyethyl cellulose disk after exposure to the atmosphere at 400° C showed the formation of multiple phases, with little to no potassium pyrosulfate detected. Reaction depletion of the pyrosulfate occurred. In addition, electrolyte was dissolved in an 80%/20% ethanol/toluene solution at 25° C. This solution is the solvent used in the polyvinyl

binder system discussed in earlier reports. The solution was dried with low heat, and filtered. X-ray diffraction, performed on the resulting solid, showed, again, a reaction had taken place. This result was expected, as pervious attempts to use the polyvinyl binder system had resulted in unusable material and membranes, confirming these methods did not represent the solution to in situ electrolyte introduction.

The most successful method of electrolyte introduction is to assemble the cell components minus the electrolyte, and raise the temperature under an air atmosphere. The matrix used was a tape cast ceramic. Organic components are burned away as the cell reaches its operating temperature of 400°C, leaving a porous ceramic matrix 50% porous by volume. Electrolyte is first brought to cell temperature, then introduced to the matrix through a hole cut in the upper housing for this express purpose. The molten electrolyte, by capillary action, is drawn into the porous ceramic, forming a viable membrane for use in testing. The hole used for electrolyte introduction is then sealed.

This method resulted in a practical cell, with a wet seal able to withstand a pressure of up to 1"H_2O both across the membrane and to the environment. All removal results utilized electrolyte introduction in this manner.

Table VII: Table of attempted electrolyte disk manufacture.

#	wt% Elect.	T(oven) (° C)	cycles	Oven Time	MW polymer	Mill Time (hr)	Results
6	66.7	155	3	7	900000	0.5	usable disk
7	81.4	100	3	10	900000	0.5	15% usable
9	66.7	165	3	10	900000	0.5	20% usable
10	50.0	155	3	15	900000	0.5	40% usable
11	33.3	162	6	16	900000	0.5	usable disk
12	66.7	156	1	7	100000	1.0	25% usable
13	66.0	158	2	10	100000	1.0	usable disk
15	85.7	158	2	10	100000	1.0	usable disk
16	80.0	158	2	10	100000	1.0	90% usable
17	75.0	158	2	10	100000	1.0	usable disk
18	85.7	158	2	10	100000	2.0	10% usable
19	75.0	158	2	10	900000	2.67	70% usable, but brittle
20 *	69.4	------	1	---	30000	1.0	60% usable
21 *	71.4	------	1	---	30000	1.0	85% usable
22 *	62.5	------	1	---	300	1.0	90% usable
23	85.7	158	3	20	100000	1.0	75% usable
24 *	55.5	------	1	---	300	1.0	90-95% usable
25 *	69.4	------	1	---	300	1.0	70% usable

* = denotes the use of hydroxyethyl cellulose, courtesy Union Carbide Corporation, which was cold-pressed.

All others use polyethylene oxide.

Electrolyte Experiments

Before any type of model for electrode wetting can be developed, the transport properties of the molten electrolyte must be known. While much data is available for potassium sulfate, little is known about potassium pyrosulfate, and even less about a mixture of potassium pyrosulfate and vanadium pentoxide. A simple experiment was performed to determine the density of the molten salt at 400° C.

A Pyrex graduated cylinder was used to determine the density. The coefficient of linear thermal expansion for Pyrex is listed as 0.033×10^{-8} [33] up to 300° C. The expansion of the cylinder due to the increase in temperature was therefore assumed negligible. The cylinder was loaded with a known weight of electrolyte, covered to maintain a constant SO_3 partial pressure, and heated. Readings were taken over a 4 hour period. The loss of weight was found to be 0.083 g ±.005 g possibly due to SO_3 formation or vaporization of any water present on the surface of the cylinder. This small loss was considered negligible. The beginning and end weights were averaged, and the density at 400° C was calculated as 1.997 g/ml ±0.05 g/ml. Error in this experiment may result from an inaccurate reading, or solidification of the molten salt when the oven was open to read the height. Solid density of the electrolyte is predicted to be 2.346 g/ml when using a correlation suggested by Prausnitz[34].

An attempt was then made to calculate the surface tension of the electrolyte. Lovering[35] has suggested Jaeger's[36] maximum bubble method as an excellent technique with which to measure the surface tension of a molten salt. The method requires the

$$p = \rho g h + \frac{2\gamma}{r} \qquad (59)$$

ability to measure the pressure required to force one N_2 bubble out of an opening at a known depth. This pressure is assumed to be due to the depth of the liquid and the force required to overcome the surface tension of the liquid, forming a bubble. The equation used is shown as Equation (59), where p=pressure, h=depth of immersion for tip of capillary, r=radius of the capillary opening, g=gravitational constant, ρ=density of the melt, and γ=surface tension. An apparatus was then developed for the experiment (see Figure 52), and a mercury manometer was used to measure the pressure difference.

The result is encouraging, although the range is large. The manometer read only a 6 mmHg difference, providing the largest relative source of error, and was treated as such in the analysis. The final value for surface tension from the maximum bubble pressure method was 138.8 dynes/cm ± 33.4 dynes/cm.

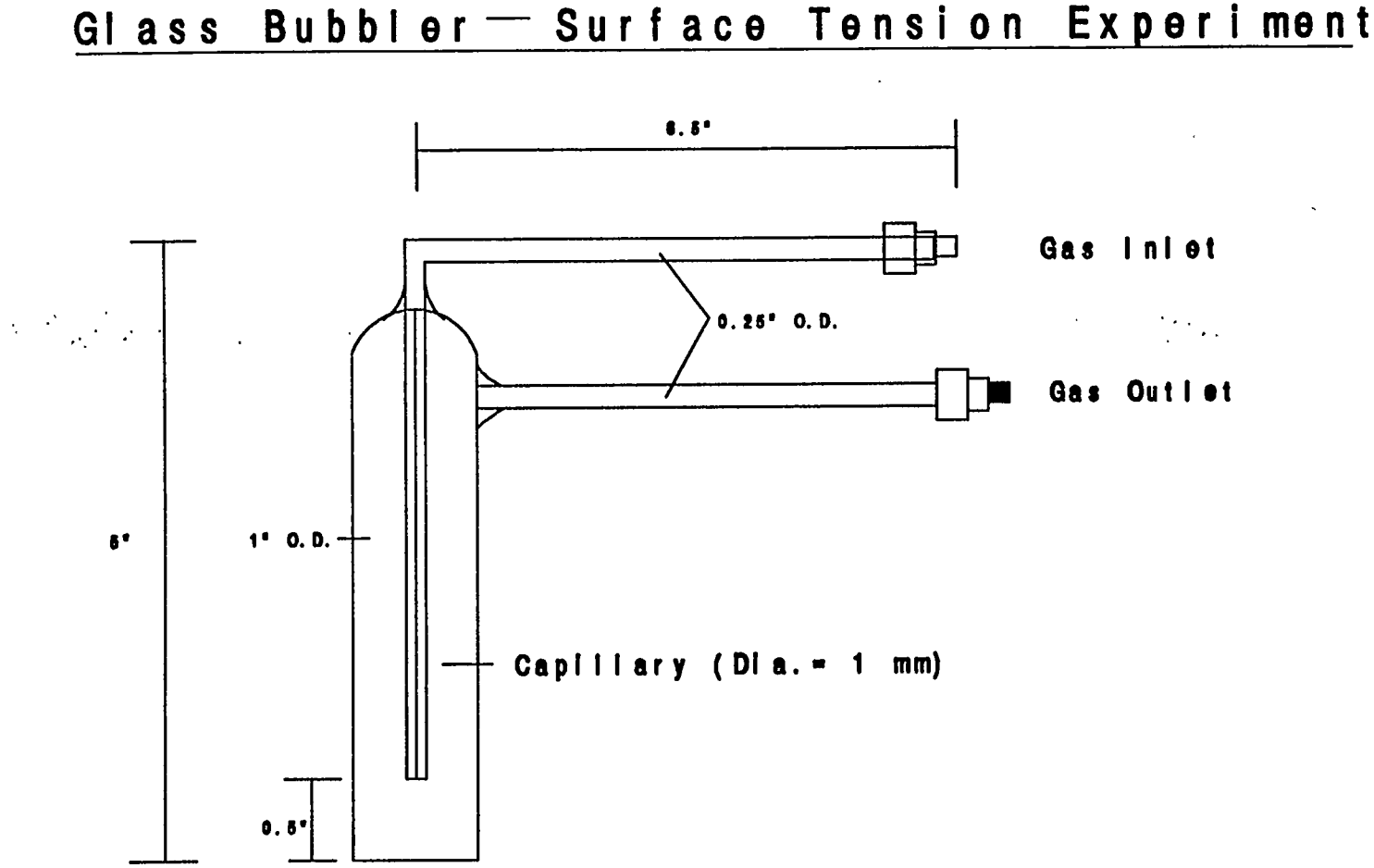

Figure 52: Capillary apparatus used in an attempt to determine the surface tension of molten electrolyte.

Matrix

General analysis was conducted on several candidate matrix materials. These included a magnesium oxide (MgO), zeolites, two borosilicate glass preparations, silicon carbide, three silicon nitride materials, crystalline and amorphous silica (SiO_2), and zirconia (ZrO_2).

Magnesium Oxide

Work initially used hot pressed MgO as a matrix material Franke[26] found that the MgO was actually a matrix precursor, with the true matrix material being formed through reaction with the electrolyte:

$$2MgO + 2K_2S_2O_7 \rightarrow K_2Mg_2(SO_4)_3 + K_2SO_4 \qquad (60)$$

so that the $K_2Mg_2(SO_4)_3$ became the true matrix material, and the resulting potassium sulfate dissolved in excess electrolyte.

Zeolite

Zeolites were screened via a preliminary test. The zeolites were dried in a vacuum desiccator for 48 hours, mixed with a quantity of uniform electrolyte (a single preparation of 5wt%V_2O_5 in $K_2S_2O_7$ heated to 400°C) and placed in sealed Pyrex tubes seen in Table VIII.

As the blends were heated, the electrolyte melted and penetrated the pores of the zeolites. Silicalite (ZSM-5) had wet spots of electrolyte throughout while other zeolites absorbed all of the molten salt. The difference in behavior was attributed to the polar nature of the zeolite. 13X, 4A, and 5A have lo SiO_2:Al_2O_3 ratios, making them highly polar. the nature of the matrix attracts the electrolyte and permits absorption in the pores. Silicalite, with a ration of 280, was non-polar and thus had reduced absorption.

Borosilicate

The borosilicate glass materials were prepared by wet milling <325 mesh (<44 microns) glass for 6 or 7 days.

Several tapes were cast from a blend of 45 volume percent (^{V}/o) glass in vinyl butyryl binder (Metoramic B73305). Varying results were found upon burnout, depending on drying conditions. Some tapes dried too rapidly, causing minor mud cracks on the surface. These mud cracks caused cracking of the membranes upon heating to T > 450° C. When drying conditions were better controlled, no cracking resulted in the membrane, allowing complete wetting of the matrix with electrolyte.

Zirconia

Two full cell tests were conducted during this quarter with Zircar fabrics. The fabric is made from yttira-stabilized (8 ^{W}/o Y_2O_3) zirconia, in either knitted or woven form. Since these materials worked well in the H_2S removal process, preventing gas crossover and retaining sufficient electrolyte, they were tested here.

During full cell testing, performance of the fabric decayed over time. Cell resistance increased, to the point of prohibiting passage of current. Post-mortem analysis showed the fabric to react with the $K_2S_2O_7$ electrolyte, leaving the electrolyte phase enriched in K_2SO_4. The remaining membrane was water soluble, confirming the reaction of the fabric, with the formation of water soluble zirconyl sulfates. These fabrics were dismissed as viable membrane matrices.

Silica

Amorphous SiO_2 was tested, pressed by a new leach technique developed at Georgia Tech. The chemical stability of this material needed to be tested, as well as the ability of the electrolyte to saturate the matrix, as crystalline silica is known to react with pyrosulfate. To this end, two samples of different manufacture were exposed to 90wt% $K_2S_2O_7$/ 10wt% V_2O_5 at 400° C in Pyrex petri dishes for 48 hours in air. The results were then analyzed using SEM and X-ray diffraction.

The first sample (10-90) surface was non-discernable (see Figure 54). The counterpart to this sample, which was tested as described above, wet throughout with electrolyte. The SEM analysis, however, only picked up what may be frozen electrolyte on the surface, as seen in Figure 55.

The second sample analyzed (3070) was of greater porosity, and apparently greater pore size than the first. The most striking feature of the surface is the rod-like formations. This matrix material easily saturated with electrolyte at a much greater

speed than the 10-90 sample. The resulting SEM of the saturated material is shown below.

The exposed samples were cooled, and x-rayed without washing (see Figure 56). Potassium pyrosulfate/vanadium pentoxide peaks were seen. The amorphous peak seen in the pure sample was also present. An extensive analysis of the possible sulfur and vanadia species failed to show any new phases due to reaction. This result indicates a chemical inertness of this proposed matrix material, but does not verify any electrochemical stability, as this material is very similar in structure and properties to the previously rejected ZrO_2.

DuPont's LUDOX AS-40 silica particle suspension was investigated also. When removed from suspension, the large agglomerates of silica formed, which were ground. However these particles did not wet with the electrolyte. Other silicas from Degussa showed the same inability to wet. Crystalline silica has been shown by other researchers to react with sulfate ions.[37]

Silicon Nitride/Silicon Carbide

One silicon carbide samples and two silicon nitride samples were obtained courtesy Phillips Petroleum, and one silicon nitride sample was obtained courtesy Oak Ridge National Laboratories. Particle analysis of each sample is shown in Table IX.

Samples of each material were subjected to chemical testing to determine chemical stability before use as a matrix material. Each material, seen in Table X, was exposed

to $K_2S_2O_7$ for 7 days at 400°C. These tests identified several stable chemical matrix materials for further study.

Several matrix materials were then used in full cell studies to evaluate relative polarizations, and identify the most favorable material for extended testing. Evaluation of the overpotential seen in Figure 57 suggests that of those materials tested, Si_3N_4 provided the most favorable polarizations.

Manufacture

Three methods of matrix manufacture were attempted, with varying success:

(1) Hot/Cold Pressing and Sintering

(2) Slip casting

(3) Tape casting

Pressing and Sintering

Dry powder was packed uniformly into a die of 3" diameter, to thicknesses of 1mm to 1.5mm. The die was then taken to a hydraulic press, with a applied pressure of 1132 psig. The resulting disk is then transferred to a firing plate, covered, and placed in an oven with a slow temperature ramping to 1150° C, held at that temperature for a period of time, and slowly brought back down to room temperature.

The first attempt resulted in an amalgamation of alumina and silicon nitride. The silicon nitride disk, after pressing, was fired on an alumina firing plate in an oxygen atmosphere. An unidentified liquid phase formed, resulting in warping of the disk, and the general defacing of the alumina firing plate,[38] and yielded a highly densified new phase, seen in Figure 58. Such a phase is not desired. Although it may be inert to the system, the ceramic will not allow impregnation by the electrolyte to any appreciable extent. Interconnecting microchannels are necessary for migration of sulfate from cathode to anode where it can be oxidized.It was suggested[39]that the firing be done in an inert atmosphere of nitrogen, and on a surface of either silicon nitride or silicon boride. In addition, a solid-phase diagram was prepared, shown in Figure 59, to ensure the material obtained from the process was the material desired.

A reaction-bonded plate of silicon nitride was obtained from Norton Industrial Ceramics. A test disk of 1" diameter was pressed and fired under high purity nitrogen (Holox, 99.97 purity), with excellent results. The plate obtained, however, was not large enough to support a 3" diameter disk.

Discussion with Paul Kohl, Professor, Georgia Institute of Technology, revealed that the chemical vapor deposition (CVD) of pure Si_3N_4 onto Si wafers was common technology. Four such wafers were prepared by Martin Ceiler, Chemical Engineering, Georgia Institute of Technology, with ~9000Å of pure silicon nitride deposited onto the surface.

A 3" diameter disk was pressed at a pressure of 1132 psig, and fired under high purity nitrogen. The resulting disk was found to be of sufficient mechanical strength,

The first attempt resulted in an amalgamation of alumina and silicon nitride. The silicon nitride disk, after pressing, was fired on an alumina firing plate in an oxygen atmosphere. An unidentified liquid phase formed, resulting in warping of the disk, and the general defacing of the alumina firing plate,[38] and yielded a highly densified new phase, seen in Figure 58. Such a phase is not desired. Although it may be inert to the system, the ceramic will not allow impregnation by the electrolyte to any appreciable extent. Interconnecting microchannels are necessary for migration of sulfate from cathode to anode where it can be oxidized.It was suggested[39]that the firing be done in an inert atmosphere of nitrogen, and on a surface of either silicon nitride or silicon boride. In addition, a solid-phase diagram was prepared, shown in Figure 59, to ensure the material obtained from the process was the material desired.

A reaction-bonded plate of silicon nitride was obtained from Norton Industrial Ceramics. A test disk of 1" diameter was pressed and fired under high purity nitrogen (Holox, 99.97 purity), with excellent results. The plate obtained, however, was not large enough to support a 3" diameter disk.

Discussion with Paul Kohl, Professor, Georgia Institute of Technology, revealed that the chemical vapor deposition (CVD) of pure Si_3N_4 onto Si wafers was common technology. Four such wafers were prepared by Martin Ceiler, Chemical Engineering, Georgia Institute of Technology, with ~9000Å of pure silicon nitride deposited onto the surface.

A 3" diameter disk was pressed at a pressure of 1132 psig, and fired under high purity nitrogen. The resulting disk was found to be of sufficient mechanical strength,

although this was not explicitly tested except in handling. It is known that the sintering of pure silicon nitride results in a final porosity of approximately 65% at a temperature of up to 2073 K[40]. The final porosity of the sintered membrane was estimated to be 50%, with incomplete sintering at the low firing temperatures.

The disk was used in a full scale run. Cracking was heard upon cell assembly, but the test proceeded in the hope that the electrodes had broken, leaving the membrane intact. The introduction of electrolyte into the matrix was an unusually slow process, and consequentially, excess electrolyte was added, flooding the electrodes. The concern that, in a time period of 1 hour, the matrix had not been completely wetted was found to unjustified post-mortem, as the small capillaries seem to simply take a longer amount of time to properly wet. The additional electrolyte plugged the outlet tubes. They were immediately cleaned, but gas-crossover began in the interim. The disk, upon examination, was noted to have a few hairline fractures, possibly due to assembly rather than post-mortem examination.

Slip Casting

Slip casting of the silicon nitride was attempted. Slip casting, is the mixing of the ceramic into a slurry, and pouring the slurry into a mold. The solvent is drawn off by the mold, leaving the resulting ceramic in the desired shape. Thickness is controlled by the solvent/ceramic ratio, speed of casting, and relative solvent humidity conditions. The casting solution may contain only the solvent, or some mixture of solvent, binder,

surfactant, or dispersant, all of which will affect the casting ability and resulting ceramic piece.

The attempt was made, again using the Phillips Petroleum silicon nitride, in conjunction with water as the solvent, and using Darvan C, courtesy Konrad C. Reiger of the R.T. Vanderbuilt Company, Inc., as the dispersant, to slip cast a membrane. Darvan C has a low ash content on burnout, and has shown low foaming in Vanderbuilt tests.

A slurry was mixed in a beaker, with DI-H_2O (18.3 Ω-cm), Darvan C, and silicon nitride in a, respectively, 48.3 wt%/0.3 wt%/51.4 wt% mixture, for a total of 20.570g. Mixture viscosity was visually estimated as correct. The slurry was then poured into the full cell housings, with electrodes in place, and the top housing was pressed onto the slurry top to form a membrane of a thickness of approximately 1.5mm. Unfortunately, the electrodes and housings were dry, and the water was quickly absorbed into the electrodes, setting the slurry in a less-than-ideal configuration. No seal was ever developed while used in full cell tests with an estimated amount of electrolyte, and the cell test was terminated. The resulting membrane utilizing this method was determined to be too thick in comparison to tape casting and pressing methods, as well as difficult to implement in method.

Tape Casting

The casting procedure used utilizes a polyvinyl butyryl binder, in a benzene/toluene solvent. This prepared mixture, including some dispersants and

surfactants, was obtained from Metoramic Sciences. The binder (see Table XI for characteristics of binders used) is added in an appropriate quantity, such that, after burnout, the resulting ceramic and ash left will occupy 50% by volume of the apparent volume of the ceramic disk.

After binder mixing, additional solvent and surfactant is added as needed to keep the solution at an appropriate viscosity. The slurry is mixed in an alumina ball mill, and is sonicated prior to casting.

Casting takes place on an appropriate surface, either glass, galvanized steel, or teflon, depending on the surfactant and dispersants used in formulation. Spacers are used so that a doctor blade may be drawn across the surface at a height of 1 mm relative to the surface. The mixture is poured onto the surface, and the doctor blade is drawn across to produce a uniform height. The wet tape is then covered completely to slow down the evaporation of the solvent, allowing the tape to dry uniformly, without cracking or undue stress. Drying is done overnight, or as required.

The resulting 0.30mm thick (corresponding to approximately 70% solvent by volume i the original slurry) green tape is then removed from the substrate, and cut to the proper form. It can be pressed or combined with other tapes as desired, as it is extremely pliable at this point. As the tape is subjected to higher and higher temperatures, as in full cell tests, the organics volatilize with oxygen, and burn out completely by 380° C, according to a Metoramic Sciences TGA, leaving only a small amount of ash. The resulting ceramic matrix may then be impregnated with electrolyte.

Various problems have arisen in the application of this much-desired process. The use of B (SiC) was attempted with little success except at low (11% ceramic) loading levels of the tape. The results of various attempts can be seen in Table XII. The one B membrane that did cast (#3, Table XII) was used, and was shown to have inadequate ceramic volume to maintain the matrix. A higher volume percentage ceramic is needed.

Another problem arose when attempting to cast C (Si_3N_4) due to the small particle size, with such a large surface area (80 m^2/g). There is a constant problem of surface wetting by the polymer due to the large surface area. The natural alleviation of this problem is the addition of binder to the system. This will result, however, in the reduction of volume percent ceramic, which leads, as previously discussed, to a mechanically intolerable system.

Additional solvent is then the possible solution. The result, however, tends to choose one of two avenues: the large amount of solvent evaporation leads to a cracked green tape; or the mixture is not homogenous, with viscous and less-viscous phases present, resulting in an non-uniform green tape. Neither of these two results is at all desirable.

Additional surfactant has been tried in an attempt to reduce the amount of solvent required to obtain a homogenous mixture. This carries its own problems: solvent evaporation will be slowed down at the surface, as the surfactant increasingly inhibits easy solvent evaporation as it travels to the surface with the solvent and accumulates due to its lower vapor pressure. Again, internal stress may result, as solvent is trapped inside the drying tape, resulting in cracking of the tape.

Solutions to this problem were discussed with Metoramic Sciences[41]. Among the solutions discussed is the variation of solvents to from just ethanol and toluene to include possibly acetone or MEK. Some of these may not be feasible, however, as the rate of evaporation would increase in some cases, possibly leading to cracking. Additional surfactants were also been discussed, including acetates, high carbon acids, and possible phosphoric acid, along with some amides, aminos, and polyesters.

Tape cast C and F, however, have shown excellent results due in part to their low surface area to weight ratios. Figure 60 shows the results of loading levels of 50 vol% F, after the binder is burned out. It can easily be seen that there exist interconnecting channels into which electrolyte can be impregnated. The picture does exhibit surface roughness, a sign that the particles are not as structured as might be desired. This may lead to lower capillary force at the surface, and possible loss of electrolyte from the matrix, neither of which is desired. Scrap was tested in air at 400° C to insure that the structure did in fact wet properly, and capillary action would carry the electrolyte through the ceramic structure.

To correct this problem, the tape is pressed prior to use in full cell testing. This pressing will tend to remove any trapped gases, and order the particles, especially at the surface. The results of such pressing can be seen in Figure 53. The surface of the membrane is much more uniform than the unpressed membrane. In addition, average pore size was qualitatively reduced, leaving smaller pores. Testing showed this matrix would saturate with molten electrolyte, though not as quickly as matrices with larger pores.

Membranes used in full cell testing generally consisted of two tapes, cut to appropriate size, and pressed together at approximately 9000 psig. These tapes were then placed in the cell under O_2 flow and allowed to burn out at 350° C. Electrolyte was introduced to the cell at this point, and the cell was sealed. Thickness of the membranes used averaged about 0.55mm.

Table VIII: Zeolite Mixture Test Samples. Electrolyte was 5wt%V_2O_5 in $K_2S_2O_7$.

Sample #	Zeolite	Mix Composition
1	13X	1.0000g 13X 0.9968g electrolyte
2	Silicalite	0.9633g Silicalite 0.9583g electrolyte
3	4A	0.9564g 4A 1.0007g electrolyte
4	5A	0.9564g 5A 1.0038g electrolyte
Control	-	0.9903g electrolyte

Table IX: Si_3N_4/SiC powder characteristics.

Binders									
Name	SC-P		SN-R		SN-P		Oak Ridge National Laboratory		
Manufacturer	Phillips Petroleum		Phillips Petroleum		Phillips Petroleum		UBE Ind., Ltd.		
Designation	B		C		D		F		
Formula	SiC		Si_3N_4		Si_3N_4		Si_3N_4		
surface area, m^2/g	10		90		5		10.9		
Particle size, µm	0.3		0.2		2.0		0.5		
Composition, wt%									
Si	69.0		58.5		59.0				
N			32.0		37.5		>38.0		
O	2.0		7.7		2.5		1.29		
C	29.0		1.8		1.0		<0.2		
trace, ppm	<400		<400		<400		<300		
Phase Composition	Beta >99%		Amorphous		Alpha >95%		Alpha >95%		

Table X: Results of chemical stability testing of candidate matrix materials.

Material	Result
Control	Decomposed to K_2SO_4
MgO	Reacted to $K_2Mg_2(SO_4)_3$
borosilicate glass	Amorphous - inconclusive
Silicalite	New phase - unidentified
SiO_2	Amorphous - inconclusive
SiC (B)	Stable
Si_3N_4 (C)	Stable
Si_3N_4 (D)	Stable

Table XI: Characteristics of Metoramic Sciences binders and modifiers.

Binders		
Name	K565-4	B-73305
Resin Type	Acrylic	Vinyl
Solvents	Isopropyl alcohol Heptane	Toluene Ethyl alcohol
Solids	24.89% (% of residue)	22.3%
Viscosity	60 cps	550 cps
Specific Gravity of residue	1.0	1.0
Specific Gravity of binder	0.79	0.88

Modifiers:		
Name:	M-1111	M-1114
Used when casting on:	glass/plastics	steels
Percentages to add to slurry:	0.1-1%	0.05-1%

Table XII: Ceramic Tape Casting

#	Ceramic	Vol% ceramic	Binder	Modifier	Results
1	SN-R (C)	50.0	Vinyl	M-1114	Would not flow despite sonication
2	SN-R (C)	48.3	Vinyl	M-1114	Additional solvent; cracked upon drying
3	SC-P (B)	11.0	Acrylic	M-1111	Cast well; pliable tapes
4	SC-P (B)	50.0	Acrylic	M-1111	Did not cast well; cracked upon drying
5	SC-P (B)	30.0	Acrylic	M-1111	Not homogen ous; cracking
6	SC-P (B)	40.0	Acrylic	M-1111	Cracked on drying

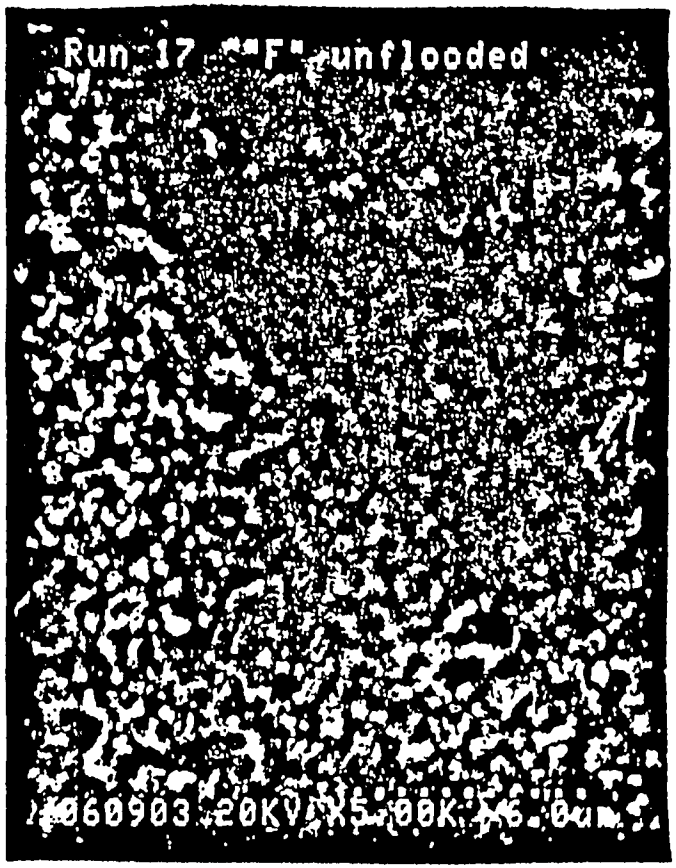

Figure 53: Pressed, tape cast F, showing an ordering of the surface over the unpressed tape.

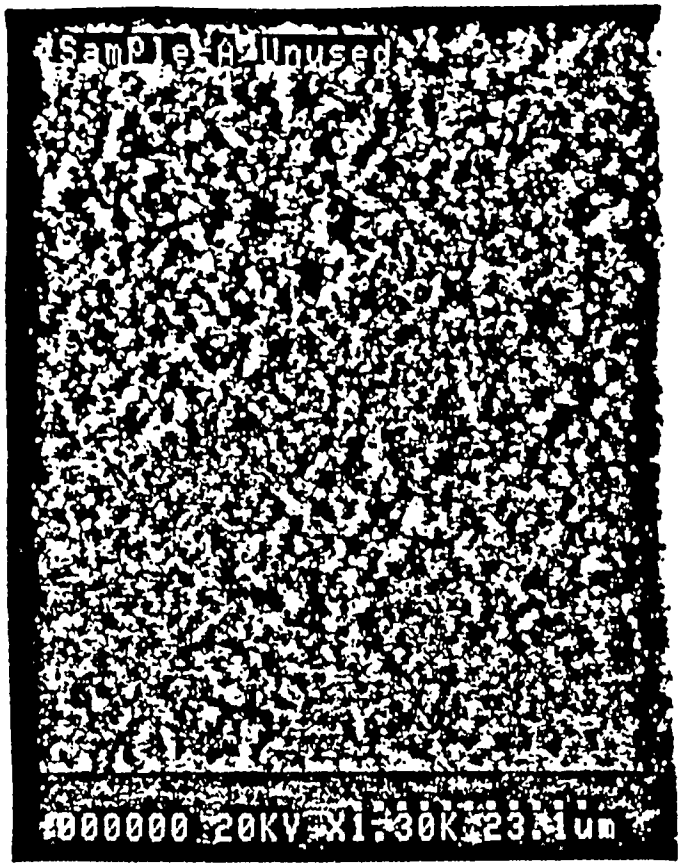

Figure 54: 10-90 amorphous SiO_2 micrograph.

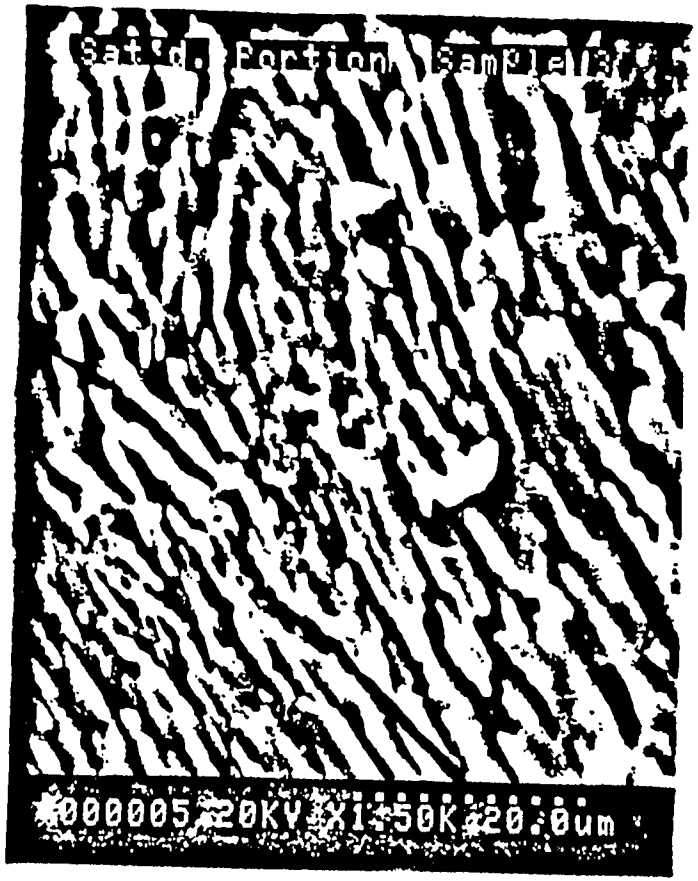

Figure 55: Micrograph of 10-90 amorphous SiO_2 saturated with electrolyte.

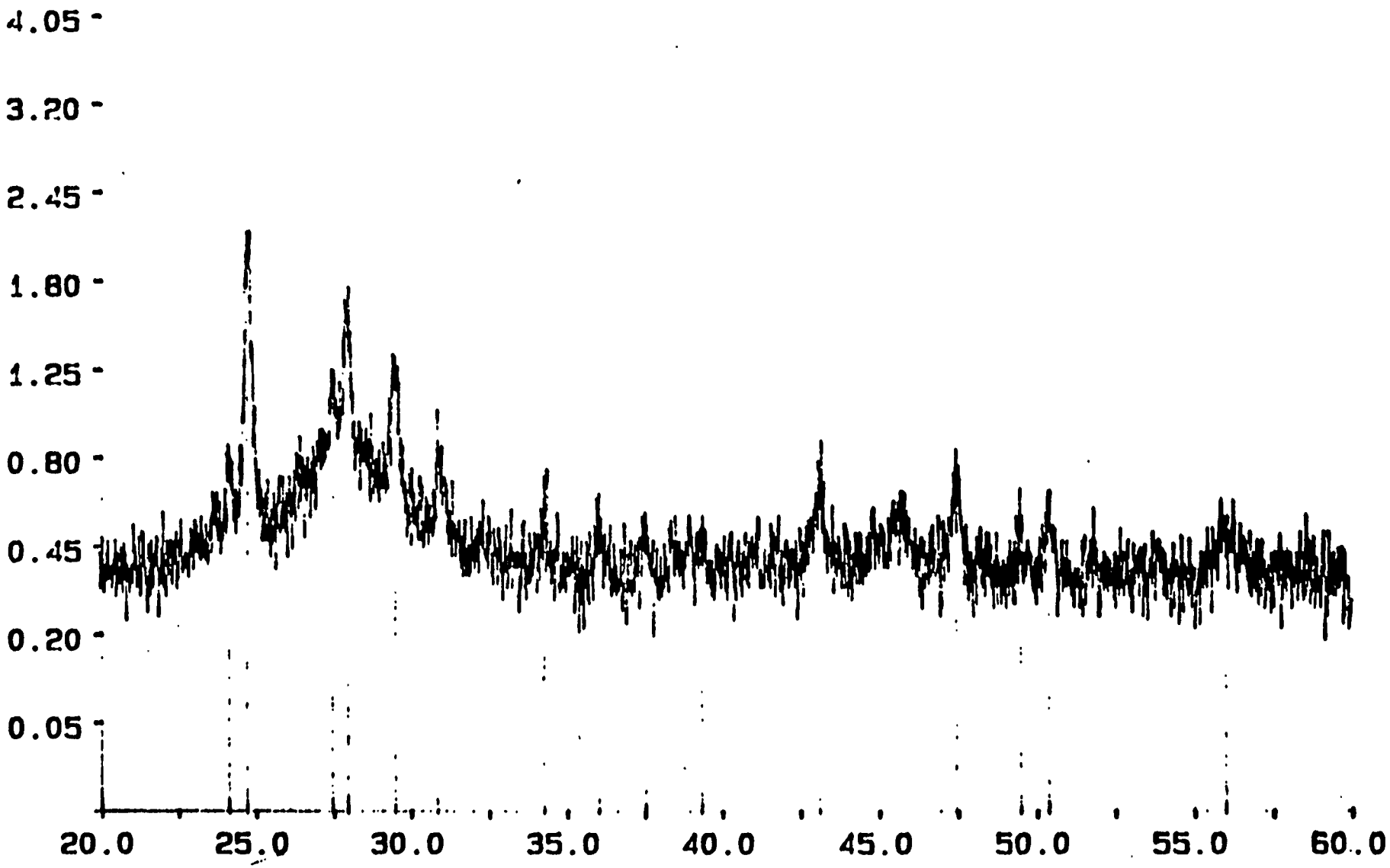

Figure 56: X-ray result of SiO_2 sol gel membrane after chemical testing.

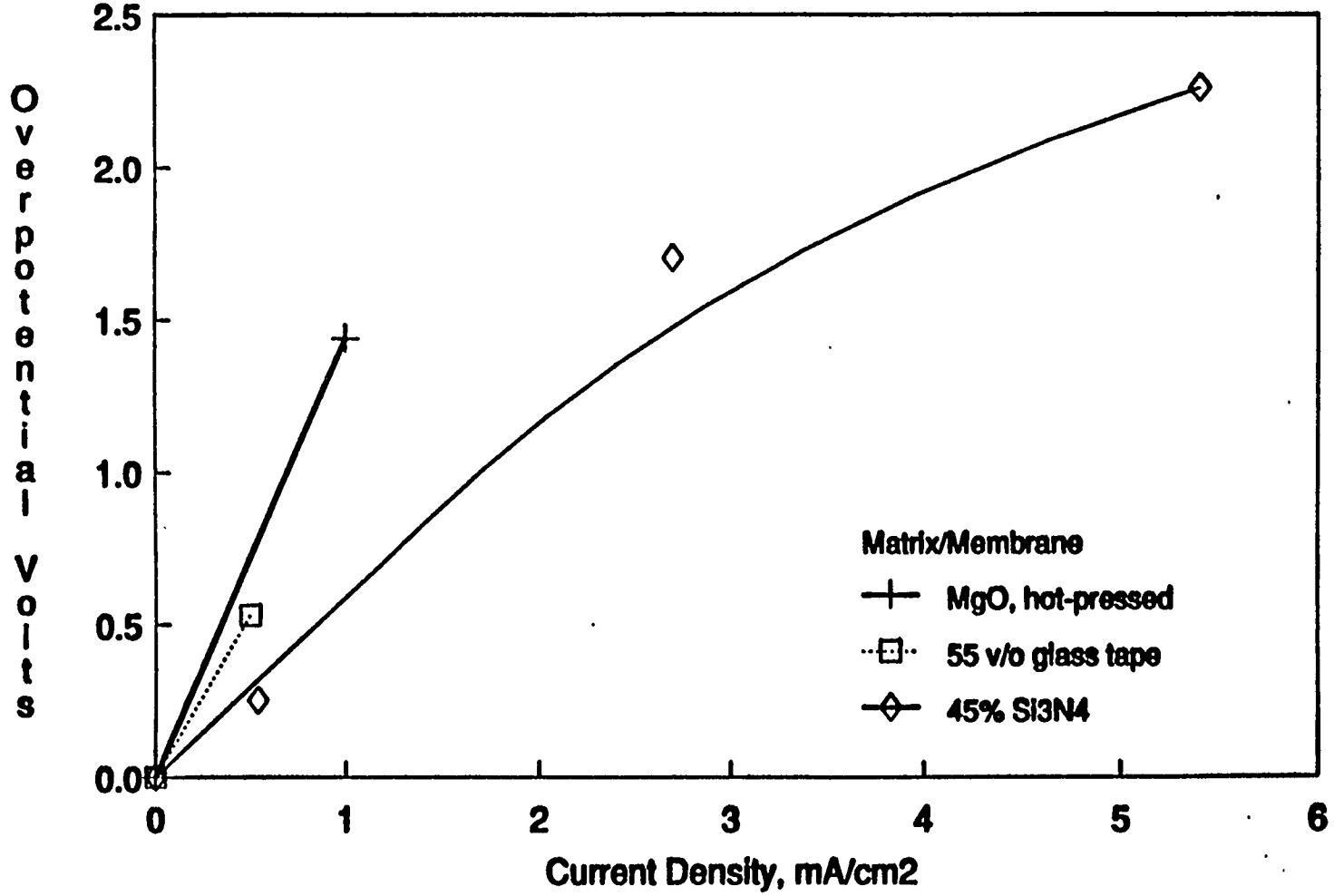

Figure 57: Cathodic polarization performance of different matrix materials using lithiated NiO electrodes.

Figure 58: Si_3N_4 sintered on alumina in air environment.

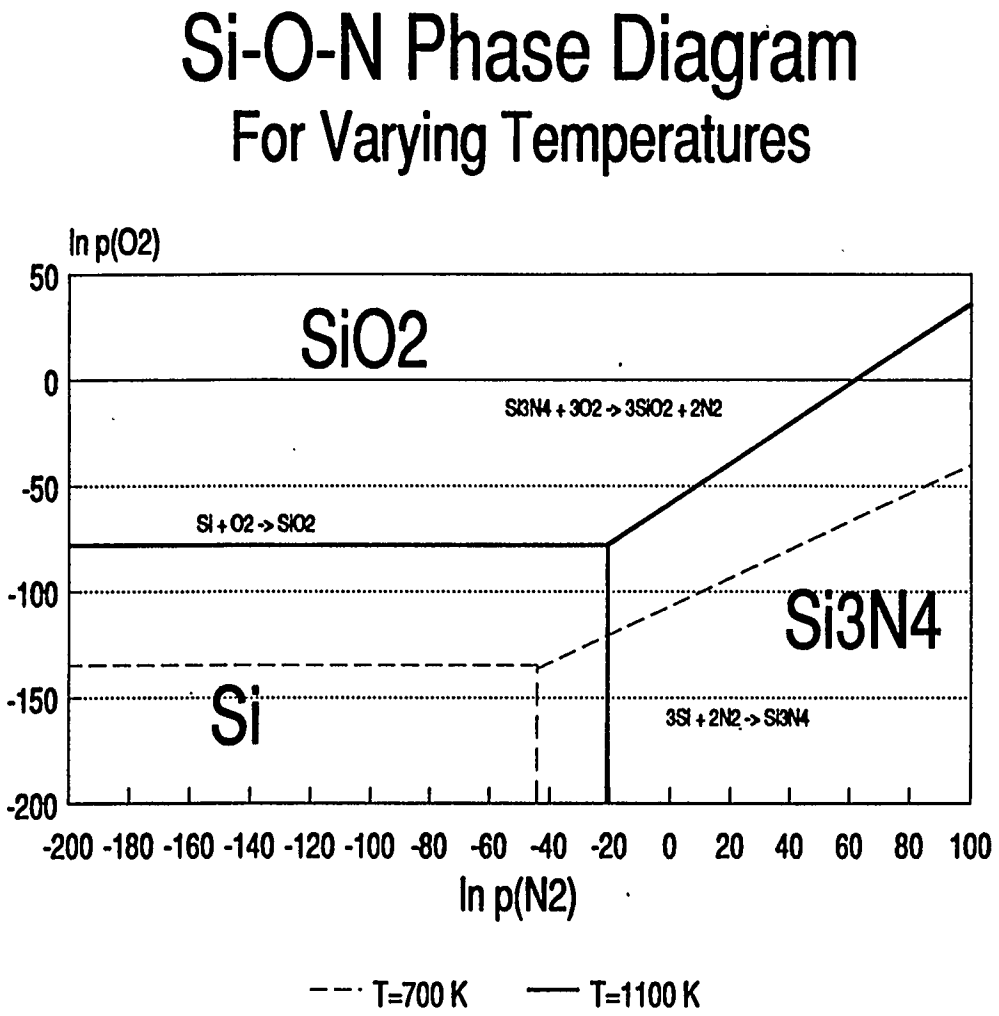

Figure 59: Silicon-oxygen-nitrogen phase diagram for the sintering of silicon at varying temperatures.

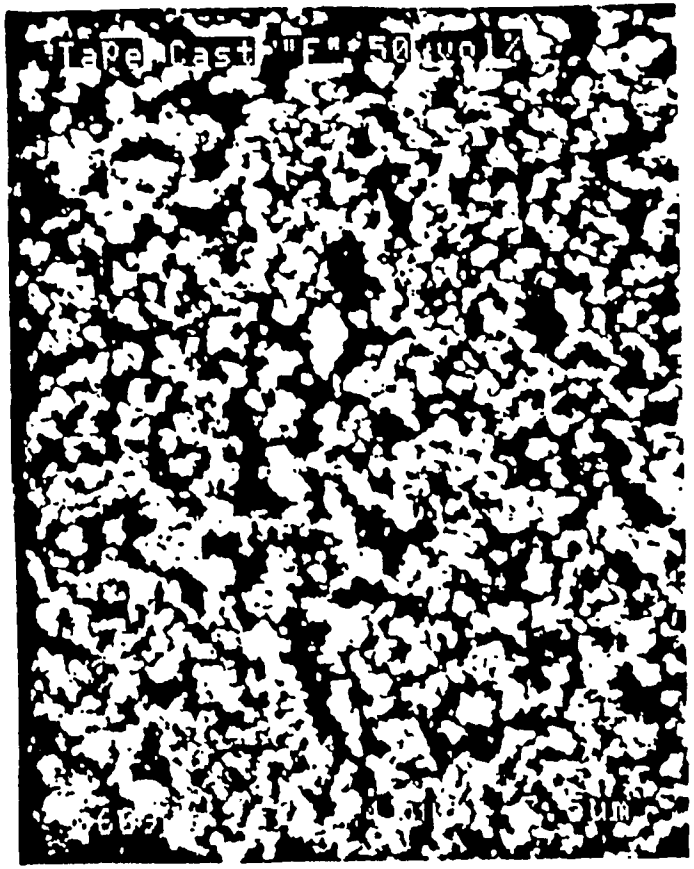

Figure 60: Tape cast F, unpressed, after binder burnout. 50 vol% loading.

FULL CELL TESTING

A laminated two-tape membrane was tested with lithiated NiO electrodes, achieving higher current densities and good polarization. The cell still produced quality data after 28 days on-line, compared to very early experiments which produced quality data for only three or four days. Most of this endurance came from the use of chemically stable electrode and matrix materials.

This configuration was very efficient at removing SO_3, showing visible decreases in the cathode exit plume three minutes after current was applied. A net generation of SO_3 at the anode was also detected within the first several minutes. Removal of 72% of inlet SO_x was achieved with current equal to 90% removal (50 mA). The residual SO_x detected in the outlet stream was partially in the form of SO_2, coming from the electrochemical reduction of $K_2S_2O_7$ (1). At low current densities, this generation was not a

$$S_2O_7^{2-} + 2e^- \rightarrow 3SO_4^{2-} + SO_2 \qquad (61)$$

problem, but as current densities exceeded 1.0 mA/cm^2, SO_2 generation became detectable. As the current density is increased, the gas flow increases in a linear fashion, sweeping the generated SO_2 away from the electrode surface.

The SO_2 generation was seen to increase with increasing current. At 50 mA, with 90% removal current equal to 100 mA, SO_x removal was 72%. The removal was in excess of 45% because of residual removal (30%) at open circuit. This phenomena always occurs if the electrolyte contains excess sulfate. When the current was doubled to that equal to

90% removal, removal dropped to 56%. During this run, SO_3 was barely visible in the cathode outlet stream at 100 mA, confirming the presence of higher levels of SO_2 in the effluent.

At 5 mA/cm^2, the incoming gas stream (275 ml/min, 36 cm/sec superficial velocity) did not remain in the inlet tubes long enough to provide adequate heating. The gas then enters the Pt pre-oxidation catalyst bed below 400° C, kinetically preventing equilibrium conversion to SO_3 (99% SO_3). Also, since the gas enters the cell cold, it chills the surface of the electrode, causing partial freezing of the SO_4^{2-} enriched catholyte, increasing the polarization at the cathode. The oxidation of the inlet SO_2 was solved by installing an auxiliary reactor, towards the end of this run, to convert the SO_2 to SO_3 before entering the cell. This did not solve the problem of SO_2 generation, because the gas partially cooled between the auxiliary reactor and the cell entrance. A modified cell design, allowing longer residence time in the heated tubes, should stop this problem.

After the auxiliary reactor was installed, several applied current experiments were applied. Although the results exhibited the same general trend of SO_2 generation with increasing current, removals were several percentage points higher using the auxiliary reactor, but not outside the range of experimental error. SO_2 generation was quantified via gas chromatography, and showed that above 20 mA current, SO_2 was present in the cathode outlet stream, at a level of ~13% of inlet concentration.

Currents as high as 200 mA (10.8 mA/cm^2 at the cathode) were reached for 10 minutes (after 3 hours at 100 mA), but with unacceptable voltages (-4.4V at cathode, +9V at anode) due to the cool gas stream and low SO_2 oxidation mentioned above.

Only minor degradation in performance was detected throughout the experiment. The electrolyte membrane did show some decay in performance, as measured by solution resistance and gas crossover. Many of the experiments were conducted at current levels above the system's ability to remove SO_x, due to the previously mentioned limitations. This had the effect of a net consumption of electrolyte through the electrochemical reactions at both the cathode and anode. The cathodic reaction (62) can

$$S_2O_7^{2-} + 2e^- \rightarrow 3SO_4^{2-} + SO_2 \qquad (62)$$

result in a net loss if the generated SO_2 is not oxidized, as seen in this experiment. The anodic reaction (63) can also consume electrolyte, since it proceeds unimpeded. After

$$SO_4^{2-} \rightarrow SO_3 + \frac{1}{2}O_2 + 2e^- \qquad (63)$$

running above removal limitations, the membrane is "dried", increasing resistance and eventually allowing gas crossover.

When gas crossover was seen, additional electrolyte was added, with the effect of stopping crossover, but with no effect on polarization. In a cell with high surface area enhancement electrodes, excess electrolyte has the effect of flooding electrode pores and increasing polarization. Because the present electrodes have a low enhancement factor (12x), excess electrolyte did not cause pore flooding. Any excess that could not be held in the membrane ran out the sides of the cell.

Overpotential behavior for all runs was very reproducible. Figure 61 demonstrates the reproducibility of the data, with only a minor shift in the initial anodic behavior between runs. The cathodic drift to more negative potentials over time shows a gradual

accumulation of SO_4^{2-} on the electrode, due to the less than theoretical removals (described earlier).

A standard polarization curve of overpotential versus applied current density is shown in Figure 62 for the present cell in comparison with previous cells. Note that the present configuration, with 45% Si_3N_4 and no flooding, shows substantial improvement in polarization performance over the other membranes. Five times as much current was passed with only a 50% increase in overvoltage driving force. This shows that the proper selection of matrix material and processing conditions can result in substantial performance increases, even with the above mentioned problems.

Another successful run was conducted with Fibrex electrodes and two 42 vol. % ceramic tapes laminated together. Superb seals were formed between the membrane and housings, but a decrease in sealing ability was noticed as the run progressed. Removal was quite high (>90%) and equivalent to stoichiometry, within the bounds of experimental error.

With applied current equal to 90% stoichiometric removal, cathodic removal of SO_3 reached 90% or greater, given adequate time. Several levels of V_2O_5 electrolyte loading were used, for reasons explained below. Figure 63 shows removal data after ten minutes of applied current. The data point at 12.5 mA/cm^2 was obtained by following a different current path (5 mA/cm^2 = 36% removal for 2 hrs. then 10 mA/cm^2 = 72% removal for 2 hrs.) which generated the required sulfate ions for high SO_3 removal. Figure 64 shows removal data for the same runs, but after one hour. Removal is seen to be near 90%, in accordance with stoichiometry, for most currents, within the bounds of

experimental error. Removal in excess of stoichiometry may be due to reaction with sulfate ions which have accumulated since current was applied, during the periods of lower removal, but is not outside the experimental error.

Looking at removal rates for 690 cc/min of cathode gas, excess removal above the stoichiometric level is seen for all applied currents in Figure 65 This is due to residual and excess sulfate in the electrolyte which is quickly neutralized by any SO_3 present in the gas phase. The excess sulfate is caused by the generation of SO_2 at the cathode (described next). Residual sulfate in the electrolyte from previous runs produces removal at zero current.

With the present configuration, a new phenomenon was observed. As current was applied, SO_2 was seen to exit the cathode, Figure 66. This is possible from the electrochemistry of the system as seen by Scott[42] in free-electrolyte, but had not been observed before in high surface area (perovskite) electrode full cell tests. As current rises, SO_2 is generated at a faster rate, one which overcomes the rate of oxidation by V_2O_5 in the electrolyte. It appears that SO_2 is diffusing out of the porous cathode before it can contact sufficient V_2O_5 and is carried off by the passing gas stream. Calculations of outlet flow rates showed that one-half of the generated SO_2 is being oxidized by the V_2O_5 and removed at the cathode, for a 5 wt% V_2O_5 electrolyte. To overcome this problem, more V_2O_5 in $K_2S_2O_7$ was added to the cell through the reference port. At 7 wt.% V_2O_5 in the electrolyte, three-quarters of electrochemically generated SO_2 was oxidized and removed, Figure 67.

At 10 wt.% V_2O_5, approximately 5/8 of generated SO_2 was oxidized and removed according to calculation of the slope of the line through the data with applied current (Figure 68). This rate of oxidation is less than that for the 7 wt.% V_2O_5 study, but two major differences were present: First, flow was continuously provided at a level such that 90% stoichiometric removal would occur at 12.5 mA/cm^2, so that SO_2 which escapes the electrolyte at lower current densities does not have sufficient residence time to diffuse back to the electrolyte. Second, SO_2 was present at zero current, showing that the pre-oxidation catalyst was not saturated with an equilibrium level of SO_2 at the start of the run. Post-mortem analysis will confirm actual V_2O_5 loading.

At the anode, SO_3 generation is seen to deviate from stoichiometry at all V_2O_5 levels, Figure 69 and Figure 70. This discrepancy can be explained by two causes. The first, gas leakage out of the wet seal, accounts for most of the discrepancy at the higher V_2O_5 and current levels. The second cause is attributed to residual sulfate ions accumulating at the anode, as seen by cathodic SO_2 generation data. When SO_2 is generated at the cathode and not oxidized and removed, excess sulfate ions accumulate in the electrolyte and migrate to the anode under the influence of the applied electrical potential. Sulfate is either oxidized or raises the melting point of the electrolyte to the point where the electrolyte freezes on the anode surfaces. Excess sulfate at the anode will absorb electrochemically generated SO_3 and neutralize it to form the $S_2O_7^{2-}$ ion. This second phenomenon is confirmed by polarization data.

The effect of increasing V_2O_5 content is minimal after this short duration. After one hour of applied current (Figure 71), a greater effect of V_2O_5 loading is observed. As

V_2O_5 content increases, polarization decreases. The anodic polarization suffers from sulfate accumulation at the lower V_2O_5 loadings. This finding proves that increased vanadia loadings oxidize more of the cathodically-generated SO_2 before it can escape from the electrolyte.

Also, as each current application progressed, the anodic overpotential and electrical resistance were seen to increase with time. This phenomenon confirms that accumulated sulfate migrates to the anode, where it raises the melting point of the electrolyte and retards the anodic electrochemical reaction. The increase in resistance shows that the sulfate is building up in the area of the electrical contact.

Electrochemical kinetic data can be obtained by properly treating the overpotential data. The Butler-Volmer equation of electrochemical kinetics,

$$i = i_0[e^{(1-\alpha)\eta F/RT} - e^{-\alpha\eta F/RT}] \qquad (64)$$

can be applied at low overpotentials in the linearized form of

to determine i_0, the exchange current density. The other parameters are R, the gas constant, n, the number of electrons involved in the charge transfer reaction, and F,

$$i_0 = -\frac{RT}{nF}\left(\frac{di}{d\eta}\right) \qquad (65)$$

Faraday's constant. Data from the present run was reduced using equation (2) and is presented in Table XII, along with data from Franke[43], who used $La_{0.8}Sr_{0.2}CoO_3$ electrodes. These data show that the electrochemical kinetics at the cathode have

improved 50% under the same conditions of electrolyte composition and temperature (5%, 400° C), further substantiating the improved performance of the lithiated nickel oxide electrodes. With an increase in V_2O_5, the exchange current density has increased four times. While there is some improvement here, free electrolyte studies have shown the exchange current density to be 30 mA/cm^2 in SO_3-saturated electrolyte. The discrepancy here can be attributed to partial flooding of the electrode pores and diffusional resistances.

Another full cell test used a 49 volume percent silicon nitride tape cast matrix with 10 wt.% V_2O_5 in $K_2S_2O_7$ electrolyte, lithiated NiO electrodes and Macor housings with platinum leads. Some difficulty was encountered during start-up with insufficient electrolyte loading, but was corrected with electrolyte additions through the reference electrode port in the top housing. Also, an excessive pressure drop was detected through the pre-oxidation catalyst bed at high flow rates.

Operation with 50 or 100 mA did produce some SO_2 at the cathode outlet, a possibility from the electrochemical reduction of pyrosulfate:

$$2S_2O_7^{2-} + 2e^- \rightarrow 3SO_4^{2-} + SO_2 \qquad (66)$$

Generation of SO_2 was 11% at 50 mA and varied from 17% to 24% at 100 mA, relative to inlet flow rate. For SO_3, removal (relative to equilibrium conversion of inlet SO_2) at 50 mA was 89% and 80% to 83% at 100 mA for a flow rate equal to 90% stoichiometric removal. One of the electrodes was kept in a vacuum desiccator and later analyzed with Electron Surface Characterization Analysis (ESCA). Investigation of the resulting peaks

showed no Ni-S bonds present, negating the possibility of nickel sulfides or sulfates as corrosion products.

The increase in SO_2 generation is due to a combination of factors. First, SO_2 generation is directly proportional to applied current, but does not follow the same slope in Figure 72. Second, as current increases, so does the gas flow rate, which means any gas escaping the membrane has a lower residence time and therefore lower contact time with the V_2O_5 in the electrolyte, however, the slope again does not follow that of the stoichiometric curve in Figure 72. Third, V^{5+} in the vanadium complex is reduced by SO_2 to V^{4+}, which has limited solubility in the melt. If this complex is not re-oxidized by gaseous oxygen, precipitation occurs, reducing the amount of catalyst available for SO_2 oxidation. This appears to be the case with the data.

Calculations of the rates of absorption of SO_2 and O_2 into vanadia-pyrosulfate melts and the re-oxidation of V^{4+} were performed to see if the melt chemistry is limiting removal performance. The work of Holroyd and Kenney[44] for SO_2 absorption into films of molten $V_2O_5/K_2S_2O_7$ can be applied to the present process to show that the initial rate of absorption is 36×10^{-9} gmol/cm^2/min. At 100 mA of current, SO_2 is electrochemically generated at the rate of 15.5×10^{-6} gmol/min. Complete absorption, assuming total escape of generated SO_2, would require a melt surface area of 430 cm^2, or an electrode surface area enhancement of 21.5. These numbers increase linearly with increasing current. Holroyd and Kenney also investigated the reoxidation of V^{4+} in the same melts[45] and found that V^{4+} has a maximum solubility of 4% at 400° C. From their reaction constants, the rate of reoxidation in this system can be calculated as 14.5×10^{-6} gmol/cm^2/min for

4% V^{4+}. With the rate of reoxidation being orders of magnitude faster than the absorption of SO_2, this step cannot be limiting.

However, Mars and Maessen[46] determined that there was a deviation from their normal kinetic behavior at lower temperatures (T < 415° C) for sulfuric acid catalyst pellets. They attributed this to either an increase in the rate-retarding effect of SO_3 or the formation of sulfovanadates, which would stabilize V^{4+}, reducing the rate of reoxidation. Both the rate of SO_2 absorption and the rate of reoxidation could be limiting and therefore an experiment will be conducted next quarter to determine the conversion of SO_2 to SO_3 bubbled through molten 10 wt.% $V_2O_5/K_2S_2O_7$.

Experimentation then focused on determination of the feasability of using commercial sulfuric acid catalyst (Haldor-Topsoe VK38) in the gas channels of the flow cell to convert the electrochemically generated SO_2 to SO_3 for removal. A tests was performed using thin cylinders of catalyst trimmed from 6 mm x 6mm catalyst pellets. This test showed a mass transfer limitation to the reaction rate (the horizontal asymptote in Figure 73) with a maximum rate of 10×10^{-6} moles SO_2/min or 30×10^{-6} moles SO_2/min/g catalyst at 400° C. At 375° C, this reaction was 5% slower, Figure 74.

Franke[47] shows the electrochemical reduction of the pyrosulfate as shown in Equation (66). This reaction must occur at the electrode/electrolyte interface due to the electron transfer required.

$$SO_2 + O_2 + 2e^- \rightarrow SO_4^{-2} \qquad (67)$$

$$2SO_2 + 2SO_4^{-2} \rightarrow 2S_2O_8^{-2} \quad (68)$$

$$SO_2 + O_2^{-2} \rightarrow SO_4^{-2} \quad (69)$$

$$E = E^o - \frac{RT}{nF}\ln\left(\frac{x_{SO_4^{-2}}\gamma_{SO_4^{-2}}}{P_{SO_2}P_{O_2}}\right) \quad (70)$$

The SO_2 then reacts with the superoxide ion according to Equation (69) and also with sulfate ions present. For the SO_2 to enter the gas stream, it must diffuse through the electrolyte, and into the gas stream. This mass transfer action is in direct opposition to the diffusion of SO_3 from the gas stream to the electrolyte where it reacts. (SO_3 dissolves in the electrolyte, and quickly reacts with the sulfate ion to form the pyrosulfate ion.) Should the superoxide ion not be present (due to the reduction of the vanadium pentoxide) in high enough concentration at the interface, the SO_2 can escape the cell, possibly the cause of the SO_2 production. The overall cathodic cell reaction can be written as seen in Equation (67). The Nerstian potential for this reaction can be written as in Equation (70), where the activity for the gaseous species is approximated as the partial pressure in atmospheres, and the activity of the solvated species is the mole fraction times the activity coefficient. E^o is the standard reversible potential, and E is the equilibrium potential. It would be suspected that increasing the partial pressure would have the effect of pushing the equilibrium to the right, thus producing more sulfate ions, reducing the amount of SO_2 production. while lowering the equilibrium potential.

The anodic overall reaction can be written as in Equation (71), so an increase in

$$SO_4^{-2} \rightarrow SO_3 + \frac{1}{2}O_2 + 2e^- \qquad (71)$$

the dissolved O_2 would increase the reaction resistance unless the availability of the SO_4^{-2} is relatively high.

Another possible explanation for the low removal is the removal of O_2 and SO_2 to form pyrosulfate through a complex of reactions utilizing complexes of vanadium

$$O_2 + 2[K_2\text{-}V_2O_4\text{-}3SO_3] \rightleftharpoons 2[K_2O\text{-}V_2O_5\text{-}2SO_3] + 2SO_3 \qquad (72)$$

$$[K_2O\text{-}V_2O_5\text{-}2SO_3] + 2SO_3 \rightleftharpoons [K_2O\text{-}V_2O_5\text{-}4SO_3] \qquad (73)$$

$$[K_2O\text{-}V_2O_5\text{-}4SO_3] + 2e^- \rightleftharpoons [K_2O\text{-}V_2O_4\text{-}3SO_3] + SO_4^{2-} \qquad (74)$$

$$2SO_3 + 2SO_4^{2-} \rightleftharpoons 2S_2O_7^{2-} \qquad (75)$$

pentoxide. The sum of the reactions contained in equations (72) through (75) is shown

$$O_2+SO_4^{2-}+2SO_3+2e^-+[K_2O\text{-}V_2O_4\text{-}3SO_3] \rightleftharpoons 2S_2O_7^{2-}+[K_2O\text{-}V_2O_5\text{-}2SO_3] \qquad (76)$$

in equation (76). The net result is the formation of pyrosulfate and a vanadium oxide complex through the utilization of oxygen, sulfate, and sulfur trioxide, and the use of two electrons. This mechanism is suggested by McHenry[48], and could explain the

apparent difference between the stoichiometric removal levels, and the actual removal levels.

The cell, again with pellets of VK38 in the flow channels, was run with the simulated flue gas over the cathode side of the cell at a 500 cc/min flowrate, and a pure N_2 sweep over the anode side of the cell. Removal data at this flow rate can be seen to be higher than that of stoichiometric removal rates in Figure 75. This may be due to the absorption of the gas into the cell in an attempt to reach a solubility equilibrium, to the presence of sulfates at the electrode surface, or to the method of mass flow evaluation.

As in the past, it was noticed that the polarity of the cell increased over time as seen in Figure 76, possibly due to the formation of a large, insoluble amount of sulfate at the surface of the electrode. The addition of 1g of electrolyte to the system decreased the polarity of the cell by approximately 65% at virtually constant stoichiometric removal rates. Should the reason for the increased cell polarity be the formation of a layer of sulfate, such a response would be expected, as the addition of the pyrosulfate/pentoxide mixture would tend to dissolve the sulfate formation, and place fresh pyrosulfate at the gas/molten salt/electrode interface. SO_2 production at the cathode was observed as the total applied current increased.

After taking a reading of the cell at 100 mA and a 500 cc/min flowrate, the partial pressure was doubled, and a measure of the SO_2 generation was taken. Figure 78 shows the extrapolated values obtained. It was not known, however, how much of this change in SO_2 generation was due to the electrochemistry of the cell, and how much was due to the oxidation (and possibly increase in activity) of the VK38 pellets in the channel. The

cell was then run for an additional 24 hours to determine the long term effects of doubling the O_2 partial pressure, and additional electrolyte was added. Figure 60 shows that the effect of the doubling of the O_2 was effective in reducing the SO_2 generation by 73%, with continuing decrease as time progressed, for a relatively constant cathodic potential of -6.2 Volts. The effect of the addition of electrolyte to the potential has already been established, but the SO_2 generation was again lowered, this time initially by about 50%. As the cathodic potential began to increase, the SO_2 generation also increased. This would suggest that the theory that the solidification of SO_4^{-2} on the electrode surface over time might be partially responsible for inability of the electrolyte to internally utilize the SO_2; the decreasing surface area available for O_2 transport could force the equilibrium in Equation (67) to the right-hand side in a perpetuating cycle.

Upon breakdown, the relative color of the VK38 pellets in the channel showed a change in color only for the pellets nearest the exit, suggesting that any in-channel conversion of SO_2 to SO_3 was taking place primarily at the exit, at approximately 0.36 micromoles/min based on one pellet. However, the change due to the partial pressure of O_2 present was not known. It was therefore determined that a full-scale cell test should be implemented without the VK38 pellets in the flow channels.

The temperature of the cell was brought up slowly under pure O_2 on both the cathodic and anodic sides in the attempt to insure the full burnout and removal of the organics from the two ceramic and four electrolyte tapes. As the run continued, the wet seal was determined to be virtually perfect, having the ability to withstand large pressure gradients. Unfortunately, the mass flow measurements did not converge

throughout the experiment, suggesting the absorption or adsorption of the gas into the organic present. Organic was observed in the exit tubes, and was cleaned. This process was to no avail as the mass balances continued to be in error, and more organic material streamed out of the cell. Measurements should therefore be considered relative only to this cell, and not compared against previous data.

Data was evaluated at $P(O_2)$ of 0.03, 0.06, and 0.12 atm, at flowrates of 500cc/min to 545cc/min. Increases from 500cc/min were due to the addition of O_2. Figure 79 shows a limitation, probably due to mass transfer, on the cathode side, increasing with O_2 partial pressure, while the anode shows a decreasing limitation with increasing cathodic O_2 partial pressure. Evaluation of the data at low overpotential leads to the exchange current densities seen in Table XIV. These values are in agreement with earlier values (at 0.03 atm O_2, and 10wt% V_2O_5) seen in Table XIII, but the removal rates obtained are far from stoichiometric as seen in Figure 80. These results suggest slower overall kinetics with increasing O_2 partial pressure, indicating a trade-off between increased reoxidation of the V^{4+} to V^{5+} and overall reaction rate.

With the inability of the mass flows to balance, the error involved is substantial. On average, the mass balances were 50% in error. Examination of the rate of SO_2 production shows a definite decrease from a partial pressure of 0.06 atm to 0.12 atm, but, for this same cell, the initial partial pressure of 0.03 has a lower production rate in the high current region, despite a large slope in the low current region (see Figure 81). The error in the mass balances denies any qualitative analysis of the effects of the O_2 partial pressure on the cell. The exceedingly high cell polarizations seen in Figure 79 at high

current densities may come from the inability of the cell to remove SO_3 from the cathode stream, thus channeling the current into internal reactions. This inability of the cell to achieve lower SO_2 production may be due to organics present from the burnout, reducing the surface area available for mass transfer. In addition, the SO_4^{-2} formation at the surface may further reduce the available surface area, and lead to further formation of SO_2 over time. The increasing polarization of the cell over time may explaining the conflicting SO_2 production at low partial pressures, as the initial runs were done at low partial pressures, without addition of electrolyte at any point during the run.

Table XIII. Exchange current densities.

wt. % V_2O_5	T, ° C	i_o, mA/cm^2
5%	400	0.052
7%	400	0.115
7%	425	0.106
10%	400	0.133
5%, Franke[2]	400	0.033

Table XIV: Variation of exchange current densities with O_2 partial pressure.

$P(O_2)$, atm	Exchange Current Density, mA/cm^2
0.03	0.135
0.06	0.082
0.12	0.050

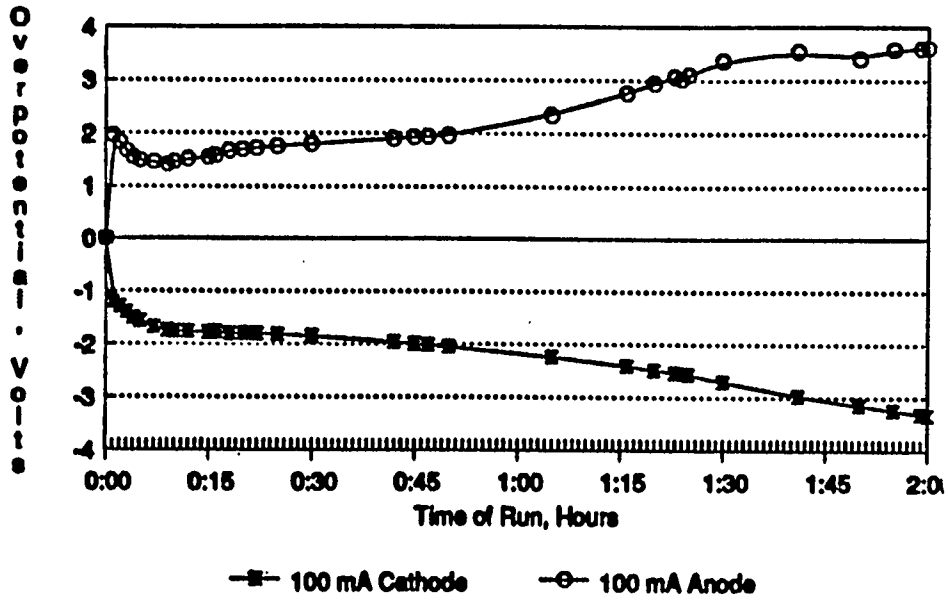

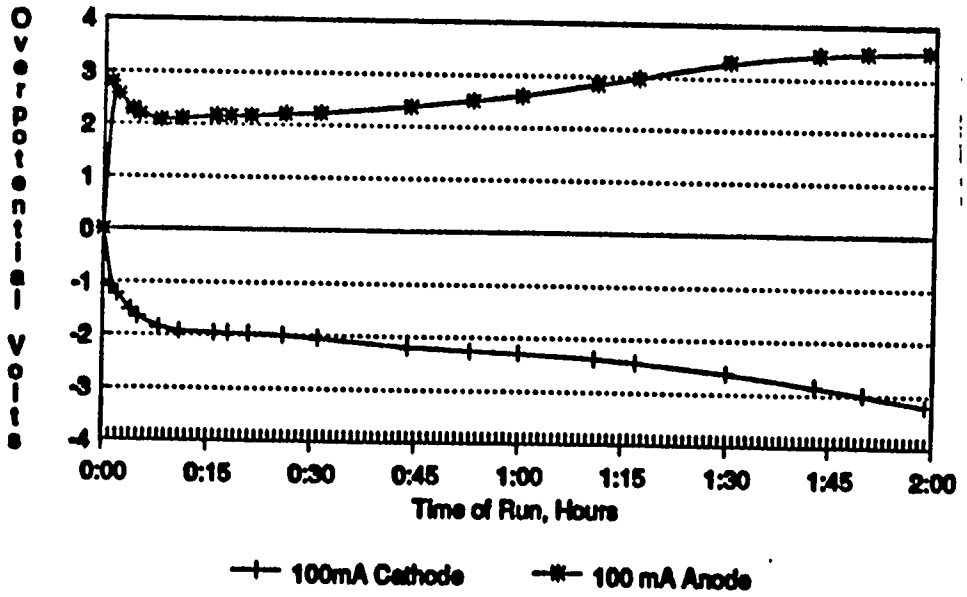

Figure 61: Comparison of overpotentials between runs utilizing identical components.

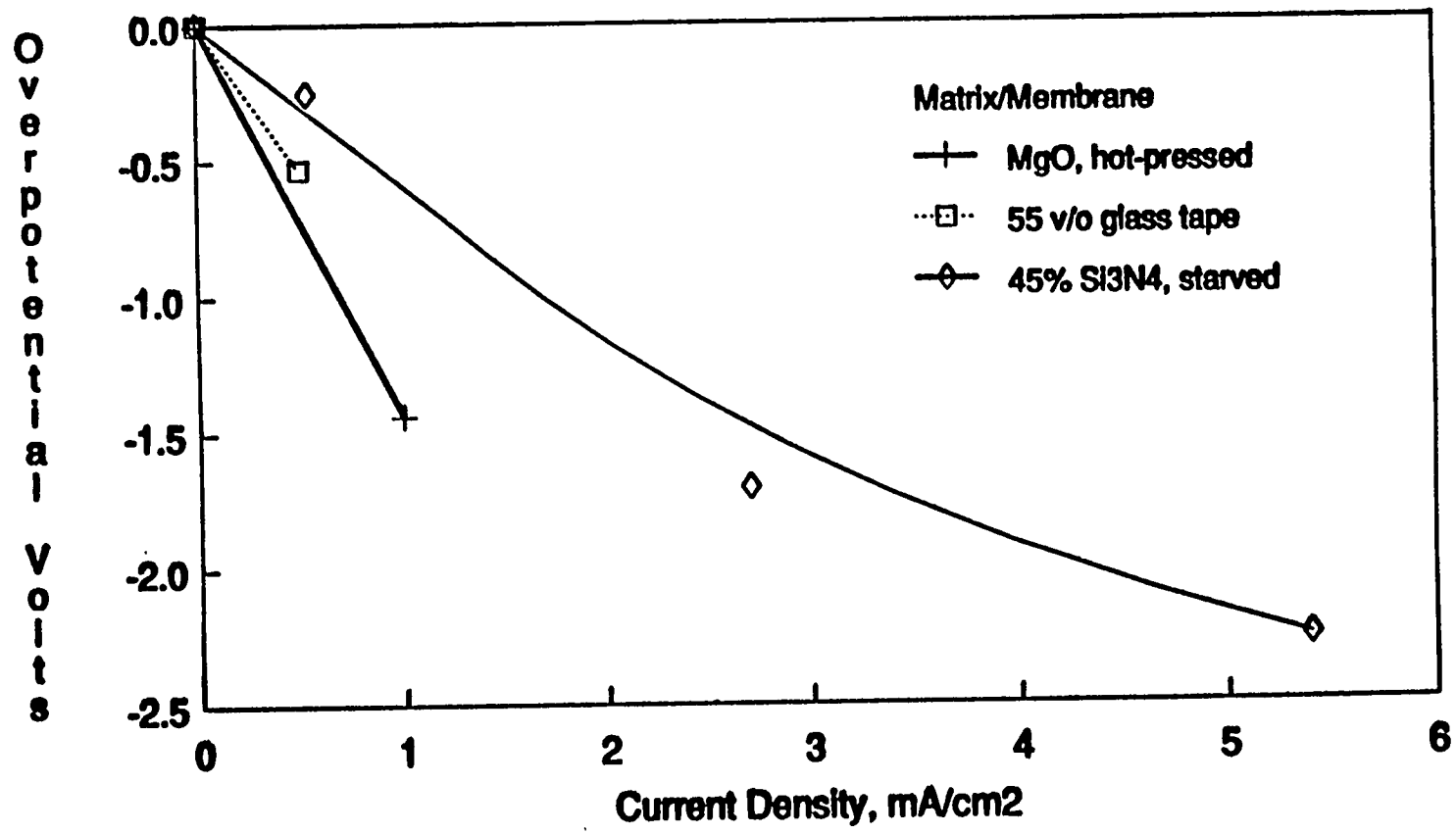

Figure 62: Overpotential versus applied current density comparison of the present and previous tests.

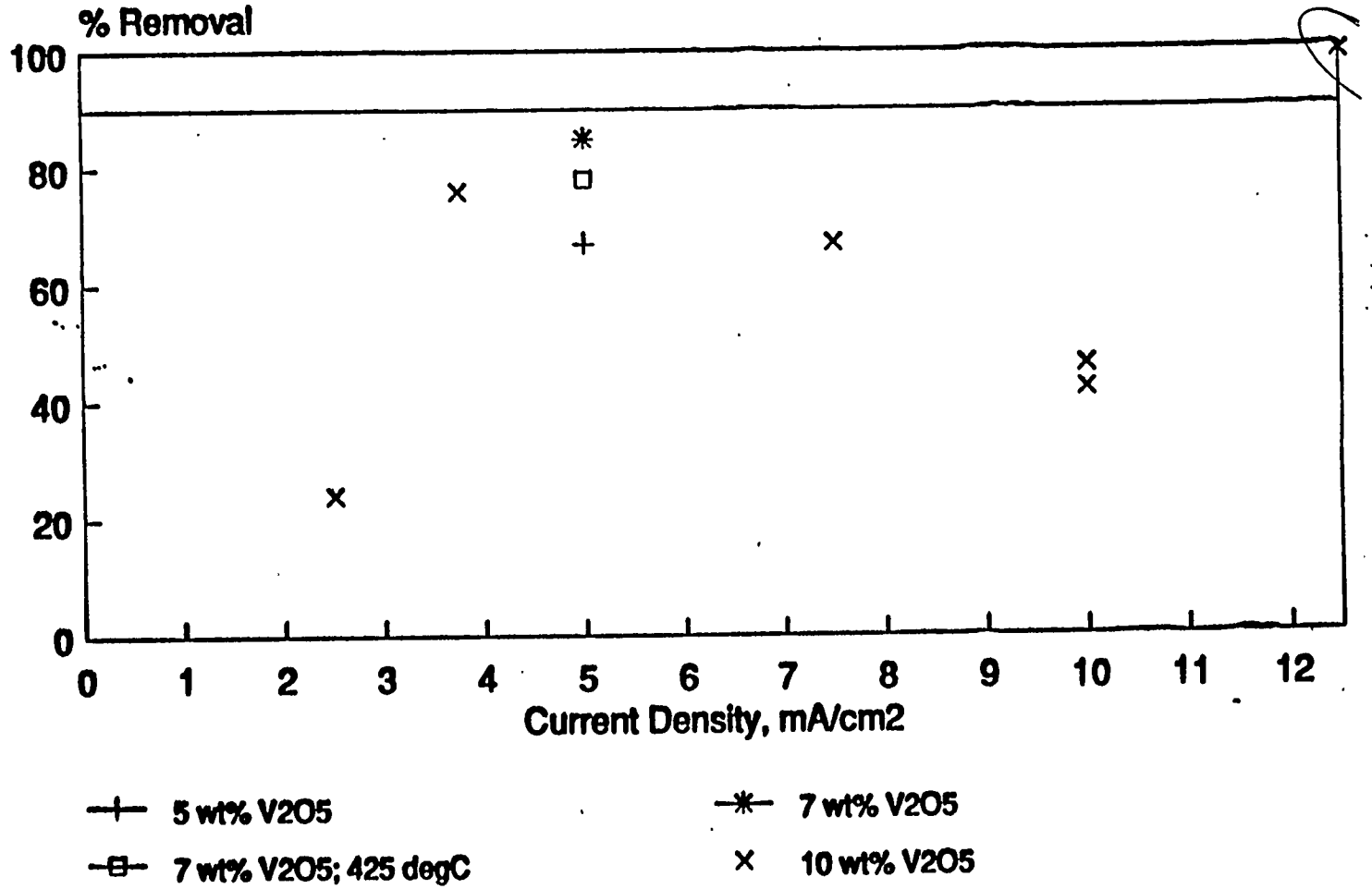

Figure 63. Cathodic removal of SO_3 after 10 minutes applied current. Flow of 0.3% SO_2, 3% O_2 in N_2 equal to that required for 90% removal at applied current.

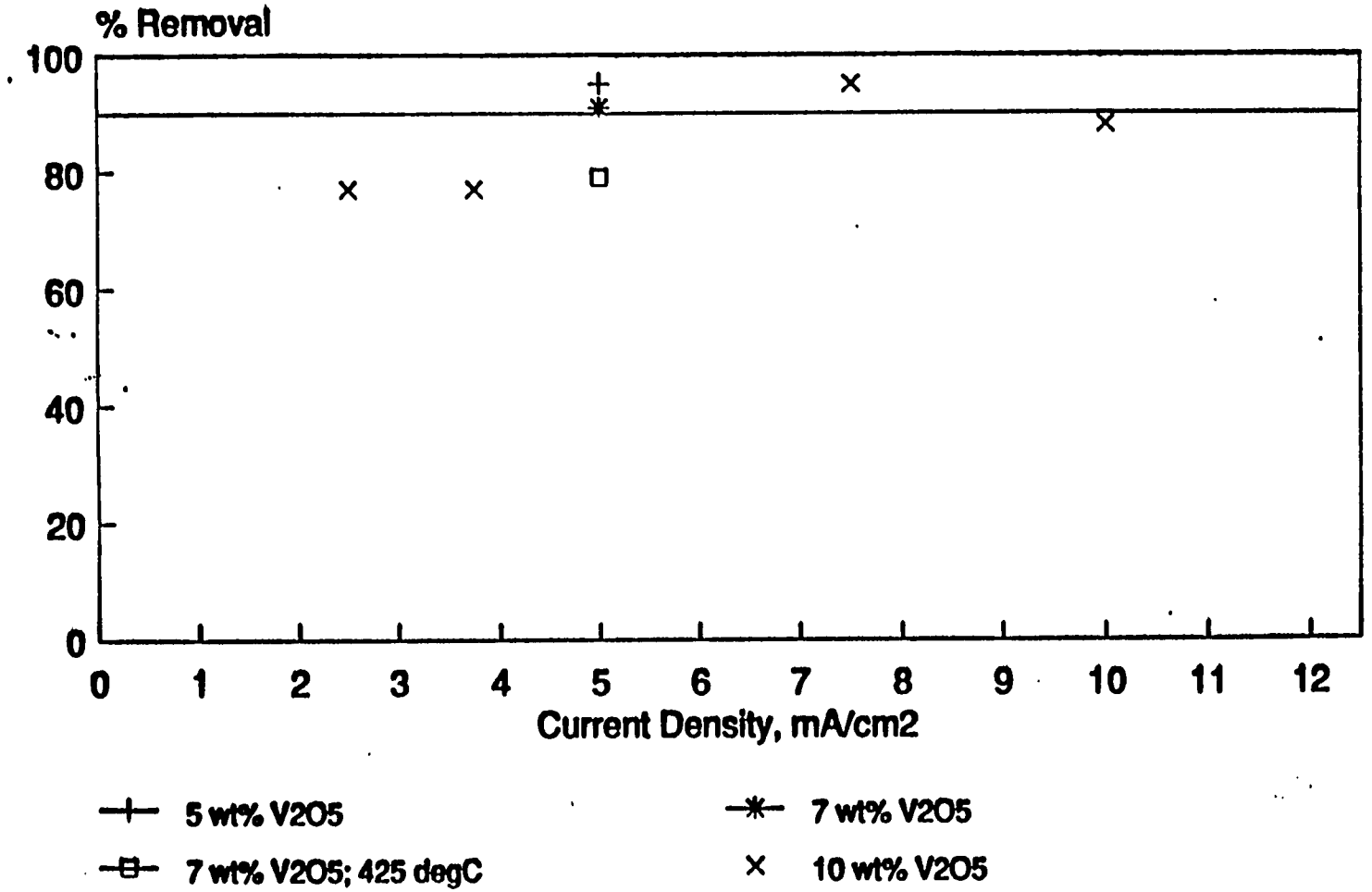

Figure 64. Cathodic removal of SO_3 after 60 minutes applied current. Flow of 0.3% SO_2, 3% O_2 in N_2 equal to that required for 90% removal at applied current.

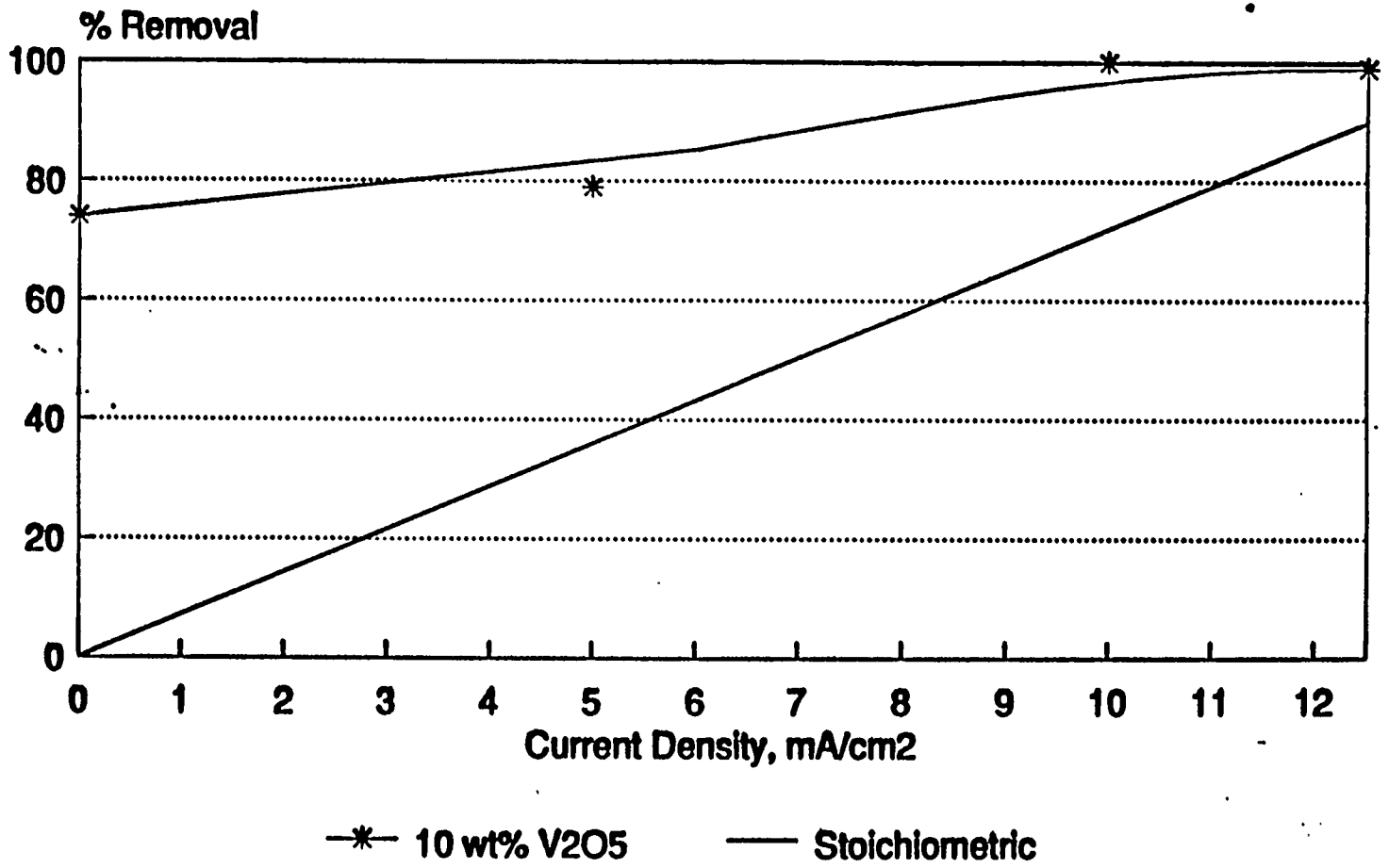

Figure 65. Cathodic removal of SO_3 with current. 690 cc/min of 0.31% SO_2, 3% O_2 in N_2 fed to cathode. All inlet SO_2 oxidized to SO_3. Line represents stoichiometric removal.

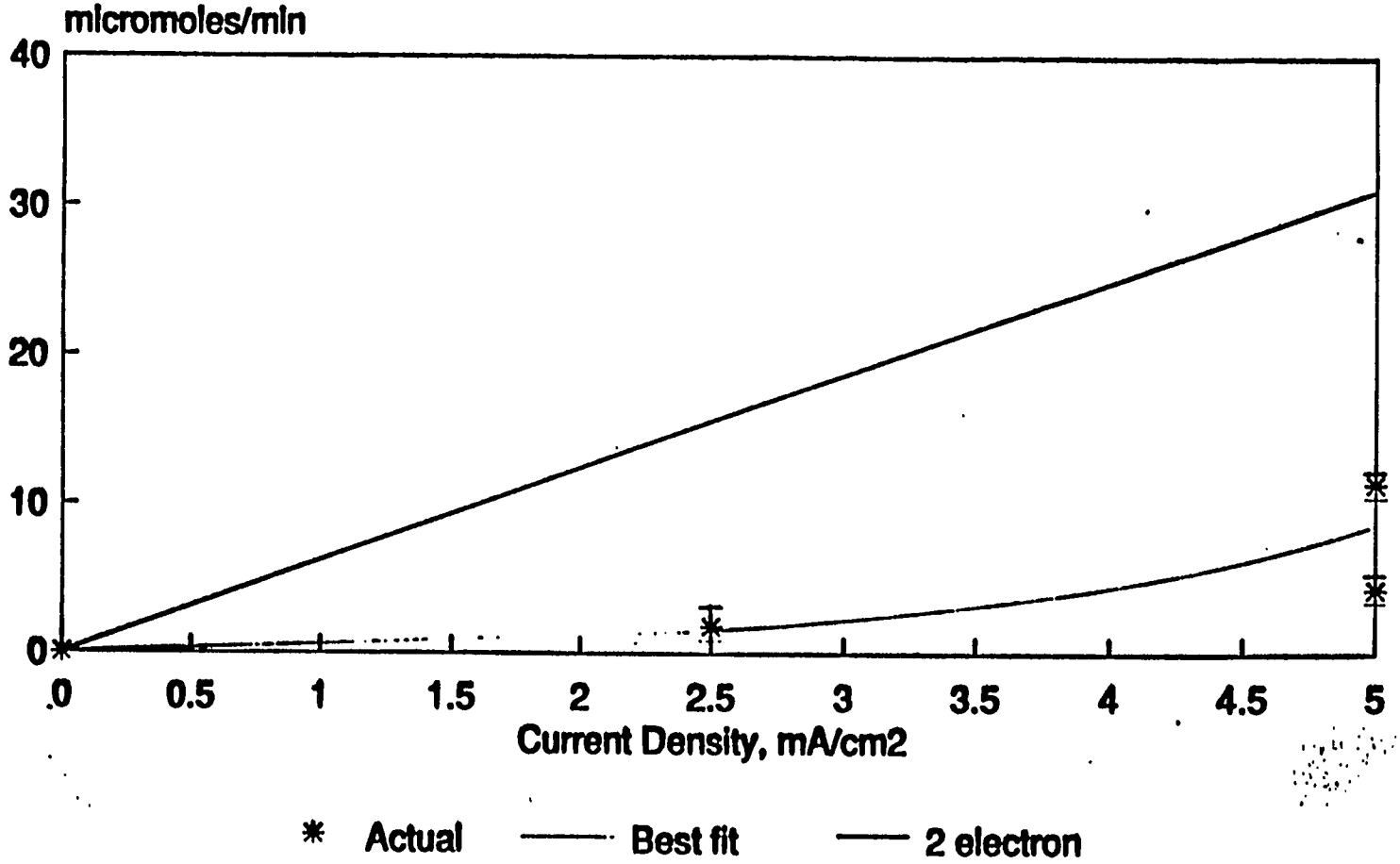

Figure 66. Cathodic SO_2 generation with applied current, with flow for 90% stoichiometric removal of inlet SO_2. 5 wt.% V_2O_5 in electrolyte.

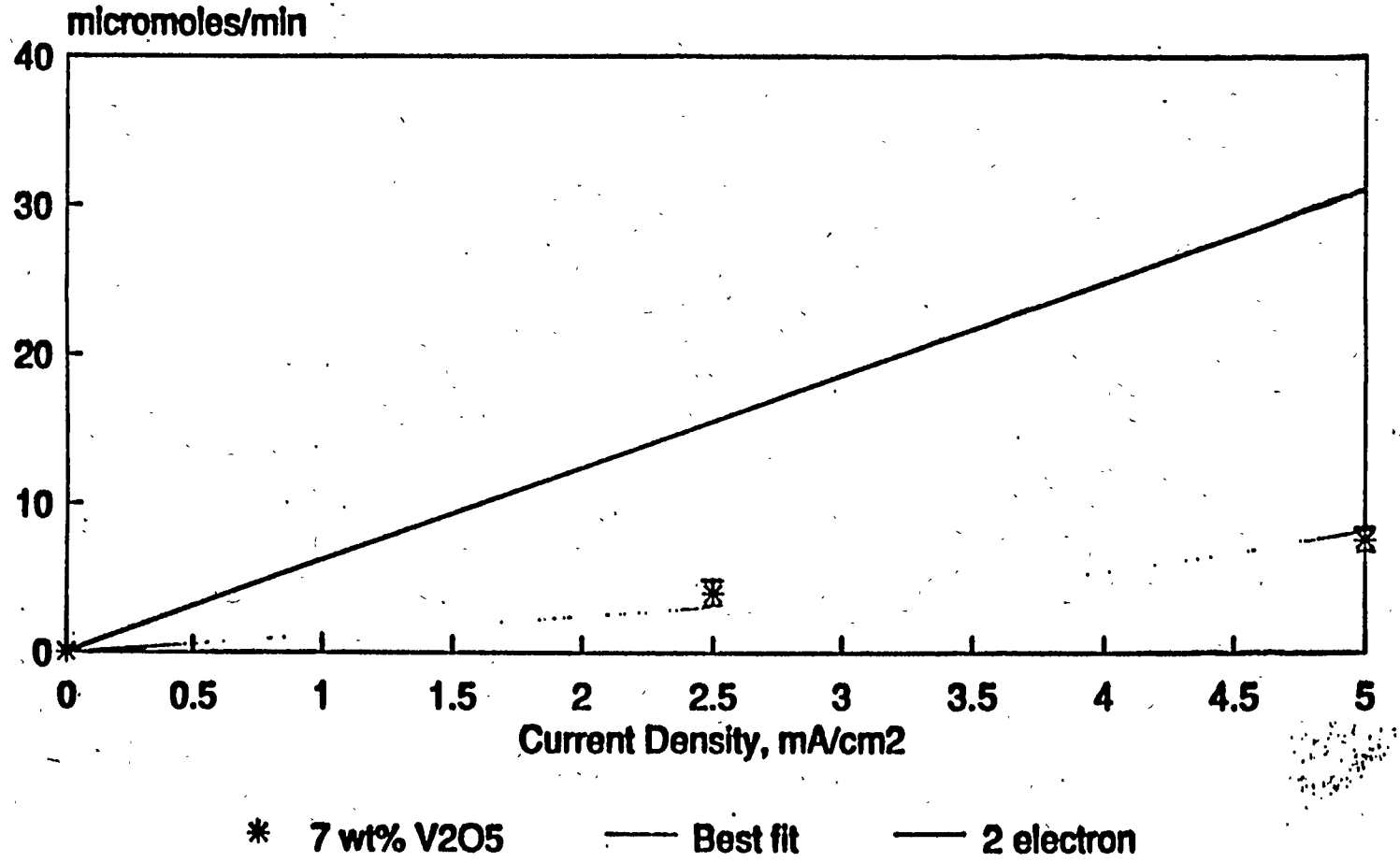

Figure 67. Cathodic SO_2 generation with applied current, with flow for 90% stoichiometric removal of inlet SO_2. 7 wt.% V_2O_5 in electrolyte.

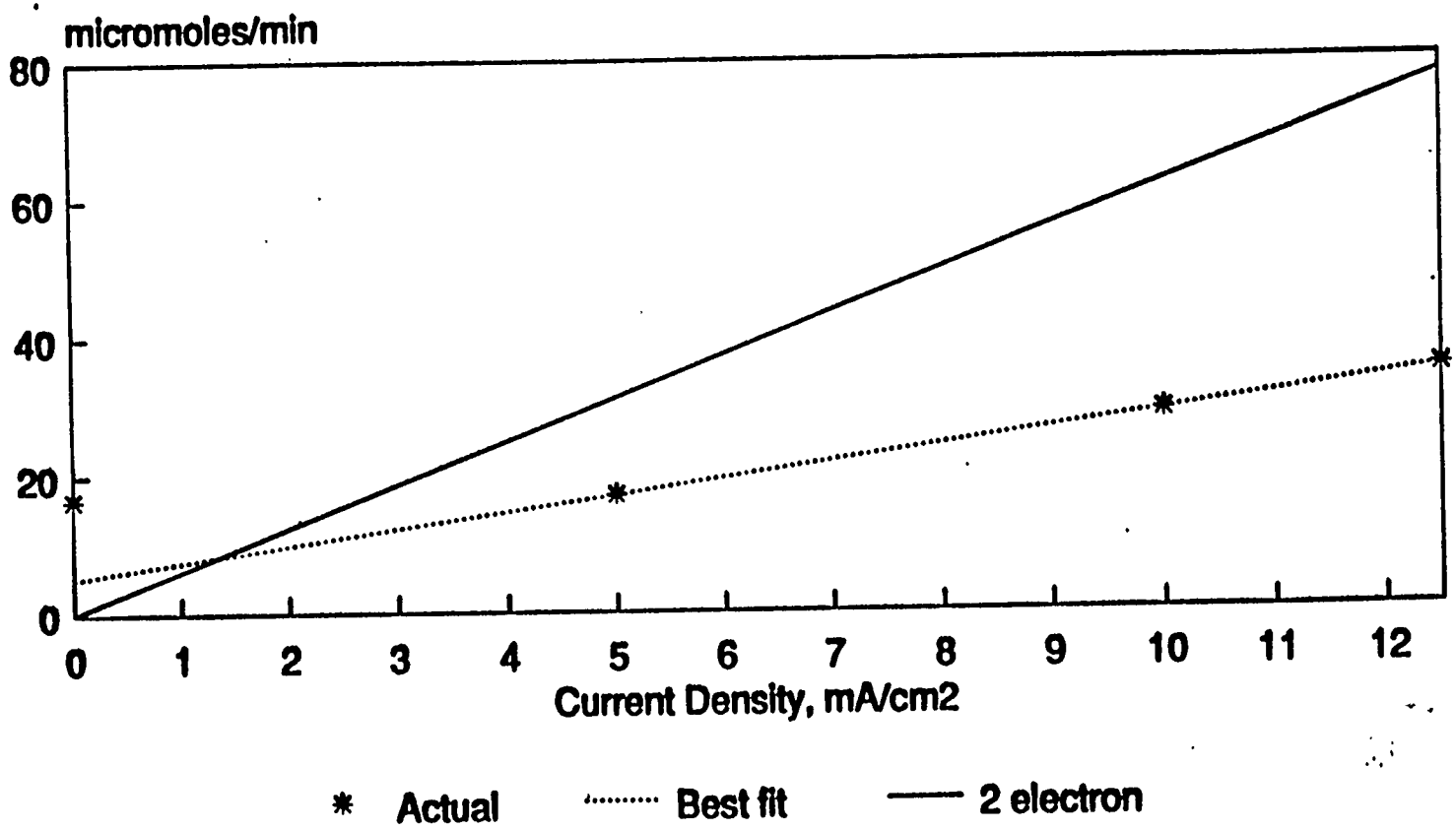

Figure 68. Cathodic SO_2 generation-Flow for 90% stoichiometric removal at 12.5 mA/cm^2. 10 wt.% V_2O_5 in electrolyte.

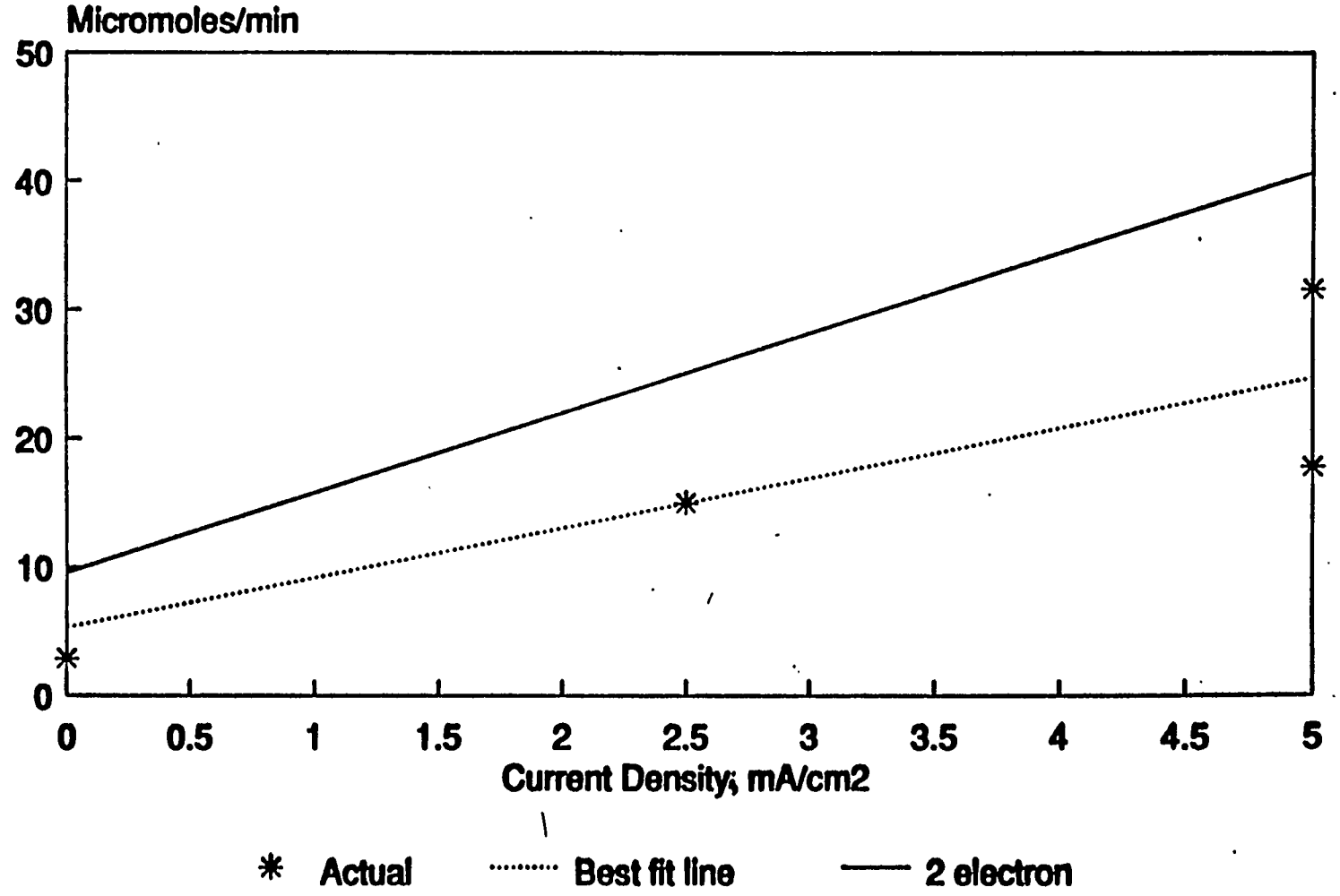

Figure 69. Anodic SO_3 generation, 5 wt.% V_2O_5 in electrolyte. Offset in calculated rates is due to oxidation of SO_2 fed to the anode side.

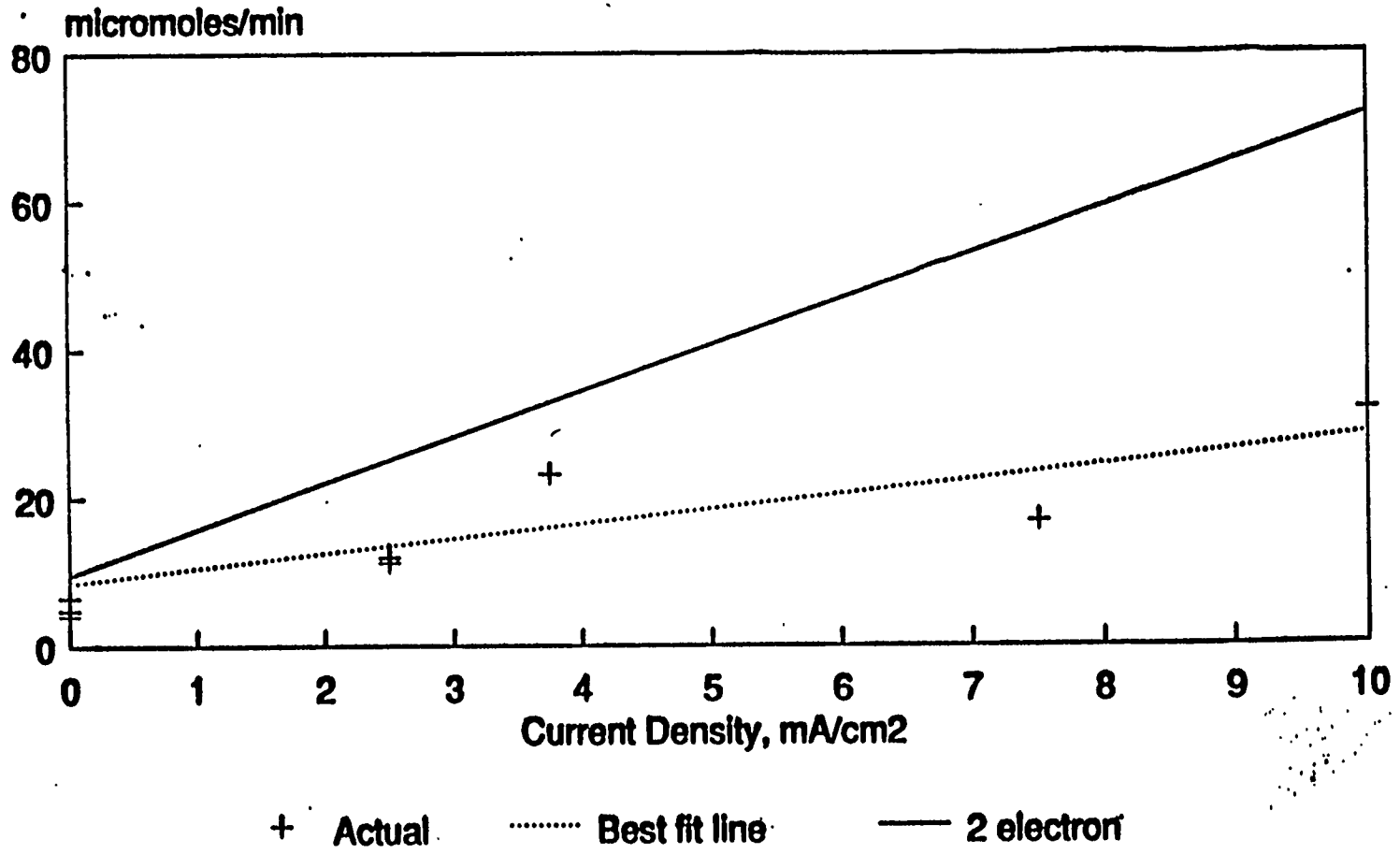

Figure 70. Anodic SO_3 generation, with 10 wt.% V_2O_5 in electrolyte. Offset in calculated rates is due to oxidation of SO_2 fed to the anode.

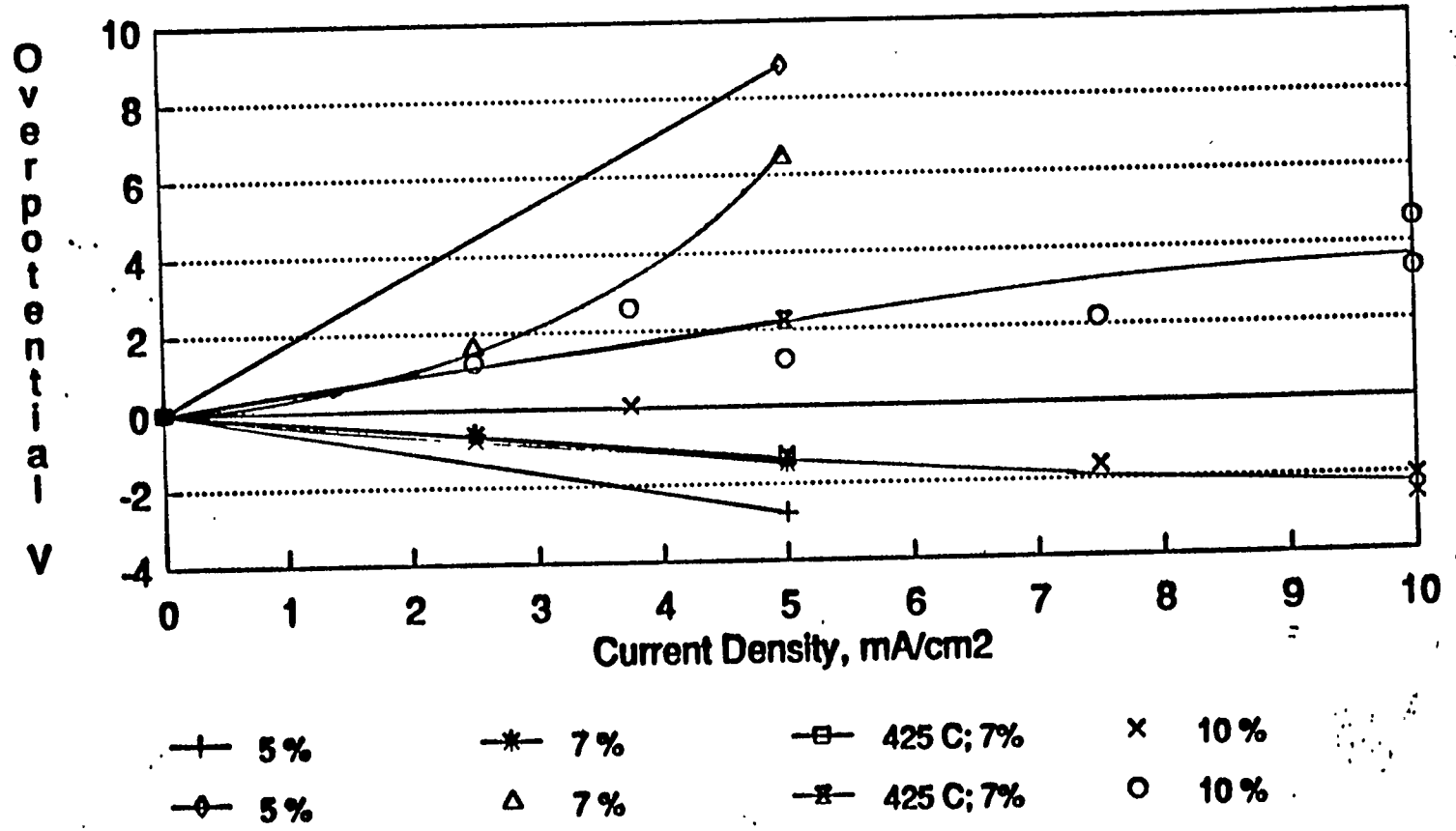

Figure 71. Polarization curves after 60 minutes of applied current.

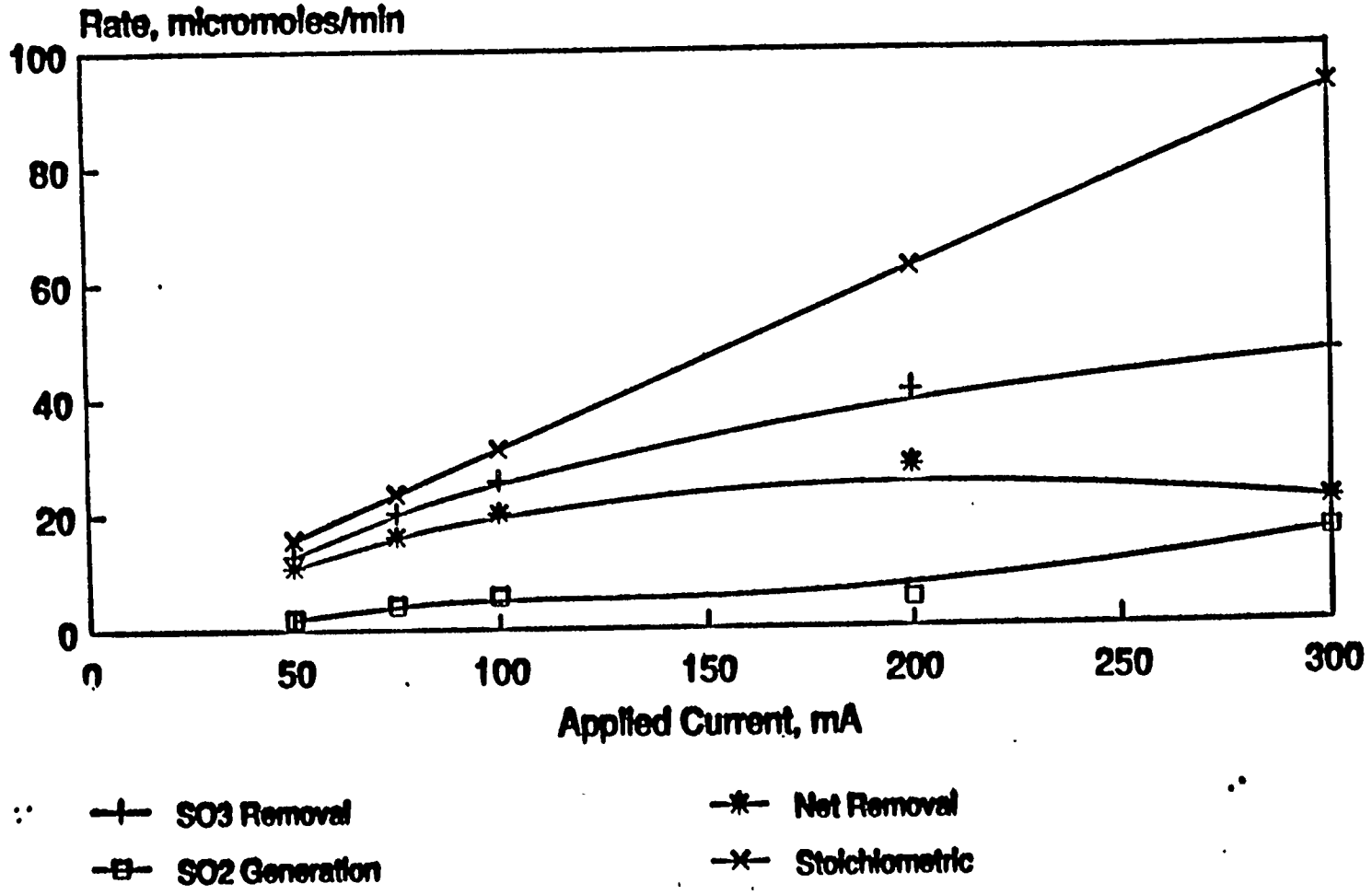

Figure 72:SO_2 generation and SO_3 removal as a function of applied current.

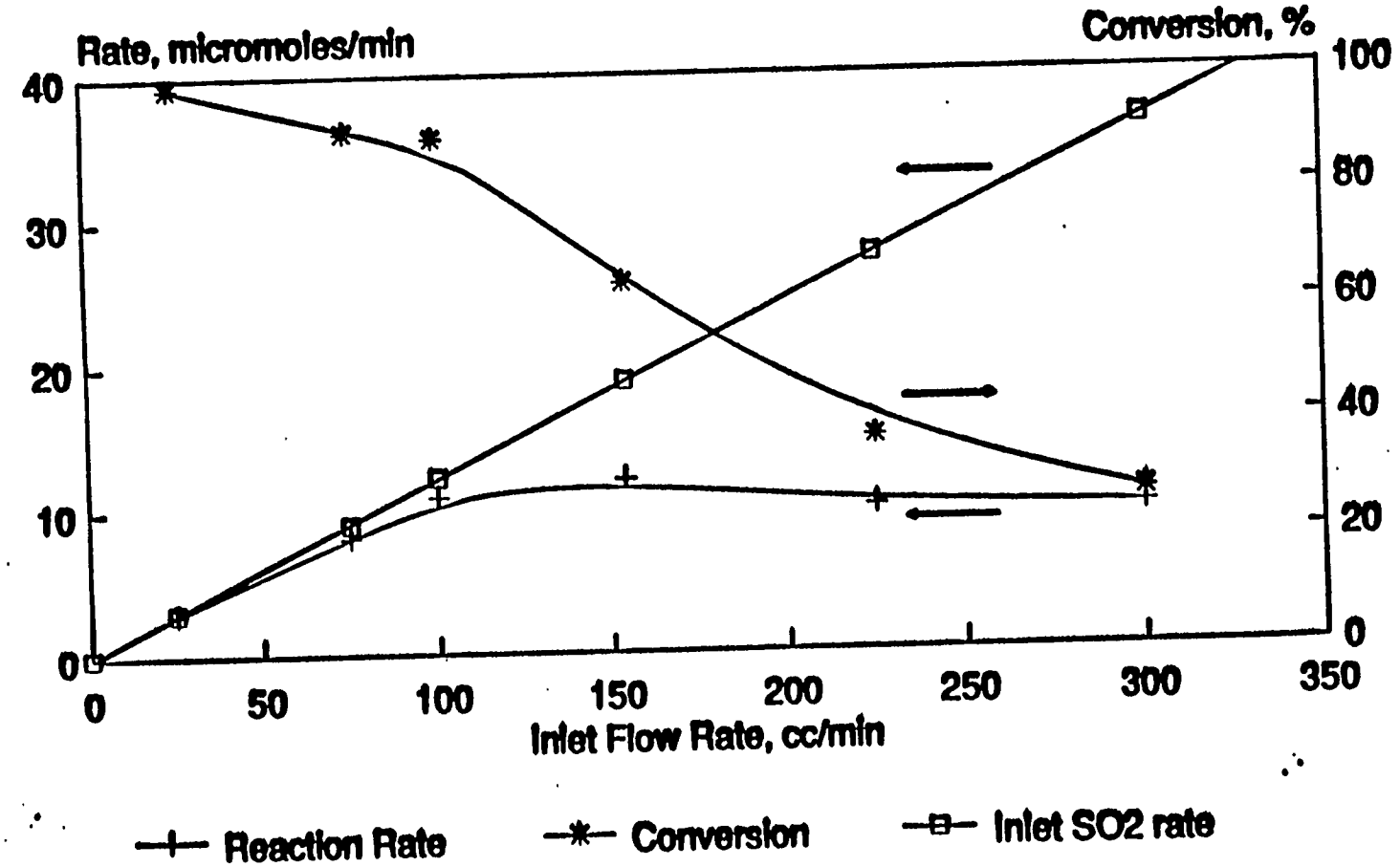

Figure 73. Rate and percent conversion of SO_2 over thin cylinders of VK38 catalyst at 400° C.

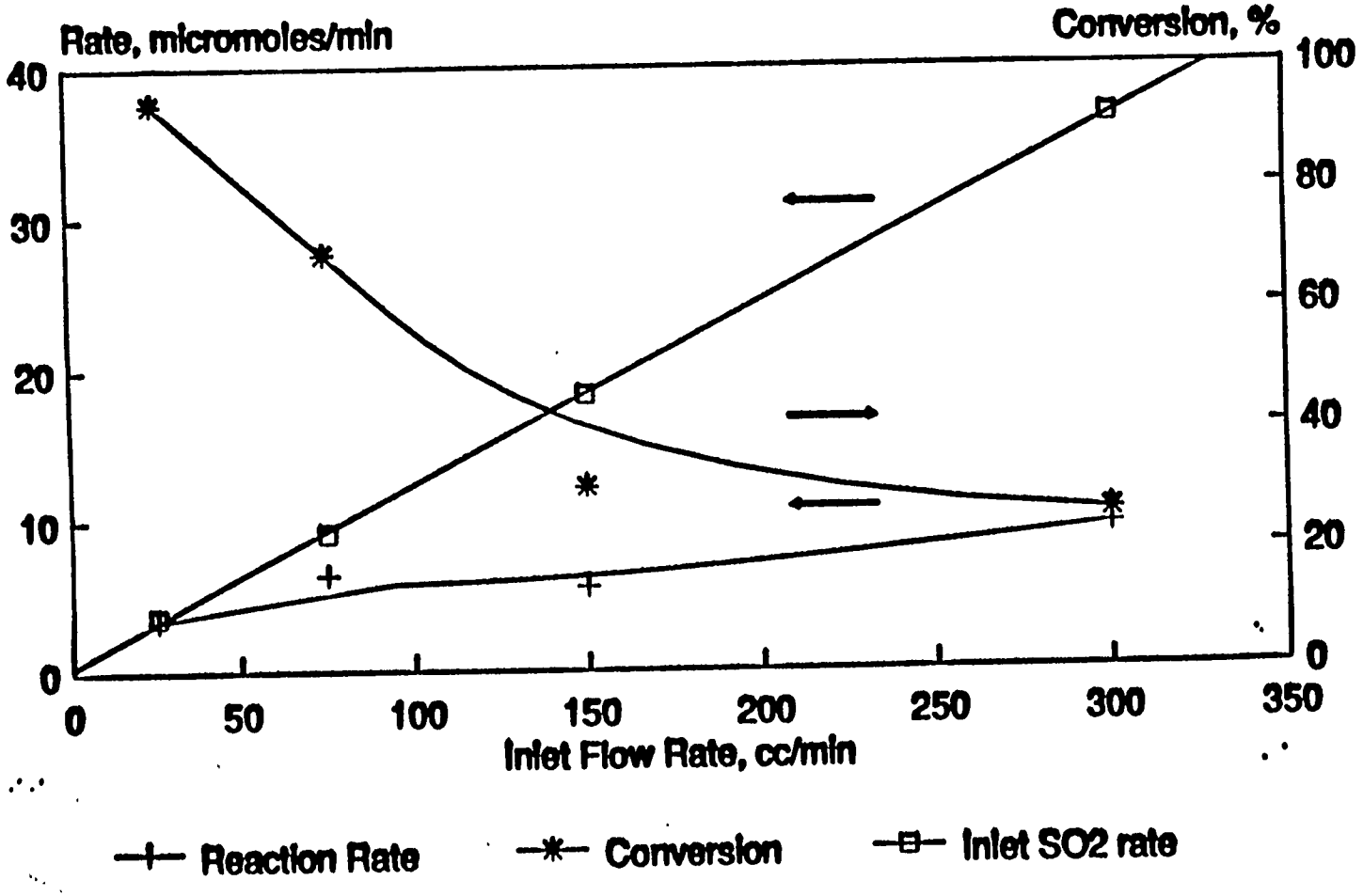

Figure 74. Rate and percent conversion of SO_2 over thin cylinders of VK38 catalyst at 375° C.

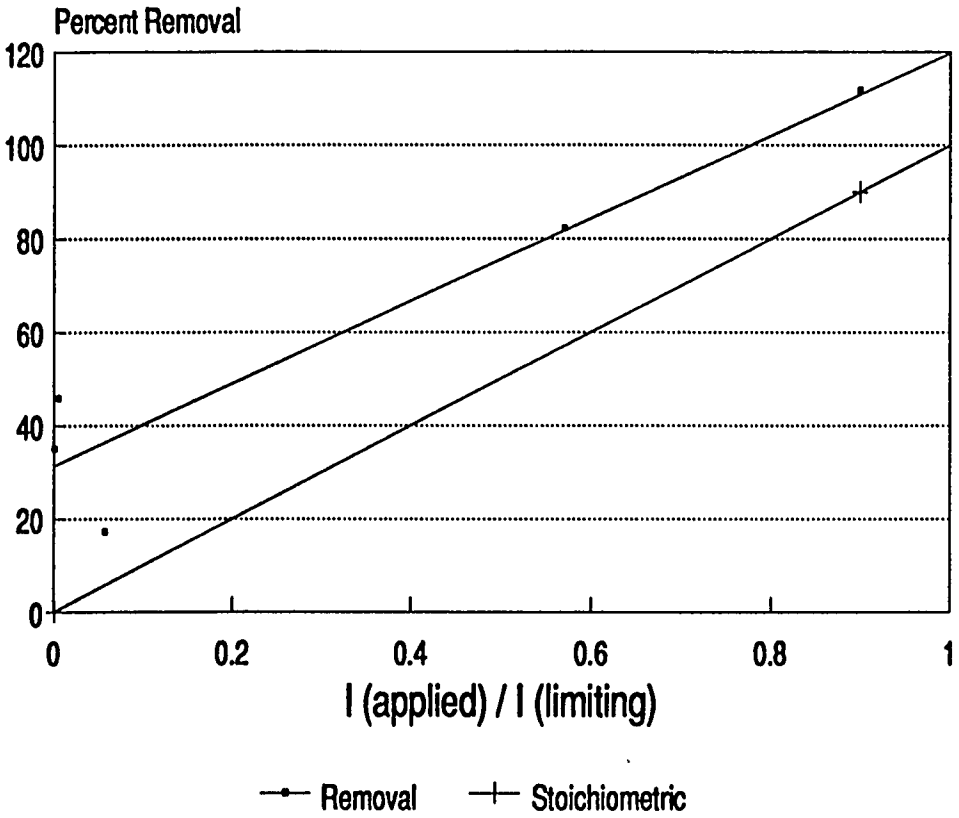

I (limiting)= 196 mA

Figure 75: The removal rate for the second run of the quarter.

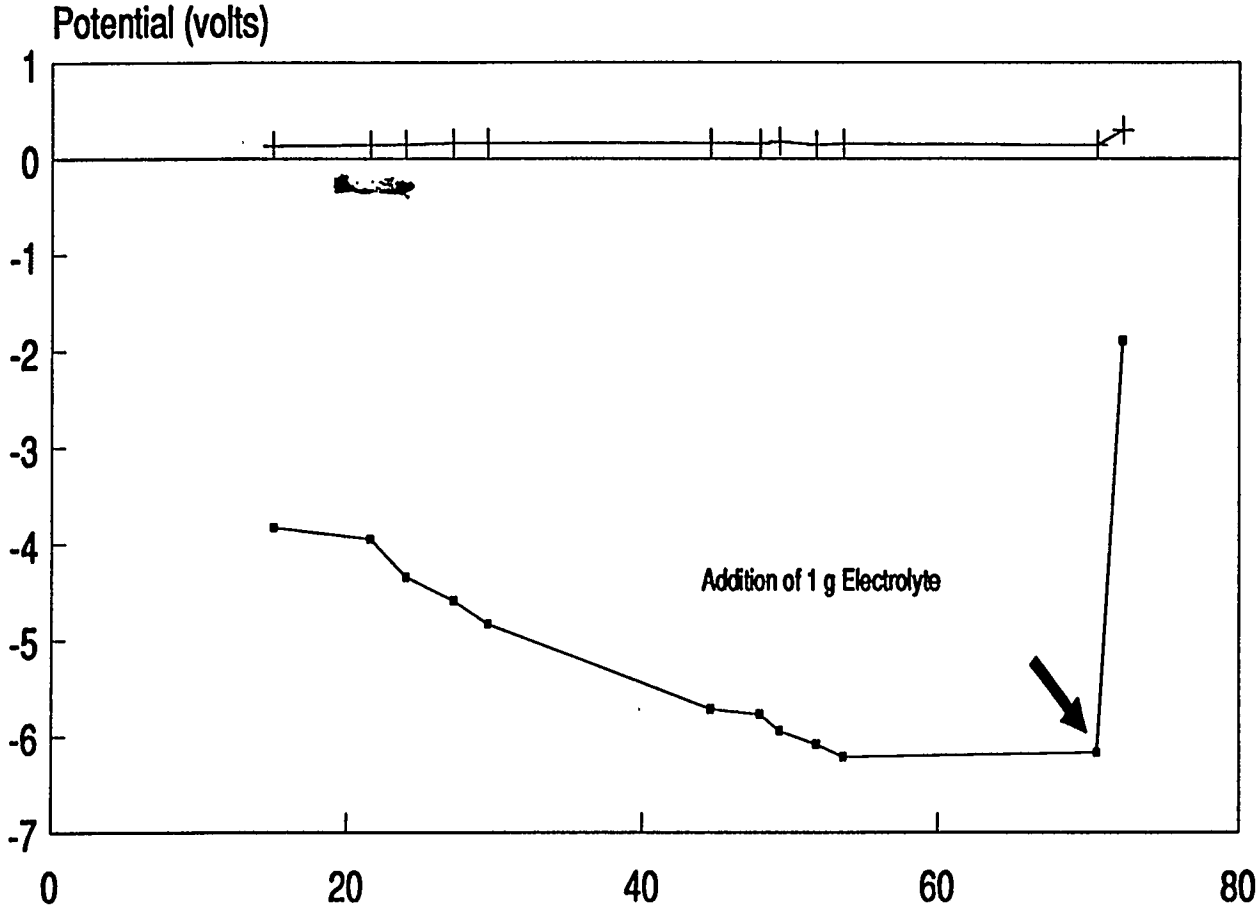

Figure 76: The general increase of the polarity of the cell dropped by 65% with the addition of 1g electrolyte.

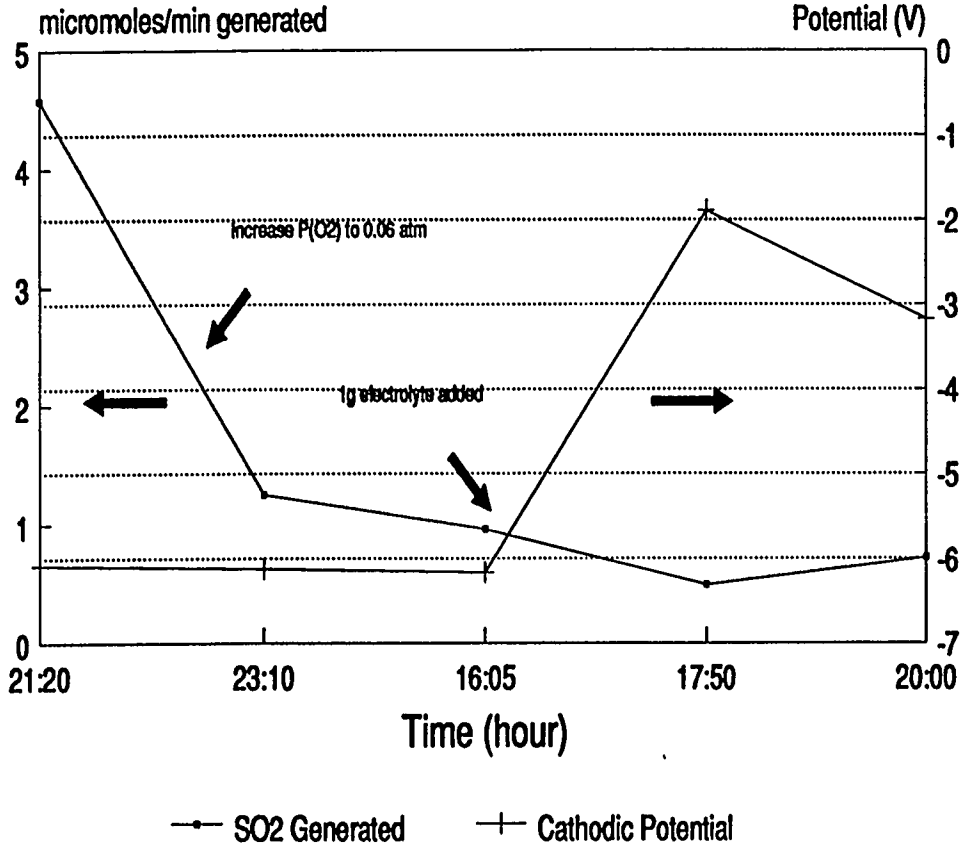

Figure 77: The change in both the cathodic potential and SO_2 generation with the increase in $P(O_2)$ and the addition of electrolyte.

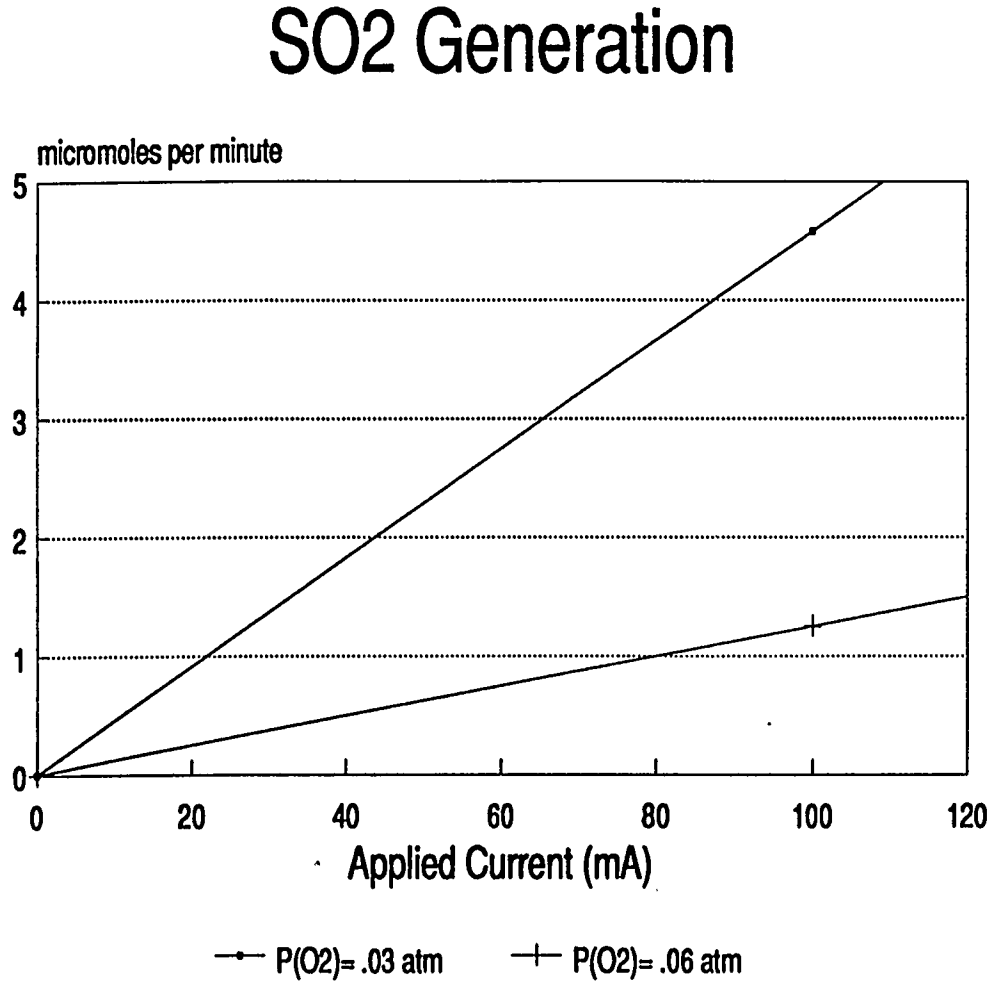

Figure 78: The extrapolated SO_2 generation for Run 2 with a change in the partial pressure of O_2 from .03 atm to .06 atm.

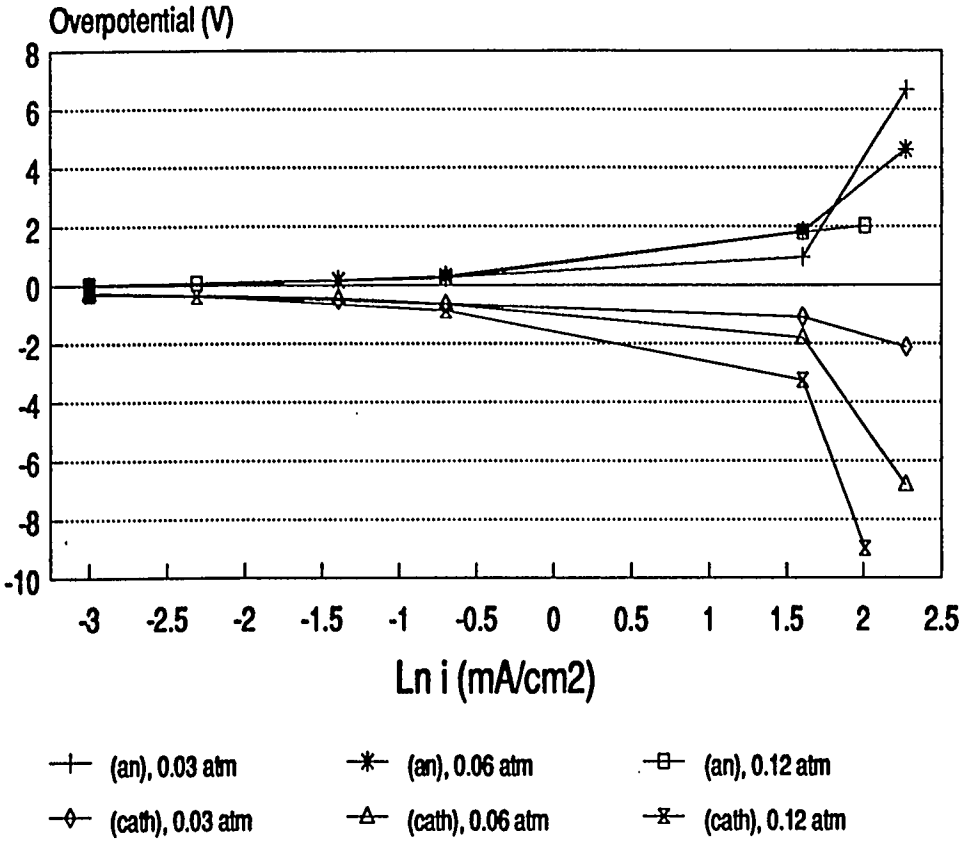

Figure 79: The variance of Overpotential (Volts) with ln i (mA/cm^2) at P(O_2)=0.03 atm, 0.06 atm, 0.12 atm.

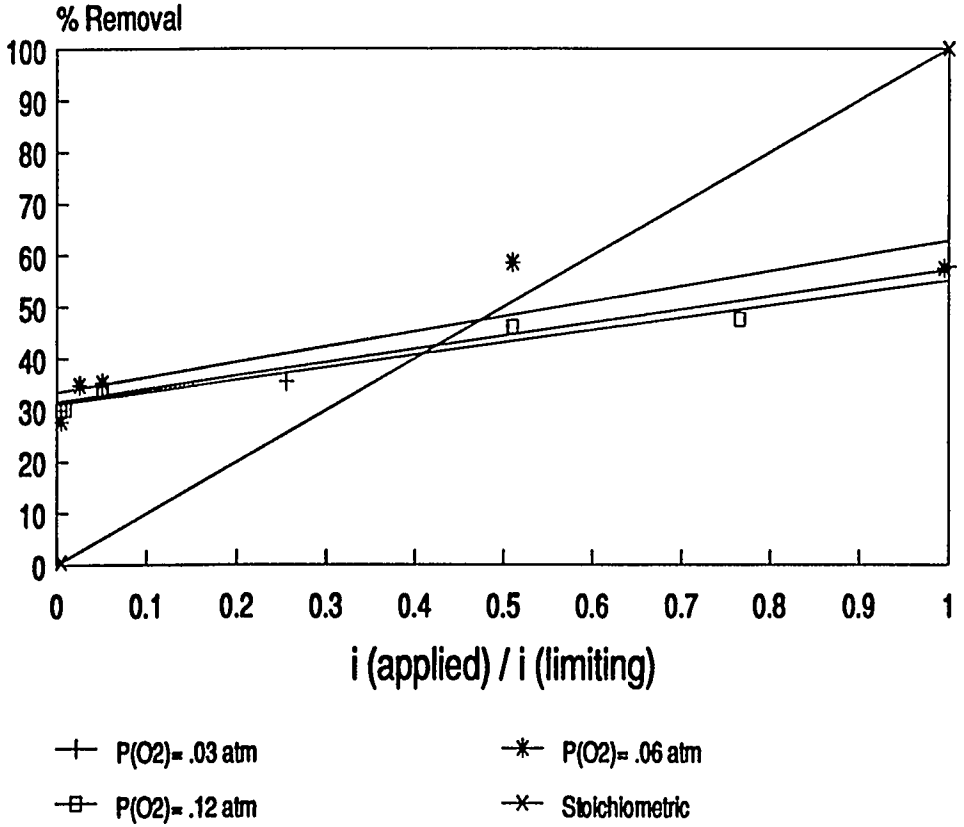

i(limiting)=19.8 mA/cm2

Figure 80: Removal rates based on cathode SO_x for varying O_2 partial pressures.

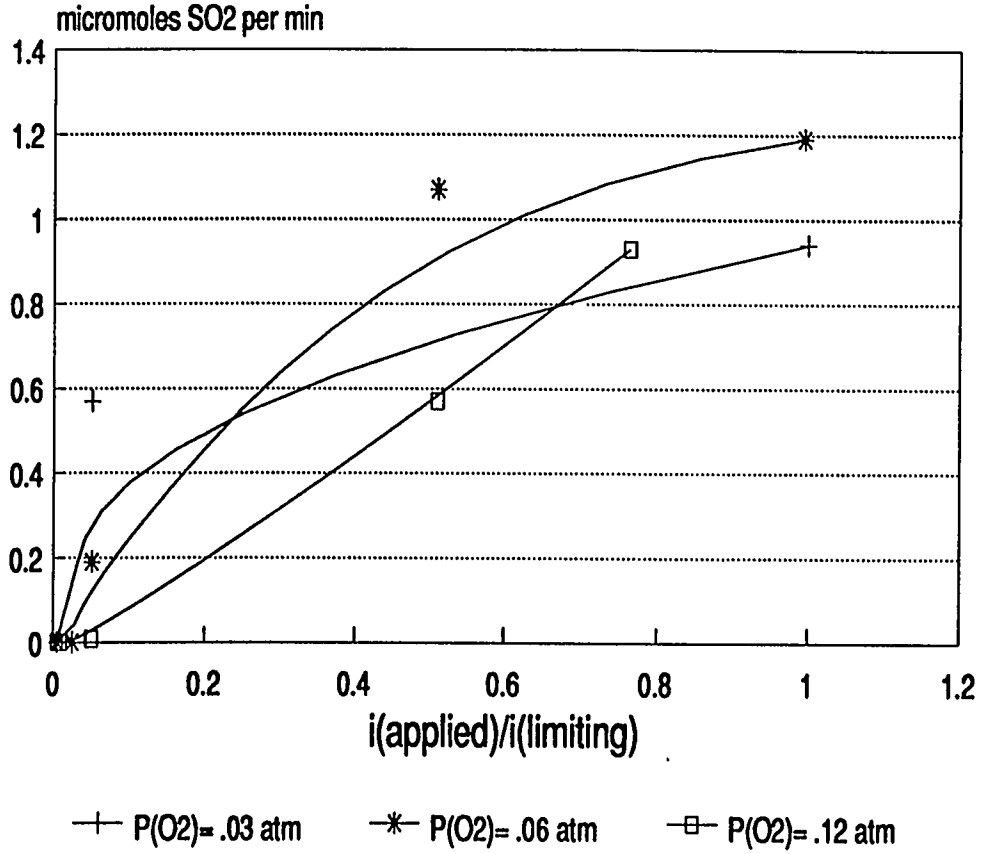

i (limiting)=19.8 mA/cm2

Figure 81: The production variance of SO_2 on the cathode side with various $P(O_2)$ for a constant flowrate.

CONCLUSIONS

Strides have been made in material development for the SO_2 removal system. New lithiated NiO electrode have been developed, representing a great improvement over the previously used pervoskite electrodes. The electrodes have been shown to match the pore size specifications as well as exhibit chemical and electrochemical stability in the full cell system.

The greatest improvements have been seen in the development of the ceramic matrix. Of the vast materials tested, a good chemical and electrochemical match was found in the Si_3N_4 materials. In addition, the new tape casting method allowed the manufacture of extremely thin matrices with simple handling characteristics. The resulting matrix showed improvements over previously used matrices such as the MgO, as well as other materials tested.

Finally, the overall removal system has been shown to exhibit 90% removal at near 100% current efficiency, over a wide range of current densities. The one remaining problem, the evolution of SO_2 from the cathodic reactions, may be solved through the use of higher active area, necessitating the development of even electrodes with even smaller pore sizes. However, the results with the new materials prove extremely promising.

CONCLUSION

The H_2S cell has demonstrated over 90% removal capabilities in the 1000-100ppm, 100-10, and 10-1ppm H_2S ranges. This excellent removal has been accompanied by economically feasible current efficiencies, with the highest current efficiencies (100%) in the 1000-100ppm H_2S range. The lower current efficiencies experienced at polishing levels should still prove economically sound due to the low overall power requirement at those levels.

Yttria-stabilized densified zirconia membranes have shown a high degree of compatibility with the current system. Selective removal has been demonstrated in full cell testing as well as chemical and electrochemical stability in the basic environment. For polishing applications, lithiated Ni converted to NiO in-situ proved most useful for both cathode and anode materials, similar to the molten carbonate fuel cells. However, at H_2S concentrations above 100ppm, a molten nickel sulfide state was shown to exist at the cathode, hindering high H_2S removal efficiencies. This caused a shift toward Co cathodes proven to be stable and highly conductive in the carbonate environment.

The SO_2 removal cell consistently demonstrated 90% removal at near 100% current efficiency using a simulated flue gas stream of 3000ppm SO_2. O_2 was demonstrated as crucial to the removal process due to the regeneration of V_2O_5 from the V^{4+} state.

After a number of materials had been tested, the tape-casting of Si_3N_4 was found to provide the most suitable membrane with respect to the chemical and electrochemical

stability in the highly acidic environment of the cell. In addition, the Si_3N_4 matrices was shown to provide lower polarizations than other candidate materials.

A new electrode, lithiated NiO was developed for use in the cell, and was found to resist the corrosive effect normally found with NiO in a sulfate-rich environment. Polarizations with these electrodes also led to their use in full cell system.

As this research period ended, focus was on increasing the electrode surface area available for reaction through the use of small electrode pore sizes. This method will also require the development of a ceramic matrix of smaller particle size.

ENDNOTES

1. S. H. Langer and R. G. Haldeman, *J. Phys. Chem.*, **68** (1964) 962.

2. J. Winnick, R. D. Marshall, and F. H. Schubert, *I. E. C. Pr. Des.*, **13** (1974) 59.

3. H. S. Lim and J. Winnick, *J. Electrochem. Soc.*, **131** (1984) 562.

4. D. Weaver and J. Winnick, *J. Electrochem. Soc.*, **134** (1987) 2451.

5. S. Alexander and J. Winnick, 6th *Symp. Sep'n Sci. and Tech.*, in press.

6. K. A. White and J. Winnick, *Electrochem. Acta*, **30** (1985) 511.

7. E. K. Banks and J. Winnick, *J. Appl. Electrochem.*, **16** (1986) 583.

8. D. Weaver, Ph. D. Thesis, Georgia Institute of Technology, 1988.

9. Austin, I.G., and Mott, N.E., Adv. Phys., 18, 41 (1969).

10. Kingery, W.D., Brown, H.K., Uhlmann, C.R., Introduction to Ceramics, 2nd. ed., Wiley, New York, 1976.

11. Ellingham, J.T., *J. Soc. Chem. Ind.*, **63**, 125, (1944).

12. Weaver, D., Electrochemical Removal of H_2S from Multicomponent Gas Streams, Georgia Institute of Technology PhD Dissertation, 1988.

13. Barin, I., and Knacke, O., Thermochemical Properties of Inorganic Substances, Springer-Verlag, Berlin, (1973).

14. Barin, I., and Knacke, O., Thermochemical Properties of Inorganic Substances - Supplement, Springer-Verlag, Berlin, (1977).

15. Preto, S.K., Tomzcuk, Z., et. al., *J. Electrochem. Soc.*, **130**, (1983).

16. Ingram,M.D., and Janz, G.J., *Electrochemica Acta*, **10**, (1965).

17. Babcock, K., and Winnick, J., *J. Chem. E. Data*, **33**, 1988.

18. Iacovangelo, C., and Karas, B., *J. ELectrochem. Soc.*, **133**, 1986.

19. Hamling, B., and Lattimer, R., *Advanced Materials and Processes*, June, 1986.

20.Flood, H.; Förland, T., *Acta. Chemica. Scandinavica*, **1** (1947), 781-789.

21. Flood, H.; Boyle, C., *Zeitschrift für Elektrochemie*, **66** (1962), 184.

22. Boreskov, G. K., *et. al.*, *J. Gen. Chem. USSR*, **24** (1954), 21.

23. Fang, W. C.; Rapp, R. A., *J. Electrochem. Soc.*, **130** (1983), 2335.

24. Park, C. O.; Rapp, R. A., *J. Electrochem. Soc.*, **133** (1986), 1636.

25. Shores, D. A.; Fang, W. C., *J. Electrochem. Soc.*, **128** (1981), 346.

26. Franke, M. D., Electrochemical Flue Gas Clean-Up, Ph.D. Thesis, Georgia Institute of Technology, 1988.

27. Scott, K. D.,Electrochemical Flue Gas Desulfurization, Ph.D. Thesis, Georgia Institute of Technology, 1985.

28. Townley, D.; Winnick, J., *I.&E.C. Proc. Desgn. & Develop.*, **20** (1981), 435.

29. Salzano, F. J.;Newman, L., *J. Electrochem. Soc.*, **119** (1972), 1273.

30. Flood, H.; Kleppa, O. J., *J. Am. Chem. Soc.*, **69** (1947), 998.

31. Karydis, D. A., *et. al.*,"Extended Abstracts," *J. Electrochem. Soc.*, **93-1** (1993), 2017.

32. Karydis, D., *et. al.*, "Extended Abstracts," *J. Electrochem. Soc.*, **93-1** (1993), 2027.

33. Hodgman, Charles D. et. al., Eds., Handbook of Chemistry and Physics, 42nd Edition, 1960-1961, Chemical Rubber Publishing Company, Cleveland, Ohio, 1960.

34. Prausnitz, J.M., Lichtenthaler, R.N.,deAzevedo, E.G.,Molecular Thermodynamics of Fluid-Phase Equilibria, Prentice-Hall, New Jersey, 1986.

35. Lovering, Gale et. al., Molten Salt Techniques vol. 1, 1983.

36. Jaeger, F.M., "Z. Anorg. Chem.," 101, 1 (1917).

37.Burrows, B.W., and Hills G.J., *Electrochim. Acta.* **15**(1970), 445.

38.Risbud, S.H., Zangvil, A.,*J. Matl. Sci.*, **18**(1983), 998.

39. D.N. Hill, Professor, Ceramic Engineering, Georgia Institute of Technology, personal communication.

40. Chin G.Y., Advances in Powder Technology, American Society for Metals, 1982, p.293.

41. Mark Wesselman, Electro Scientific Industries, personal communication.

42. Scott, K. D., Fannon, T. and Winnick, J., *J. Electrochem. Soc.*, **135**, 573, 1988.

43. Franke, M. and Winnick, J., *I&EC Research*, **28**, 1352, 1989.

44. Holroyd, F. P. B. and Kenney, C. N., *Chem. Eng. Sci.*, **26**, 1963, 1971.

45. Holroyd, F. P. B. and Kenney, C. N., *Chem. Eng. Sci.*, **26**, 1971, 1971.

46. Mars, P. and Maessen, J. G. H., *J. Catalysis*, **10**, 2, 1968.

47. Franke, M. and Winnick, J., ***J. Electroanalytical Chemistry*, 238**, 163, 1987.

48. McHenry, Dennis John, Development of an Electrochemical Membrane Process fir Removal of SO_x/NO_x from Flue Gas, Ph.D. Thesis, Georgia Institute of Technology, 1992.